T H E U N I V E R S I T Y O F M I C H I G A N

COLLEGE OF ENGINEERING
Department of Mechanical Engineering
Heat Transfer and Thermodynamics Laboratory

THE DYNAMICS OF GAS-VAPOR BUBBLES IN BINARY SYSTEMS

Poul S. Larsen

John A. Clark

ORA Project 04268

under contract with:

NATIONAL AERONAUTICS AND SPACE ADMINISTRATION
GEORGE C. MARSHALL SPACE FLIGHT CENTER
CONTRACT NO. NAS-8-825
HUNTSVILLE, ALABAMA

administered through:

OFFICE OF RESEARCH ADMINISTRATION ANN ARBOR

November 1963

This report was also a dissertation submitted by the first author in partial fulfillment of the requirements for the degree of Doctor of Philosophy in The University of Michigan, 1963.

ACKNOWLEDGMENTS

The authors wish to express their appreciation to Professors Gordon J. Van Wylen, Joseph J. Martin, Vedat S. Arpaci, Herman Merte, Jr., Richard E. Sonntag, and Wen-Jei Yang, for their interest and cooperation in serving as members of the Doctoral Thesis Advisory Committee.

TABLE OF CONTENTS

TABLE OF CONTENTS (CONT'D)

LIST OF TABLES

LIST OF FIGURES

LIST OF FIGURES (CONT'D)

LIST OF FIGURES (CONT'D)

LIST OF APPENDICES

NOMENCLATURE

Roman

a	coefficient, polar amplitude
A_o	constant, Equation (56)
b	constant, Equation (81)
c	molal specific heat at constant pressure
C	constant Equation (119)
C_H	coefficient, Equation (69)
C_M	coefficient, Equation (69)
$\mathfrak{D}$	mass diffusivity
E	functional notation $E() = \exp()^2 \cdot \operatorname{erfc}()$, Equations (106) and (107)
f	frequency, parameter function, function
F	ratio of heats of phase transition, $F = h_{fgB}/h_{fgA}$
h	enthalpy
I	integral, Equation (69)
INT	integral, Equation (127)
Ja	Jakob number, defined by Equations (50) and (111)
k	thermal conductivity
K	expression, Equation (66), Henry law constant, Equation (94)
Lu	Lukomskiy number, defined by Equations (50) and (101)
L1	reference length, Figure 30
L2	reference length, Figure 30
M	expression, Equation (66), molecular weight in Appendix I
n	order of harmonic
N	mole flux, expression in Equation (66)

p	pressure, partial pressure when subscripted
P	dimensionless bubble size, $P = R/R_O$
$\dot{q}$	spherical surface source
Q	relative dimensionless bubble size, $Q = (P - 1)/(P_\infty - 1)$
r	radial independent space variable
R	bubble radius, universal gas constant in Appendix I
Re	Reynolds number for bubble motion, $Re = 2 \cdot R \cdot V/\nu$
R(I)	equivalent bubble radius from I-th frame of film
t	time
T	temperature
U	variable, $U = P\dot{P}/Lu$
v	velocity
V	velocity
VMAX	asymptotic bubble volume
VO	initial bubble volume
VR	volume, defined in Figure 30
V(I)	visible volume from I-th frame of film, defined in Figure 30.
w	relative bubble size, $w = P/P_\infty$
x	molefraction of component A
y	independent space variable measured from bubble interface in the direction of the liquid phase
Y	spherical zonal harmonic, dimensionless similarity variable, $Y = y/\sqrt{\alpha' t}$

Greek

α	thermal diffusivity
δ	uncertainty on

ϵ	density deficienty, $\epsilon = 1 - \rho''/\rho'$
Θ	dimensionless temperature, defined by Equations (50) and (112)
λ	phase-growth constant, defined by Equation (97)
μ	$\mu = \cos\psi$
ν	kinematic viscosity of the liquid
ξ	intermediate time between t' and t
ρ	partial molal density
σ	surface tension
τ	dimensionless time, $\tau = \alpha' t/R_o^2$
ϕ	function, defined by Equation (118)
ψ	polar angle
ω	cyclic frequency

Subscripts

A	component A
B	component B
c	bubble center, collapse
eq	equivalent
fg	liquid-gas phase transition
H	heat
M	mass
r	radial
R	at the bubble surface
s	interfacial
T	temperature
x	composition

o	initial, reference value
1	join point between initial and intermediate solution
2	join point between intermediate and asymptotic solution
∞	asymptotic, at a distance from

Superscripts

$()^*$	saturation, equilibrium
$()'$	liquid
$()''$	gas
$\dot{()}$	time derivative

Operators

$\bar{\nabla}.$	Nabla operator
$*$	convolution

ABSTRACT

The dynamic problem of the growth or collapse of a single stationary spherical bubble suddenly exposed to a quiescent liquid is analyzed for a binary system by means of intra-phase mass and heat transport subject to thermodynamic phase-equilibrium at the bubble interface. Two cases are studied. For the nonsoluble gas case, in which the liquid constitutes a single component, approximate solutions to bubble growth are obtained by means of the integral technique for the initial and intermediate stages and the theory of sources for the asymptotic stage of the transient. For the soluble gas case, the initial bubble behavior is predicted and a solution is given to bubble collapse in a nonvolatile liquid, in which case the gas phase constitutes a single component. Dimensionless bubble growth is governed by the Jakob number, $Ja = p\cdot(dT/dp)^* \cdot (\rho' c'/\rho'' h_{fg})$, which characterizes the rate of heat transport when phase change occurs, and the Lukomskiy number, $Lu = \mathcal{D}/\alpha'$, which gives the ratio of mass to heat diffusivity. The significant ratio, Ja^2/Lu, is shown to represent a measure for the relative significance of mass to heat transport for the rate of the process.

The growth and collapse of single bubbles is studied experimentally from high-speed film recordings. For the nonsoluble gas case nitrogen and helium bubbles were injected into water, and for the soluble gas case ammonia was used. For stationary nitrogen and helium

bubbles in water the analysis is shown to describe the average bubble growth well over a parameter range corresponding to the temperature range 150-206°F and initial bubble radii of 0.7 - 3.0 mm. The effect on the transient heat and mass transport of the observed bubble oscillations is concluded to be negligible. Translatory bubble motion is shown to cause a significant increase in the growth rate when the rising bubble has been accelerated and a flow transition has occurred. The rate of collapse of ammonia bubbles is shown to become greater when the governing rate-parameters and solubility of the gas increases and the liquid volatility decreases.

CHAPTER I

INTRODUCTION AND LITERATURE SURVEY

A. Introduction

The purpose of the present study is to analyse a particular case of the comprehensive subject of the dynamics of binary gas-liquid systems, namely the dynamics of a single gas bubble suddenly brought into contact with a volatile liquid, where either one or both of the phases may comprise two components.

The process of injecting a soluble or nonsoluble gas into a liquid has several applications. These can be associated either with the resulting mass and/or heat transfer and/or with the resulting mechanical agitation of the liquid. In gas injection-cooling the primary effect is that of heat removal from the liquid facilitated by its evaporation into injected gas bubbles until these become saturated in this component. In principle, this process is similar to stream distillation from the aspect of forced transfer of a more volatile component from the liquid phase to the gas phase, and it has found application in the cooling of cryogenic systems, especially when local and short duration sub-cooling is desired. A lumped analysis of the injection cooling process[35], based on the instantaneous attainment of the equilibrium composition in the gas phase, predicts satisfactorily the transient cooling for the average system. For certain system geometries, however, - and in particular when the gas is soluble in the liquid - this approach is inadequate and analysis of the distributed system becomes necessary. Accordingly

attention need be given the discrete processes, namely the dynamics of the bubbles, when appearing individually or in clusters in the liquid. In the present work the dynamics of the single bubble has been investigated, excluding interference from neighboring bubbles. Although translatory bubble motion will always persist whenever the gas-liquid system is subject to a gravitational field, most attention has been given the case of the stationary bubble in the later justified anticipation that the dynamic process is rapid enough to come practically to an end before appreciable motion has occurred. The effect of translatory motion invariably results in an increase in the rate of the process thus rendering the findings for the stationary bubble conservative.

To identify the present problem among the many types of binary gas-liquid dynamic problems, it is pertinent to examine the physics of the process in light of the following characterizing aspects,

(i) system geometry	dispersed liquid phase (drops, fog) separated phases (plane, nonplane interface) dispersed gas phase (bubbles)
(ii) disturbance	thermodynamic non-equilibrium pressure gradient temperature gradient concentration gradient non-equilibrium shape imposed body force field
(iii) significant process (inter/intra-phase)	mass transport momentum transport heat transport viscous dissipation capillary effects gravity effects

Although the injection cooling process in fact represents the case of a dispersed gas phase, the study of the single bubble implies separated phases. When a stream of gas is introduced into the liquid, it breaks into individual bubbles representing a more stable configuration. Related to the hydrodynamics of this process the formed bubbles may oscillate, interfere with neighboring bubbles, coalesce or further break up into smaller bubbles. The present study considers the single bubble having a spherical interface of separation, representing the thermodynamic equilibrium shape in the absence of a gravity field.

The nature of the disturbance initiating the dynamic process is primarily the thermodynamic state of non-equilibrium at the interface prevailing at the moment the bubble is introduced. This disturbance causes non-equilibrium temperature and composition distributions to be established by means of which the process is analyzed. The presence of a gravity field represents a secondary disturbance to the shape of the stationary bubble, while being a primary initial disturbance for acceleration of translatory bubble motion.

Among the listed significant processes, inter-phase and intra-phase heat and mass transport become important for the bubble size and for the types of gases and liquids under study. The inertia effects become important only in the very initial stage when the dynamic process is accelerated, covering a negligible part of the transient for the stationary bubble. For the case of the moving bubble, however, inertia, viscous, gravity, and surface effects determine the motion.

Next, the present case of bubble dynamics is identified among the many particular cases previously studied as they relate to diverse applica-

tions. The summary given in Table I has been prepared for the frequently encountered process labels and listed are the effects governing the particular bubble dynamic transient. For completeness the effects being important only in the initial stage have been included and marked with I, while the otherwise controlling effects are denoted by X.

TABLE I

SIGNIFICANT EFFECTS FOR VARIOUS BUBBLE DYNAMIC PROCESSES

	Significant effects / Bubble dynamic process label		Liquid phase			Gas phase			
			Mass transport	Momentum transport	Heat transport	Mass transport	Heat transport	Surface effects	Viscous effects
Initial microscopic size. (nucleation phenomenon)	Cavitation	vaporous		X				X	X
		gaseous	I	X				X	X
	Boiling	one-component liquid		I	X			I	
		two-component liquid	X	I	X			I	
		presence of permanent gas nuclei			X	X		I	
Initial macroscopic size	Gas-vapor bubbles (injection cooling)		X		X	X			
	Gas absorption		X			X			
	Gas desorption		X						

The cavitation and boiling processes are characterized by an initial microscopic bubble size, while gas injection cooling, gas adsorption and desorption are characterized by initial visible (macroscopic) bubble sizes. In cavitation and boiling the dynamic growth starts from nuclei, small bubbles of the thermodynamic equilibrium size corresponding to liquid superheat and the state of the interface. The transient is triggered by a sudden disturbance in pressure (cavitation), gaseous diffusion into the nuclei (gaseous cavitation) or a temperature disturbance (boiling). While in all cases the inertia and surface effects play a significant role in the very first stage of the growth, the heat transport in the liquid phase to the bubble interface required for the evaporation associated with the growth may be omitted in the study of "cold" cavitation. For "hot" cavitation, however, which, aside from the externally imposed pressure variations, physically is identical to boiling, heat transport controls growth subsequent to its initiation. The reason for this difference in behavior, alone determined by the temperature level, is found in the difference in slope of the vapor pressure curve $(dT/dp)^*$. Consider a nucleus of a certain size in thermodynamic equilibrium at the uniform bulk liquid temperature, such that the excess vapor pressure is balanced by the surface tension forces. When, started by some disturbance, the bubble has grown a small amount, the change in interface saturation temperature, ΔT, is related to the pressure change by $\Delta T = \Delta p(dT/dp)^*$. For identical nucleation size and subsequent growth, the pressure change is the same but the temperature difference which governs the rate of heat transfer depends on the vapor pressure curve. Low temperature implies

large values of the Ja-number[1]

$$Ja = \Delta T \cdot \frac{\rho' c'}{\rho'' h_{fg}}$$

which, as shown later is the governing parameter for nondimensional bubble growth controlled by heat transport in the liquid alone. Large Ja-number implies very rapid growth if heat transport were the only effect. This in turn implies that growth is governed and limited by inertia effects in such cases, and heat transport becomes insignificant. For moderate or small values of the Ja-number heat transport dictates the growth rate to be slow enough that inertia effects are of no importance.

The presence of dissolved gases in a cavitating or boiling fluid and the case of boiling of binary mixtures may necessitate the consideration of the intra-phase mass transport. As shown later in the analytical treatment, the Lu-number[2]

$$Lu = \frac{\mathfrak{D}}{\alpha}$$

is convenient for measuring the relative significance of mass diffusion to heat diffusion. Mass diffusion is significant in bubble dynamics of

---

1 Jakob number, after the late Max Jakob, referred to by Savic[53]. A dimensionless group appearing when phase change occurs in connection with the molecular diffusion of heat, change in density and release or absorption of heat.

2 Lukomskiy number, a dimensionless group appearing when mass and heat transfer by molecular diffusion occur simultaneously. Introduced in the Russian literature (see e.g. Lykov and Mikhaylov[38]). With the same notation the group is called the Luikov-number by Mikhaylov[39], and is the inverse of the so called Lewis number, criticized by J. H. Arnold in the paper by Klinkenberg[32] as an inappropriate notation, although used later in the American literature.

of boiling mixtures, important for the greater part of the dynamics of gas-vapor bubbles, controls gas absorption and desorption, but is relatively unimportant for the cases of gaseous cavitation and boiling liquids containing permanent gas nuclei.

B. Literature Survey

The dynamic phase-growth in gas-liquid systems has primarily been studied for the application to the processes of underwater detonations, cavitation, boiling, and chemical engineering unit operations involving mass transfer to or from a dispersed gas phase. As might be expected, the growth or collapse of a gas cavity in a liquid has been chronologically explored in steps of increasing complexity. The present survey of the literature is therefore conveniently divided into sections accordingly. Firstly, in isothermal bubble dynamics the sole effect of an initial pressure disturbance is considered. Next, in one-component boiling the effect of heat transport in the liquid is added, and in two-component boiling the effect of mass transport in the liquid is included, while this effect alone controls gas absorption. In the dynamics of gas-vapor bubbles heat transport in the liquid is coupled to mass transport in the gas phase at the moving boundary. Finally, attention is given the problem of interface equilibrium when mass transfer occurs.

1. Isothermal Bubble Dynamics

Bubble dynamic studies were initiated by Besant[4] who formulated the problem of bubble collapse. The solution to this problem was not given until much later by Raleigh[52], after whom the governing equation is named. A summary of the formulation and the solution to the problem of bubble

collapse neglecting the internal pressure and to isentropic bubble expansion neglecting the external pressure is given by Lamb[33]. Later, Plesset[44] modified the Rayleigh equation to account for surface tension effects and Barlow and Langlois[2] included and made specific use of the viscous dissipation in the liquid in the study of the early stage of growth of gas bubbles in a viscous plastic.

2. One-component Boiling

Because bubble growth in boiling is related to the rate of vapor formation at the bubble interface facilitated by heat transfer from the surrounding liquid, the initial phase of growth is a coupled thermal and dynamic problem. Considering surface tension and relating the excess pressure in the bubble to the temperature difference between the interface and the bulk of the liquid by Clapeyron's equation, Plesset and Zwick[46] formulated the coupled problem for a uniformly superheated liquid. It was shown that the evaporation rate did not violate the assumption of interface equilibrium, and an approximate solution was obtained. The intermediate stage of growth in which the inertia terms become less important is difficult to treat. It is, however, like the initial stage of growth of very short duration compared to the asymptotic stage of growth, and is thus generally omitted from consideration. In the asymptotic stage of growth the inertia effects are negligible and bubble growth is governed alone by heat transfer in the liquid as shown by Forster and Zuber[19] who also evaluated the magnitude of the inertia terms. For the asymptotic stage, solutions to bubble growth in a superheated liquid were obtained by Plesset and Zwick[45,46,47] assuming the temperature drop in the liquid is localized

to a thin film next to the interface. Forster and Zuber[17,18,19] obtained nearly identical solutions by the use of source theory and by approximating the fluid and boundary motion by successive differential processes of convection and conduction.

Chambré[8] analyzed, by means of similarity variable, the coupled dynamic problem of fluid flow and heat transfer in a viscous liquid surrounding a growing solid of plane, cylindrical and spherical geometry. Griffith[22] analyzed the growth of hemi-spherical bubbles on a heated surface into a liquid with a linearly decreasing superheat. Bankoff and Mikesell[1] extended the Plesset and Zwick[46] solution to the growth of spherical bubbles in a liquid initially having a linear or exponential temperature distribution. Clark, et al.,[9] formulated a simple quasi-steady model for the collapse of vapor bubbles in a boiling liquid subsequent to sudden pressurization. Collapse by condensation was controlled by heat transfer from the bubble interface into the liquid by conduction. The bubble size was assumed constant and hence convective contribution to the heat transport was ignored.

Bubble growth rates in various superheated liquids have been studied experimentally by Dergarabedian[13] who found consistency with the predictions by Plesset and Zwick[46] for the asymptotic stage of growth and small superheats. Ellion[15] measured radii and radial velocities of bubbles growing on a heated surface.

3. Two-component Boiling

Scriven[55] formulated the asymptotic stage of growth for a single spherical vapor bubble in a superheated binary mixture. Growth was controlled by heat and mass transfer in the liquid phase. By means

of the technique of similarity variables an exact solution to the postulated model was obtained analogous to the solution presented earlier by Birkhoff, et al.[6] and again used by Barlow and Langolis[2] for the similar problem of the diffusion of a gas into an expanding bubble. A significant result of the analysis was that interface temperature and composition remained constant throughout growth. The effect of finite mass diffusivity in reducing the growth rate was shown. For the special case of a one-component boiling liquid the exact similarity solution also apply, and permit comparison with the approximate solutions.

Bubble growth rates in binary mixtures of water and ethylene glycol were experimentally studied by Benjamin and Westwater[3] who found qualitative agreement with the predictions of Scriven[55]. The smaller bubbles due to slower bubble growth in boiling binary mixtures as compared to those in any of the pure components constituting the mixture, have been observed in the study of boiling and burn-out in binary mixtures by van Wijk, Vos, and van Stralen[62,61,57] and by Grigor'ev and Usmanov[23].

4. Gas Absorption

Gas absorption from a bubble rising through a non-volatile liquid was treated by Higbie[26] based on the "penetration theory" assuming that the dissolved component penetrates only a short distance from the interface into the liquid. As the bubble rises, the gas in the bubble undergoes a toroidal motion such that there is essentially no slip between the gas flow and the liquid at the interface, and fresh liquid is encountered at the top of the bubble at all times. Under these assumptions the transfer of gas to the liquid is treated as the transient diffusion into a

falling film, the exposure time taken to be the bubble diameter divided by the bubble rise velocity. Average absorption rates from rising gas bubbles (0.3-0.5 cm diameter) based on this theory has been verified by Hammerton and Garner[25] while Groothuis and Kramers[24] successfully predicted mass transfer rates during drop formation on a capillary tip. The presence of surface active agents caused a considerable decrease in transfer rates[25]. Coppock and Meiklejohn[10] studied bubble formation from horizontal circular orifices and measured mass transfer coefficients for the absorption of oxygen in water fom 0.15-0.3 cm diameter rising bubbles. Datta, Napier and Newitt[12] reported on carbon dioxide absorption in air-saturated water from rising bubbles formed from circular capillary orifices submerged under mercury to minimize absorption during bubble formation. Pattle[41,42] studied experimentally aeration of water by measuring the absorption of oxygen from air injected in various bubble sizes, and formulated the theoretical problem of gas diffusion into the liquid in terms of a coefficient of per cent uptake per unit length travelled by the bubble. The height through which small bubbles will rise through air free water before being fully absorped was measured and the average adsorption coefficient was determined. The efficiency was shown to depend strongly of liquid height over injection location, initial bubble size, and agitation.

Danckwerts[11] made a more general formulation of gas absorption in agitated liquids treating the phenomenon of surface renewal statistically by defining a fractional surface age distribution function. Lightfoot[37] employed the "stagnant liquid film" theory to predict the

effect of the chemical reaction between solvent and solute on the absorption rate. Each gas bubble is assumed surrounded by a thin stagnant liquid film through which the gas diffuses in steady state to the assumed constant bulk concentration outside the film. It is shown that only high reaction rates can change the absorption rate significantly.

5. Gas-vapor Bubbles

Lienhard[36] in a theoretical study of inception of cavitation and flashing of liquids in hydraulic equipment treats the thermodynamic stability in a superheated liquid of vapor bubbles with and without the presence of a permanent gas. He proceeds to give first a comprehensive formulation of the dynamic growth of a gas-vapor bubble containing a constant mass of gas and growing entirely owing to evaporation. Inertia, surface effects, heat transfer and liquid viscous dissipation are included in this formulation. With the attention focused on incipient cavitation the heat transfer is neglected and representative numerical approximate solutions based on the direction field method are presented. The second case treats isothermal growth resulting entirely from mass diffusion of dissolved gas in the liquid into the bubble. Neglecting liquid motion a simplified quasistatic model analogous to that of Reference 9 is postulated and the solution given.

In another recent fundamental study of the cavitation process Plesset[48] compares boiling and cavitation bubbles and gives an account of the thermodynamics of oscillating gas bubbles, including the first order damping effect of heat diffusion in the liquid. Criteria in terms of diffusion lengths, thermal properties and frequency of oscillation are

given for the thermodynamic behavior of an oscillating gas bubble in a liquid. As expected, isothermal behavior describes the bubble well for low frequencies while for higher frequencies the behavior is adiabatic. For very high frequencies, however, the behavior again becomes isothermal. Mention is made of the second order rectified diffusion phenomenon, and the stability of a growing or collapsing spherical gas bubble is analyzed. Bubble growth is stable while bubble collapse is unstable. The instability is unaffected by surface tension and becomes evident when the bubble radius has been reduced by a factor of ten from its initial value. This agrees with experimental observations of the fragmentation of collapsing bubbles. For bubbles with an appreciable amount of permanent gas the decrease in size may be insufficient to cause instability.

The problem of rectified diffusion of mass into a spherical gas bubble in an oscillating pressure field was studied in detail by Hsieh and Plesset[27]. This problem is identical to that of a spherical gas bubble carrying out an undamped harmonic oscillation. The second order effect of a net flow of mass to the gas phase by diffusion from the liquid phase is named rectified diffusion, and it arises from the greater average transfer area available during the expansion half-cycle, when the mass flow is inward, than during the compression cycle, when the mass flow is outward. The Mathieu equation of stability was furthermore investigated, indicating that the second mode of harmonic oscillation is most probable. The analytical expression for the rate of mass transfer was given and sample calculations confirmed the effect to be secondary. Strasberg[58] studied experimentally the pulsation frequency of gas bubbles formed on a

capillary tip and rising through a liquid. The zero-th order pulsation frequency was found in accord with the standard frequency of an oscillating gas bubble as calculated using the acoustic approximation, and this frequency was not significantly affected by the lower frequency oscillations (second and higher order) carried out by the bubble while departing and rising.

Approximate solutions for stationary gas bubble growth or collapse owing to mass diffusion in a nonvolatile liquid respectively oversaturated and undersaturated with the soluble gas were obtained by Epstein and Plesset[17] using a quasistatic model neglecting liquid motion, similarly to the model used by Clark, et al.[9]. The same isothermal problem of bubble growth was solved by Barlow and Langlois[2] for the considerably more general case including the inertia of the viscous liquid, surface tension, and the changing gas concentration. A numerical computer solution was carried out for the complete formulation, while approximate analytical solutions for the initial and asymptotic stages were obtained in closed form.

6. Interface Equilibrium

In the analysis of bubble dynamics in one and two component boiling systems, in the analysis of gas absorption, and in general in mass and heat transfer processes across phase boundaries, it is tacitly assumed that thermodynamic phase equilibrium exists at the interface. Strictly speaking this is incompatible with the observation that a process takes place, since the driving potential in the first approximation is proportional to the departure from equilibrium. However, if the "reaction rate" is small, the departure will be small. This will, in general, be

the case if the rate of the controlling processes - in the above cases heat and mass diffusion - are slow compared to the rate at which thermodynamic equilibirum locally can be restored. The assumption of interface thermodynamic equilibrium has been studied experimentally by Tung and Drickamer[60] and Emmert and Pigford[16] and by Scriven and Pigford[56], who measured the rate of absorption of carbon dioxide into a liquid laminar jet of water flowing at high velocity. Comparison with analytical predictions based on the assumption of interface equilibrium justified the latter. A theoretical study by Schrage[54] based on the kinetic theory seems to support the experimental studies.

CHAPTER II

THEORETICAL ANALYSIS

In this chapter the general problem is stated of the dynamics of a single bubble having no translatory motion. Based on an account of the detailed physics of the problem the corresponding general mathematical formulation is given. Re-evaluating the physics of the process a simplified - mathematically tractable - formulation is deduced. Solutions to this formulation are investigated for two cases. For the nonsoluble gas case, in which the liquid constitutes a single component, approximate solutions to bubble growth are obtained by integral technique for the initial stages and the theory of sources for the asymptotic stage of the transient, and the analytical results are presented in dimensionless form in a parametric study. For the soluble gas case the initial bubble behavior is predicted and a solution is derived for bubble collapse in a nonvolatile liquid.

A. Statement of the Problem

A spherical bubble of radius R_o containing a binary mixture of gas components A and B of uniform composition x_o'' (molefraction of the more volatile component A) and temperature T_o'' is suddenly introduced into a quiescent binary liquid mixture of components A and B of uniform composition x_∞' and temperature T_∞. The initial pressure distribution is assumed uniform throughout each phase. Figure 1(a) shows schematically this initial condition for the system.

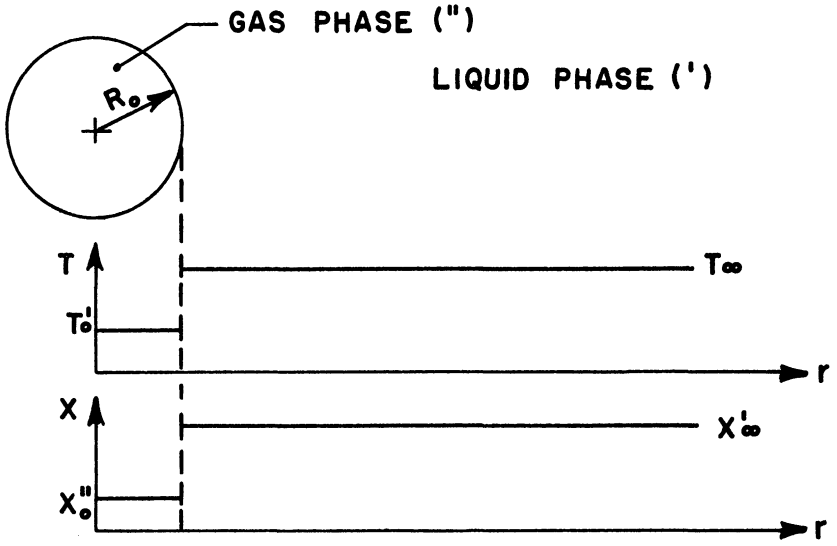

(a) INITIAL CONDITION (t = 0)

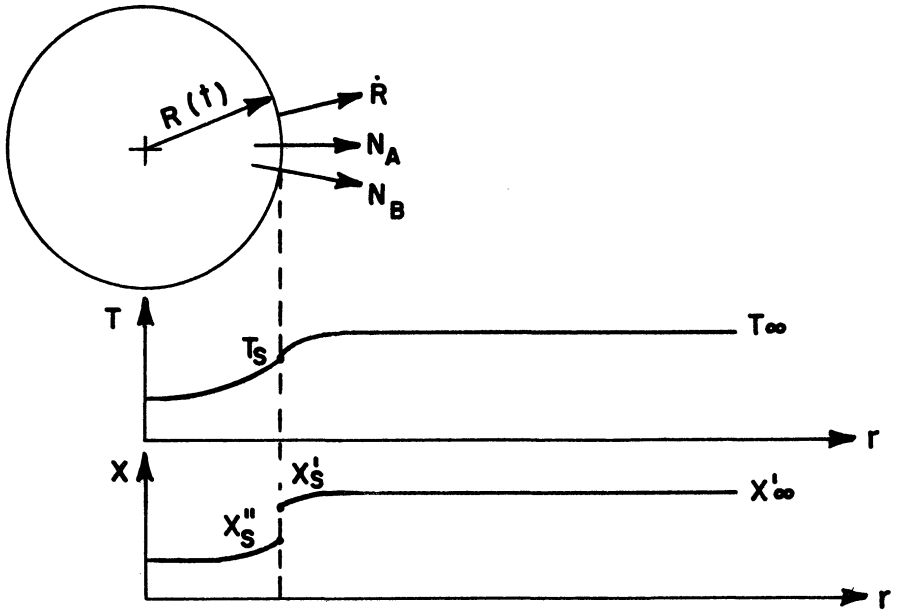

(b) INTERMEDIATE STATE OF TRANSIENT (t>0)

Figure 1. Model for General Formulation of the Bubble Dynamic Problem.

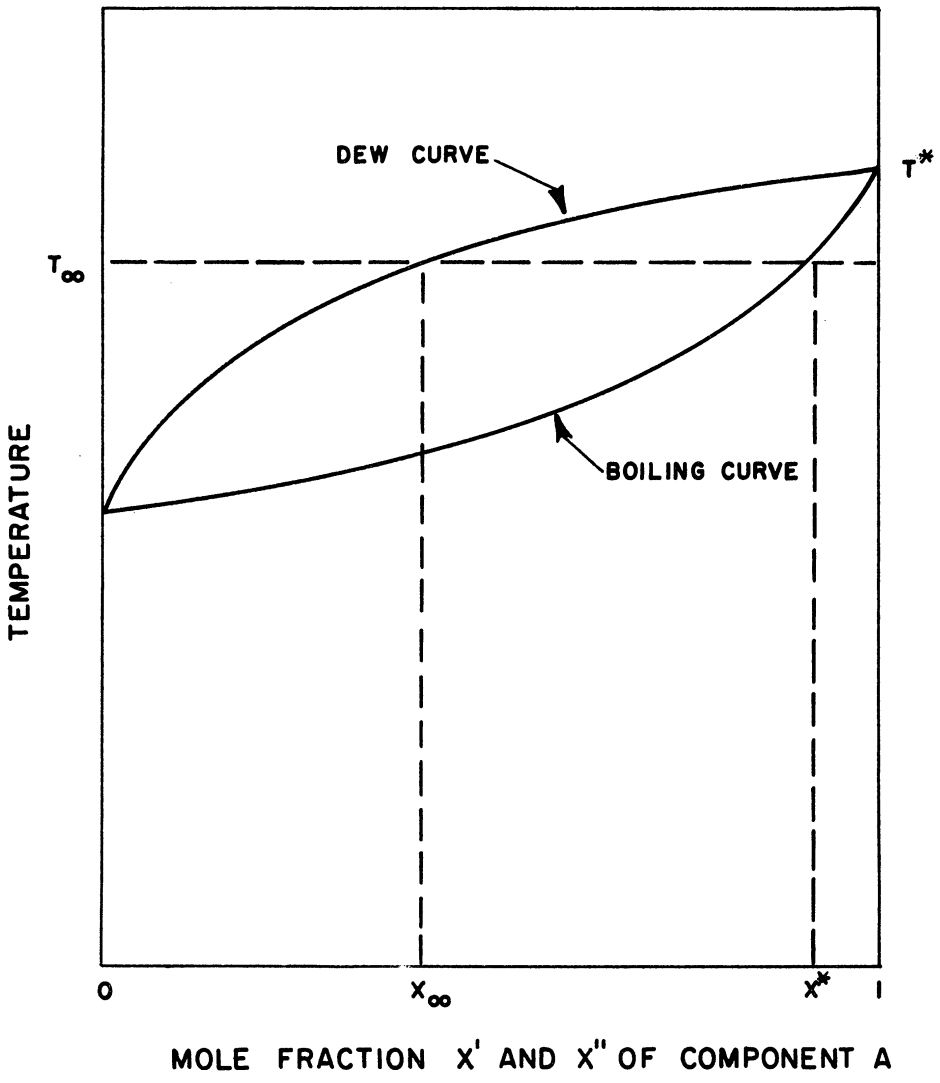

Figure 2. Isobars for Binary Phase-equilibrium (Schematic).

Owing to the initial thermodynamic non-equilibrium gas-liquid compositions and temperatures at the bubble interface, transfer of components A and/or B from one to the other phase will begin. The necessary heat liberated or absorped in this phase change is transferred to or taken from the liquid and gas, thereby changing the interface temperatures. This process procedes rapidly at the beginning of the transient until at the interface a state of thermodynamic phase-equilibrium is established,[1] whereby local values of pressure, temperature and compositions become functionally related. This initial state is considered attained instantaneously since it affects only a few molecular layers in each phase. The intra-phase non-equilibrium distributions in composition and temperature in conjunction with the pressure distribution govern the subsequent bubble growth and/or collapse. The net flow of heat to the interface satisfies at all times the requirements for the instantaneous net phase change of components A and B .

Insight into the asymptotic bubble behavior is gained by considering a typical non-azeotropic, binary phase-equilibrium diagram shown in Figure 2. Noting that the liquid phase is considered unbounded in extent, the approach to thermal equilibrium in the asymptotic stage implies a uniform system temperature identical to the initial liquid temperature, T_∞ . The persistance of two phase therefore requires the liquid to be at the saturation state, x^* . For the general case of complete miscibility

---

[1] The departure from phase equilibrium owing to interface mass and heat transfer is small as discussed in Appedix I, and omitted from the analysis.

of the two components in each phase, a non-zero asymptotic bubble size can only exist when the liquid is initially at the saturation composition x^* . The resulting gas composition is correspondingly x_∞ as shown in Figure 2. For the case of an initially super-saturated liquid, no finite equilibrium size exists. From the physics of the problem it may furthermore be seen that for the case of a soluble gas, the bubble may grow initially or collapse, depending on the initial conditions and the governing parameters for mass and heat transport. Thus, if the liquid component A is very volatile the tendency for this to evaporate may exceed the tendency for the nonvolatile gas component B to go into liquid solution, and a net growth may occur initially.

For the case of a nonsoluble gas the boiling curve of Figure 2 coincides with the line $x = 1$. The liquid may be interpreted to be saturated with respect to the nonsoluble gas component B irrespective of its temperature. Hence, a finite asymptotic bubble size of composition x_∞ is approached in all cases of a subcooled liquid, $T_\infty < T^*$. In the limiting case, the liquid is also saturated with respect to component A, $T_\infty = T^*$, and the corresponding equilibrium composition in the gas phase, $x_\infty = 1$, is approached only by unlimited growth of the bubble.

B. General Formulation

The following general mathematical formulation takes into account the simultaneous processes of mass, energy and momentum transport in both phases, all coupled at the moving bubble interface to satisfy here mass, energy and momentum balances as well as thermodynamic phase-equilibrium. Cross coupling is neglected in intra-phase transport between the transport

of one of these quantities and the driving potential for the others (Dufour and Soret effects and pressure forced mass diffusion), as predicted by the Onsager linear relations[5] of the theory of the thermodynamics of irreversible processes. The liquid is considered inviscid and incompressible and the system geometry is spherically symmetrical. In the notation used, extensive properties are on a partial molal basis. Thermal and transport properties are assumed constant.

1. Gas Phase ($0 \leq r < R$)

Intra-phase mass transport by diffusion and convection is governed by

$$\frac{\partial(\rho'' x'')}{\partial t} + \bar{\nabla}\cdot\left(\rho'' x'' \bar{V}''\right) = \mathcal{D}'' \bar{\nabla}\cdot\left(\rho'' \bar{\nabla} x''\right) \tag{1}$$

subject to the initial and boundary conditions

$$\begin{cases} x''(r,0) = x_0'' \\ \dfrac{\partial x''(0,t)}{\partial r} = 0 \\ x''(R,t) = x_s'' \end{cases}$$

where subscript s refers to the interface condition. Combining Equation (1) with the corresponding equation for component B, noting that $x = x_A = 1 - x_B$, the equation of continuity in terms of the molal density of the gas mixture, ρ'', becomes

$$\frac{\partial \rho''}{\partial t} + \bar{\nabla}\cdot\left(\rho'' \bar{V}''\right) = 0 \tag{2}$$

With the assumption of constant average thermal properties the energy transport is given by

$$\frac{\partial T''}{\partial t} + \bar{V}''\cdot\bar{\nabla}T'' = \alpha''\nabla^2 T'' + \frac{1}{\rho''c''}\frac{Dp''}{Dt} \tag{3}$$

subject to

$$\begin{cases} T''(r,0) = T_o'' \\ \dfrac{\partial T''(0,t)}{\partial r} = 0 \\ T''(R,t) = T_s \end{cases}$$

Momentum transport is given by

$$\rho''\left[\frac{\partial \bar{V}''}{\partial t} + (\bar{V}''\cdot\bar{\nabla})\bar{V}''\right] = -\bar{\nabla}\cdot p'' \tag{4}$$

subject to the initial conditions

$$\begin{cases} p''(r,0) = p_\infty \\ \bar{V}''(r,0) = 0 \end{cases}$$

In addition, an equation of state relates the density of the mixture to pressure and temperature locally

$$p''(r,t) = f(\rho'', T'') \tag{5}$$

2. Liquid Phase ($R < r < \infty$)

The corresponding formulation for the liquid phase, noting its incompressibility, becomes, for mass transport

$$\frac{\partial x'}{\partial t} + \bar{V}'\cdot\bar{\nabla}x' = \mathcal{D}\,\nabla^2 x' \tag{6}$$

$$\begin{cases} x'(r,0) = x'_\infty \\ x'(\infty,t) = x'_\infty \\ x'(R,t) = x'_s \end{cases}$$

continuity

$$\bar{\nabla}\cdot\bar{V}' = 0 \tag{7}$$

and heat transport

$$\frac{\partial T'}{\partial t} + \bar{V}'\cdot\bar{\nabla}T' = \alpha'\,\nabla^2 T' \tag{8}$$

$$\begin{cases} T'(r,0) = T_\infty \\ T'(\infty,t) = T_\infty \\ T'(R,t) = T_s \end{cases}$$

In light of the incompressible, irrotational flow, the momentum transport may be written

$$\frac{\partial \bar{V}'}{\partial t} + \bar{\nabla}\left(\frac{p'}{\rho'} + \frac{V'^2}{2}\right) = 0 \tag{9}$$

subject to the initial conditions

$$\begin{cases} p'(r,0) = p_\infty \\ \bar{V}'(r,0) = 0 \end{cases}$$

The formulation is completed with the statement of the conditions at the moving bubble interface, separating the two domains and initially subject to

$$\begin{cases} R(0) = R_o \\ \dot{R}(0) = 0 \end{cases} \tag{10}$$

where $\dot{R}$ denotes the interface velocity.

3. Interface Conditions (r = R)

In terms of mole fluxes N_A and N_B of respectively component A and B transferred from the gas phase to the liquid phase the interface mass balances, considering each phase separately, become

$$N_A = (V_s'' - \dot{R})\,\rho'' x_s'' - \mathcal{D}''\rho_s''\left.\frac{\partial x''}{\partial r}\right|_s \tag{11}$$

$$N_A = (V_s' - \dot{R})\,\rho' x_s' - \mathcal{D}'\rho_s'\left.\frac{\partial x'}{\partial r}\right|_s \tag{12}$$

Combining Equation (11) with the similar form for component B , the net mole flux results

$$N_A + N_B = (V_s'' - \dot{R})\,\rho_s'' = (V_s' - \dot{R})\,\rho_s' \tag{13}$$

With the contributions from enthalpy flux and molecular diffusion the interface heat balance becomes

$$N_A h_A'' + N_B h_B'' - k''\left.\frac{\partial T''}{\partial r}\right|_s = N_A h_A' + N_B h_B' - k'\left.\frac{\partial T'}{\partial r}\right|_s \tag{14}$$

Including the momentum flux associated with the interface mass transfer and accounting for the surface curvature by considering surface tension, the momentum balance becomes

$$p_s'' - p_s' = (V_s' - V_s'')(N_A + N_B) + \frac{2\sigma}{R} \tag{15}$$

Finally, thermodynamic phase-equilibrium provides two relations (dew curve and boiling curve) for temperature and compositions

$$x_s'' = f(T_s, p_s'') \tag{16}$$

$$x_s' = f(T_s, p_s') \tag{17}$$

C. Simplifications of the General Formulation

The following additional assumptions, discussed in detail below, are made to bring the general formulation into a mathematically tractable, yet physically meaningful, form.

(i) Inertia effects in both phases are neglected

(ii) Surface tension effects are negligible

(iii) The gas phase is adiabatic

(iv) The binary mixtures in both phases are ideal

(v) The assumed constant thermal and transport properties are evaluated at the state of the bulk liquid, p_∞ and T_∞

(vi) The thermodynamic phase-equilibrium relationship prevailing at the interface can adequately be approximated linearly.

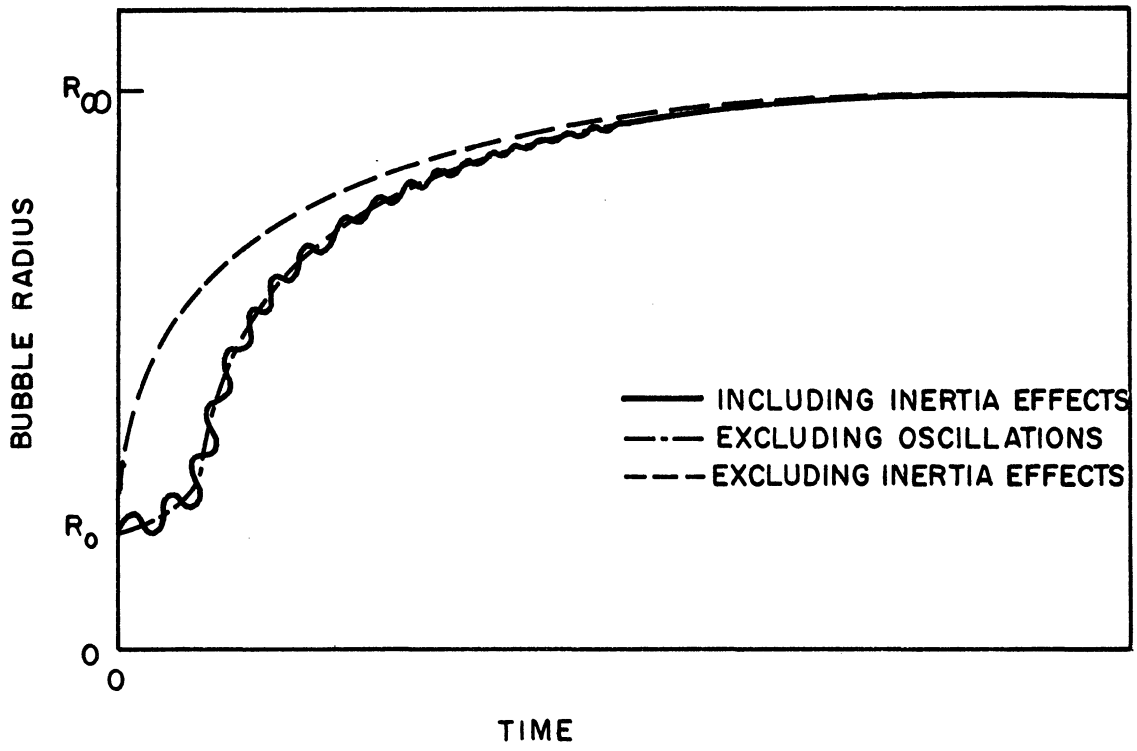

Figure 3. The Influence of Inertia Effects on Bubble Growth (Schematic).

(i) Inertia effects, primarily in the liquid phase, become important in two aspects of the bubble dynamic process as shown in schematic in Figure 3. Firstly, the initial rate of volumetric expansion of the bubble owing to mass transfer becomes finite insteady of infinite as predicted by models based on mass and heat transport alone, following the initial step-change in potential distributions. The initial acceleration of the fluids, however, takes place in a very short time (fractions of milliseconds) and may rightfully be omitted in the present case where the controlling factors for bubble growth are mass and heat diffusion.

Secondly, inertia effects become important when comparing the idealized analytical model of an initially static spherical bubble shape to the actual case of the sudden introduction of the gas phase into the liquid. Owing to the initial non-equilibrium shape in the latter case, bubble oscillations invariably will occur. The sudden introduction of the gas phase from a circular capillary may thus be visualized to give rise to a predominant mode of oblate-oblong oscillation, persisting until damped out by viscous dissipation and thermal effects. Because bubble oscillations are experimentally observable, yet neglected in the analysis, an account of this behavior is given in the following for the case of undamped oscillations governed by inertia and surface effects.

Assuming axis-symmetry the shape of the bubble surface may be expressed as a sum of spherical zonal harmonics, Y_n , superimposed the equilibrium shape which in the absence of gravity effects is a sphere of radius R

$$r(\psi,t) = R + \sum_{n=0}^{\infty} a_n(t)\, Y_n(\psi)\, e^{i\omega_n t} \qquad (18)$$

where Ψ is the polar angle and ω_n the cyclic frequency of the n-th harmonic. Based on a stability analysis Hsieh and Plesset[27] showed that the second zonal harmonic is the most unstable mode of oscillation, hence, the dominating. Because the second zonal harmonic is identical to the Legendre polynomial of first kind and second order, the first approximation for the bubble shape for the case of an undamped harmonic oscillation with cyclic frequency ω and polar amplitude a may be written

$$r(\psi,t) = R\left[1 + \left(\frac{a}{R}\right)\frac{3\cos^2\psi - 1}{2}\sin\omega t\right] \tag{19}$$

The frequency, $f = \omega/2\pi$, of this mode of oscillation may be obtained from hydrodynamic considerations, showed by Lamb[33], as

$$f = \frac{1}{\pi}\sqrt{\frac{3\sigma}{\rho' R^3}} \tag{20}$$

and the polar amplitude, a, is given from the initial conditions particular to the injection process.

A dominating mode of oblate-oblong oscillation having a frequency consistent with Equation (20) has been experimentally evidenced. The similarity of this mode to that given by Equation (19) has furthermore been substantiated by comparing from experiment the magnitude of the relative polar amplitude a/R to the magnitude of the amplitude of the relative equivalent radius R_{eq}/R, where R_{eq} is the radius of the sphere having the same volume as the deformed bubble. The analytical relationship, obtained from Equation (19) as shown in Appendix II, is

$$\frac{R_{eq}}{R} = \left[1 - \frac{3}{5}\left(\frac{a}{R}\right)\sin\omega t + \frac{3}{7}\left(\frac{a}{R}\right)^2 \sin^2\omega t - \frac{1}{35}\left(\frac{a}{R}\right)^3 \sin^3\omega t \right]^{1/3} \qquad (21)$$

As discussed in Chapter III under the evaluation of the experimental results the magnitude of the relative polar amplitude a/R varies between experiments in a random manner since it is determined by the initial displacement during formation. Typical values range from 0.01-0.10 in the first part of the transient damped out to 0.001-0.05 in the later and asymptotic stage.

For the mode of oscillations of zero-th order (spherical oscillater) the analytical study by Hsieh and Plesset[27] of rectified mass diffusion indicates that amplitudes comparable to those in the present study have a negligible perturbing effect on the mean bubble size over short periods of time. Thus, even for an initial bubble size of 1 mm and a relative pressure amplitude of 0.25 the time for doubling of the bubble radius exceeds 10^6 sec. In light of these results and owing the experimentally observed small amplitudes of oscillations in most cases, only the zero-th approximation, $r = R$, to the bubble shape will be considered in the present study. Whenever the oscillations in shape play a small role for the heat and mass transfer processes the solutions thus produced represent the time history of the equivalent mean bubble radius.

(ii) Surface tension effects are disregarded in the present study because only visible (macroscopic) bubble sizes are considered.

(iii) For relatively slow transients as well as for low frequency oscillations, as pointed out by Plesset[48], the thermodynamic behavior of the bubble is isothermal. In view of the comparatively small change in inter-

face temperature experienced during the transient and because of the low heat capacity of the gas phase, it is appropriate to neglect heat transfer to or from the gas hence to consider it adiabatic. This assumption implies that only cases for which the initial gas temperature is near the liquid bulk temperature are considered.

(iv) Ideality of the binary system implies that the heat and volume change of mixing are zero and that properties for the mixture can be obtained from those of the pure substances. When experimental phase-equilibrium relations are not available, these can thus be expressed analytically in terms of system pressure, p_∞ , and respective vapor pressures, p^* , for the pure components A and B (see e.g. Dodge[14] Eqs. (XII.3) and (XII.4)).

$$x''(T, p_\infty) = \frac{1/p_\infty - 1/p_B^*(T)}{1/p_A^*(T) - 1/p_B^*(T)} \tag{22}$$

$$x'(T, p_\infty) = \frac{p_\infty - p_B^*(T)}{p_A^*(T) - p_B^*(T)} \tag{23}$$

Ideality in the liquid phase is generally expected when the components have similar chemical structure and in particular for dilute solutions. A requirement for considering the gas phase ideal is low pressure and high temperature of the system, and particularly that its state is far removed from the critical state of either component.

(v) The evaluation of thermal properties at the bulk liquid temperature primarily introduces an error in the heat of phase transition. This error is small, however, during most of the transient because of the small temperature difference between the bubble interface and the bulk liquid.

(vi) Linear approximations to the dew curve and boiling curve of the phase-equilibrium relations are adequate for interface temperatures in the neighborhood of the liquid bulk temperature.

With the above assumption the bubble dynamics is considered governed by mass diffusion in the gas phase and mass and heat diffusion and radial convection in the liquid phase. The general formulation is accordingly simplified as follows.

1. Gas Phase ($0 \leq r < R$)

With a constant molal density ρ'' of the gas mixture, the equation of continuity, Equation (2), infers that the gas phase is stagnant and assumptions (i) and (ii) then implies that the pressure is uniformly p_∞ throughout the two phases. In terms of the potential difference, $x''-x''_o$, intra-phase mass transport from Equation (1) becomes

$$\frac{\partial (x''-x''_o)}{\partial t} = \mathcal{D}'' \frac{1}{r^2} \frac{\partial}{\partial r}\left[r^2 \frac{\partial (x''-x''_o)}{\partial r} \right] \tag{24}$$

subject to

$$\begin{cases} x''(r,0) - x''_o = 0 \\ \dfrac{\partial x''(0,t)}{\partial r} = 0 \\ x''(R,t) - x''_o = x''_s - x''_o \end{cases}$$

2. Liquid Phase ($R < r < \infty$)

In terms of the composition difference, $x'_\infty - x'$, Equation (6) for spherical symmetry becomes

$$\frac{\partial (x'_\infty - x')}{\partial t} + v_r' \frac{\partial (x'_\infty - x')}{\partial r} = \mathcal{D}' \frac{1}{r^2} \frac{\partial}{\partial r} \left[r^2 \frac{\partial (x'_\infty - x')}{\partial r} \right] \tag{25}$$

subject to

$$\begin{cases} x'_\infty - x'(r,0) = 0 \\ x'_\infty - x'(\infty,t) = 0 \\ x'_\infty - x'(R,t) = x'_\infty - x'_s \end{cases}$$

where $v_r'(r,t)$ is the radial liquid velocity, satisfying the continuity equation, Equation (7), now written

$$\frac{1}{r^2} \frac{\partial}{\partial r} \left(r^2 v_r' \right) = 0 \tag{26}$$

Omitting the notation ('), the heat transport from Equation (8) may be written

$$\frac{\partial (T_\infty - T)}{\partial t} + v_r' \frac{\partial (T_\infty - T)}{\partial r} = \alpha' \frac{1}{r^2} \frac{\partial}{\partial r} \left[r^2 \frac{\partial (T_\infty - T)}{\partial r} \right] \tag{27}$$

subject to

$$\begin{cases} T_\infty - T(r,0) = 0 \\ T_\infty - T(\infty,t) = 0 \\ T_\infty - T(R,t) = T_\infty - T_s \end{cases}$$

3. Interface Conditions (r=R)

Noting that the gas phase is stagnant, Equations (11), (12), and (13) for the interface mass balance simplify to

$$N_A = -\dot{R}\rho'' x_s'' - \mathcal{D}''\rho'' \frac{\partial x''(R,t)}{\partial r} \tag{28}$$

$$N_A = \left[v'(R,t) - \dot{R}\right]\rho' x_s' - \mathcal{D}'\rho' \frac{\partial x'(R,t)}{\partial r} \tag{29}$$

$$N_A + N_B = -\dot{R}\rho'' = \left[v_r'(R,t) - \dot{R}\right]\rho' \tag{30}$$

The energy balance of Equation (14) with assumptions (iii) and (iv) may now be written

$$N_A h_{fgA} + N_B h_{fgB} = -k' \frac{\partial T(R,t)}{\partial r} \tag{31}$$

where h_{fg} indicates the heat of evaporation of the pure component, identical to the change in partial molal enthalphy when going from liquid to gas solution because the heat of mixing is zero. The phase-equilibrium relations of Equations (16) and (17) simplify to

$$x_s'' = f(T_s, p_\infty) \tag{32}$$

$$x_s' = f(T_s, p_\infty) \tag{33}$$

where the functional relationship is linear and p_∞ is constant.

D. The Case of a Nonsoluble Gas

The case in which the gas component B is nonsoluble or has a negligible solubility in the volatile liquid component A , represents the particular case of most interest for the application to injection cooling. The bubble dynamics is then governed by mass diffusion in the gas phase and heat transport in the liquid phase. For simplicity the notation (') and (") for respectively the gas and liquid phases is left out where not needed for clarity.

1. Solutions

Although the physics of the problem has been simplified considerably in the formulation given above, an exact solution to this is not readily obtained. The mathematical difficulties may be seen to arise from the following characteristics of the problem. The transient is sought for the two spherical domains, $0 \leq r \leq R$ and $r \geq R$ of which one is semi-infinite, the other finite. The two domains are coupled at the moving interface, $r=R(t)$, where the time-wise change of the potentials for transfer is in turn coupled to the interface motion.

It is worth noting that similarity solutions exist for the chosen model either for the case of one dimensional plane geometry[34] (i.e., two semi-infinite domains as shown in part E. 1. of this chapter), or for spherical geometry for the case of initial zero bubble size[55]. In the present case, however, similarity solutions can be shown not to exist, primarily because of the finite, initially non-zero, domain of the bubble interior, but also because of the arbitrary phase-equilibrium relations imposed at the bubble interface, even when these relations are assumed to be linear.

For large values of time an asymptotic solution is obtained using source theory under the quasisteady approximation of uniform gas composition. The solutions for small and intermediate values of time, however, are obtained by the use of the mass and energy integrals of the governing differential equations employing one-parameter parabolic distributions of mass concentration and temperature in respectively the gas and liquid phases.

In applying the integral technique to a problem, suitable profiles for the dependent variables are assumed, satisfying the initial and boundary conditions, while the governing differential equations subsequently are satisfied only in their integrated forms, that is on an average over the interval in question. First introduced by Pohlhausen[49] this method has found extensive use in the solution of boundary layer problems of the viscous fluid flow. The similarity between the boundary layer concept of these problems and the concept of thermal boundary layer growth in transient heat conduction problems have lead to an increasing use of the Pohlhausen technique. Thus, Yang[63] employed the integral technique to a heat conduction problem taking into account the effect of variable thermal properties, and Goodman[21] and Poots[50,51] applied it to problems of solidification. It should be mentioned that one of the main advantages of the approximate integral technique lies in its ability to handle analytically difficult geometries. Inherent nonlinearities of a problem, however, are not eliviated by the method. The usefulness of applying the integral technique to a problem of spherical phase-growth is illustrated in Appendix III for the case of bubble growth in one-component boiling having an exact solution.

The profile for mass concentration and temperature distributions are chosen in accordance with the physics of the problem. Referring to

Figure 4(a), the shown initial conditions suggest the transient growth of a concentration and thermal boundary layer from the interface into respectively the gas and liquid phases during the first part of the transient. For the first time domain, $0 \leq t \leq t_1$, terminated when the composition boundary layer has penetrated to the bubble center, the profiles are therefore suitably expressed in terms of the time dependent penetration depths, $f_T(t)$ and $f_x(t)$, as shown in Figure 4(b). The parabolic one-parameter forms are

$$\frac{T_\infty - T}{T_\infty - T_s} = (1 - y/f_T)^2 \tag{34}$$

$$\frac{x - x_o}{x_s - x_o} = (1 + y/f_x)^2 \tag{35a}$$

satisfying the following set of boundary conditions

$$\begin{cases} T_\infty - T(0,t) = T_\infty - T_s \\ T_\infty - T(f_T,t) = 0 \\ \dfrac{\partial T(f_T,t)}{\partial y} = 0 \end{cases} \qquad \begin{cases} x(0,t) - x_o = x_s - x_o \\ x(-f_x,t) - x_o = 0 \\ \dfrac{\partial x(-f_x,t)}{\partial y} = 0 \end{cases}$$

where $y=r-R$ is the independent space variable with respect to the interface. In the second time domain, $t > t_1$, the gas composition at the bubble center, x_c, becomes affected by the mass diffusion process as the transient proceeds and the uniform equilibrium composition, x_∞, is asymptotically approached throughout the gas phase. With $x_c(t)$ as a suitable

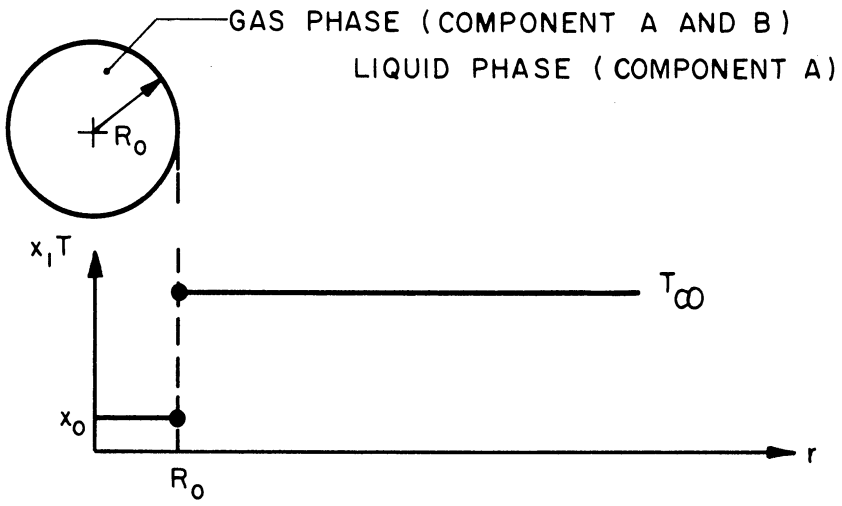

(a) INITIAL CONDITION ($t = 0$)

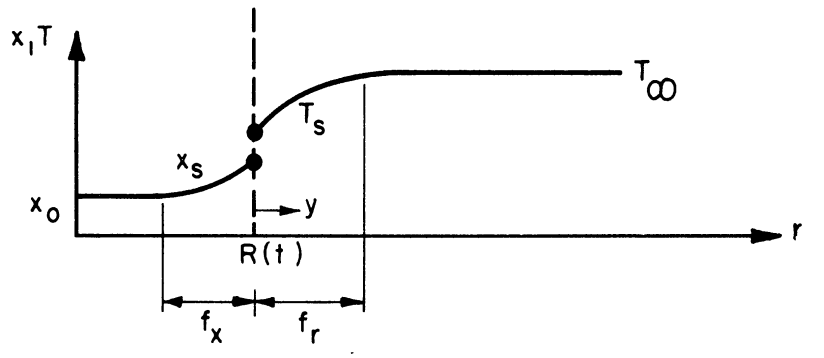

(b) SMALL VALUES OF TIME ($0 < t \leq t_1$)

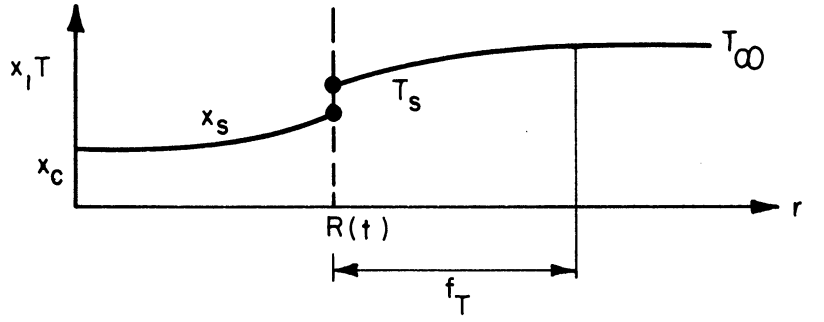

(c) INTERMEDIATE VALUES OF TIME ($t \geq t_1$)

Figure 4. Composition and Temperature Profiles. Nonsoluble Gas Case.

parameter function for this time domain, the parabolic profile for composition is written

$$x = x_c + (x_s - x_c)\,(1 + y/R)^2 \tag{35b}$$

satisfying the following set of boundary conditions

$$\begin{cases} x(0,t) = x_s \\ x(-R,t) = x_c \\ \dfrac{\partial x(-R,t)}{\partial y} = 0 \end{cases}$$

and coinciding with Equation (35a) for $t = t_1$, when $x_c = x_o$ and $f_x = R$. Noting that the need for two different profiles for the composition in the gas phase was prompted by the finiteness of this domain, it follows that the temperature profile of Equation (34) may be continued unaltered in the second time domain.

Before proceeding to obtain solutions for small and intermediate values of time, the differential formulation is further reduced. Thus, integration of Equation (26) using the liquid velocity at the bubble interface, v'_R, as reference gives

$$v'_r = v'_R \left(\frac{R}{r}\right)^2 \tag{36}$$

Combining Equations (36) and (30) a relation is obtained between the liquid velocity at R and the interface velocity

$$v'_R = \left(1 - \frac{\rho''}{\rho'}\right) \dot{R} = \varepsilon \dot{R} \tag{37}$$

where ϵ is referred to as the density deficiency. The liquid velocity distribution then becomes

$$v_r' = \epsilon \dot{R} \left(\frac{R}{r}\right)^2 \tag{38}$$

With the use of Equations (30) and (38) the interface mass balance for the gas phase, Equation (28), may be reduced to

$$\dot{R} = \frac{\mathcal{D}''}{1-x_s} \frac{\partial x(R,t)}{\partial r} \tag{39}$$

and the interface heat balance, Equation (31) becomes

$$\dot{R} = \alpha' \frac{\rho' c'}{\rho'' h_{fg}} \frac{\partial T(R,t)}{\partial r} \tag{40}$$

where now h_{fg} represents the heat of evaporation for component A. Because component B is nonsoluble in the liquid phase, the interface equilibrium relation, Equation (22) reduces to

$$x_s = \frac{p^*(T_s)}{p_\infty} \tag{41}$$

In summary the differential formulation is now given by Equations (24), (27), (38), (39), (40), and (41) subject to the initial condition $R(0) = R_o$.

Referring to the discussion of the asymptotic bubble behavior under the statement of the problem (Section IIA) the finite asymptotic bubble size, R_∞, may be related quantitatively to the initial bubble size, R_o, the initial gas composition, x_o, and the final equilibrium composition, $x_\infty(T_\infty)$, by continuity consideration. The result is

$$\left(\frac{R_\infty}{R_o}\right)^3 = \frac{1-x_o}{1-x_\infty} \tag{42}$$

a. Solution for Small Values of Time

Substituting the radial liquid velocity from Equation (38) into the energy equation, Equation (27), subsequent integration over the thermal boundary layer, $R \leq r \leq R+f_T$, and using Leibnitz' rule[29] for the differentiation of integrals with variable limits, gives

$$\frac{d}{dt}\left\{\int_R^{R+f_T}(T_\infty-T)r^2dr\right\} - (T_\infty-T)r^2\frac{d}{dt}\Big|_R^{R+f_T} + \varepsilon\dot{R}R^2(T_\infty-T)\Big|_R^{R+f_T} - \alpha' r^2\frac{\partial(T_\infty-T)}{\partial r}\Big|_R^{R+f_T} = 0 \tag{43}$$

Similarly the integral over the mass concentration boundary layer, $R-f_x \leq r \leq R$, applied to Equation (24) yields

$$\frac{d}{dt}\left\{\int_{R-f_x}^{R}(x-x_o)r^2dr\right\} - (x-x_o)r^2\frac{d}{dt}\Big|_{R-f_x}^{R} - \mathcal{D}''r^2\frac{\partial(x-x_o)}{\partial r}\Big|_{R-f_x}^{R} = 0 \tag{44}$$

Introducing the profiles of Equations (34) and (35a) into Equations (43) and (44), noting that $r = R+y$, and performing the spatial integration, gives with the use of Equations (39) and (40)

$$\frac{d}{dt}\left\{f_T^3(T_\infty-T_s)\left[\left(\frac{R}{f_T}\right)^2+\frac{1}{2}\left(\frac{R}{f_T}\right)+\frac{1}{10}\right]\right\} = \left[\frac{\rho''h_{fg}}{\rho'c'} - (1-\varepsilon)(T_\infty-T_s)\right]\frac{d(R^3)}{dt} \tag{45}$$

$$\frac{d}{dt}\left\{f_x^3(T_\infty-T_s)\left[\left(\frac{R}{f_x}\right)^2-\frac{1}{2}\left(\frac{R}{f_x}\right)+\frac{1}{10}\right]\right\} = (1-x_o)\frac{d(R^3)}{dt} \tag{46}$$

Introducing the profiles Equations (34) and (35a) into the interface heat and mass balance, Equations (40) and (39), these reduce to

$$R\dot{R} = 2\alpha' \frac{\rho' c'}{\rho'' h_{fg}} (T_\infty - T_s) \left(\frac{R}{f_T}\right) \tag{47}$$

$$R\dot{R} = 2\mathcal{D}'' \frac{x_s - x_o}{1 - x_s} \left(\frac{R}{f_x}\right) \tag{48}$$

Dimensionless quantities may now be introduced to facilitate a clear evaluation of the governing parameters. The use of a linear approximation to the equilibrium relation, Equation (41), suggests that the expression $(\partial T/\partial x)_{T_\infty, p_\infty}$ be applied as a convenient and meaningful reference temperature. Introducing Equation (41) into this expression, it becomes

$$\left(\frac{\partial T}{\partial x}\right)_{T_\infty, p_\infty} = p_\infty \left(\frac{dT}{dp}\right)^*_{T_\infty} \tag{49}$$

The initial bubble radius, R_o, being a natural reference length, the dimensionless quantities may then be summarized as

$$\left.\begin{aligned} \tau &= \frac{\alpha' t}{R_o^2} \\ P &= \frac{R}{R_o} \\ \theta &= 1 - \frac{T_\infty - T}{p_\infty (dT/dp)^*_{T_\infty}} \\ Ja &= p_\infty \left(\frac{dT}{dp}\right)^*_{T_\infty} \frac{\rho' c'}{\rho'' h_{fg}} \\ Lu &= \frac{\mathcal{D}''}{\alpha'} \end{aligned}\right\} \tag{50}$$

where Ja is the Jakob number and Lu the Lukomskiy number.[1] The linear form of Equation (41) then becomes

$$x_s = \theta_s - (1 - x_\infty) \tag{51}$$

representing the closest approximation to the dew curve in the neighborhood of T_∞ (i.e., $\Theta=1$), the value approached by T_s as $t \to \infty$.

Introducing the dimensional quantities of Equation (50) the fomulation for this time domain of dimensionless bubble growth, $P = P(\tau)$, in terms of four governing parameters, Ja, Lu, x_∞ and x_o, may be summarized to

$$\frac{d}{d\tau}\left\{ Ja\,(1-\theta_s)\,P^3\left(\frac{R}{f_T}\right)^{-3}\left[\left(\frac{R}{f_T}\right)^2 + \frac{1}{2}\left(\frac{R}{f_T}\right) + \frac{1}{10}\right]\right\} = \left[1-(1-\varepsilon)Ja\,(1-\theta_s)\right]\left(P^3\right)^{\cdot} \tag{52a}$$

$$\frac{d}{d\tau}\left\{ (x_s-x_o)\,P^3\left(\frac{R}{f_x}\right)^{-3}\left[\left(\frac{R}{f_x}\right)^2 - \frac{1}{2}\left(\frac{R}{f_x}\right) + \frac{1}{10}\right]\right\} = (1-x_o)\left(P^3\right)^{\cdot} \tag{52b}$$

$$P\dot{P} = 2\,Ja\,(1-\theta_s)\left(\frac{R}{f_T}\right) \tag{52c}$$

$$P\dot{P} = 2\,Lu\,\frac{x_s-x_o}{1-x_s}\left(\frac{R}{f_x}\right) \tag{52d}$$

$$x_s = \theta_s - (1-x_\infty) \tag{52e}$$

---

[1] See footnote on page 6.

subject to $P(0) = 1$, $f_T(0)$ and $f_x(0) = 0$.

A solution to this nonlinear formulation may be obtained for small values of time when

$$\left(\frac{R}{f_T}\right) \gg \frac{1}{2} \qquad \text{and} \qquad \left(\frac{R}{f_x}\right) \gg \frac{1}{2} \tag{53}$$

that is, when the terms $1/2(R/f)$ and $1/10$ in Equations (52a) and (52b) can be neglected compared to the term $(R/f)^2$. Physically this corresponds to omitting only the curvature effect in the terms for the time-rate of change in mass and energy over the respective boundary layers, hence the conditions of Equation (53) may be undue stringent. It may be added that in most cases the transport properties for respectively mass and heat diffusion are such that $f_x > f_T$. Hence, in view of the definition of the time domain under consideration the criterion for validity of the subsequent solution may be simplified to

$$\left(\frac{R}{f_x}\right) > 1 \tag{54}$$

With this limitation the solution leads to constant interface potentials, x_{so} and Θ_{so}, and integration is readily carried out leading to a cubic equation in bubble size P. The explicit solution of this, satisfying the conditions $f_x > 0$ for $t > 0$, may be written

$$P(\tau) = 2\sqrt{1 + \tfrac{4}{3}A_o\tau}\cdot\cos\left\{\frac{\pi}{3} - \frac{1}{3}\,\mathrm{Arccos}\left(1 + \tfrac{4}{3}A_o\tau\right)^{-\frac{3}{2}}\right\} \tag{55}$$

where the constant A_o is given by

$$A_o = \frac{Ja^2 (1-\theta_{so})^2}{1 - (1-\varepsilon) Ja (1-\theta_{so})} = Lu \frac{(x_{so} - x_o)^2}{(1-x_{so})(1-x_o)} \tag{56}$$

Equation (56) is also the implicit equation for determing the initial interface condition (x_{so}, θ_{so}) subject to Equation (52e). The criterion for validity, Equation (54), may now be written explicitely in terms of this solution as

$$P^3 - 1 < \frac{x_{so} - x_o}{1 - x_{so}} \tag{57}$$

b. Join Point $(\tau = \tau_1)$

To continue the solution from the first time domain, $0 \leq \tau \leq \tau_1$, into the second domain, $\tau \geq \tau_1$, the join point $R_1 = P(\tau_1)$ must be established. When at $\tau = \tau_1$ the concentration distribution has penetrated to the bubble center, $R/f_x = 1$ and the state of the transient is evaluated by simultaneous solution of the five equations of Equation (52). Because in most cases not close to the critical state

$$(1-\varepsilon)\ Ja\ (1-\theta_s) \ll 1 \tag{58}$$

particularly owing to the smallness of the density ration, $1 - \epsilon$, this term is omitted, and Equations (52a) and (52b) can be integrated. Rearranging the result, the five governing equations can be summarized to

$$Ja\ (1-\theta_{s1})\ P_1^3 \left(\frac{R}{f_T}\right)^{-3} \left[\left(\frac{R}{f_T}\right)^2 + \frac{1}{2}\left(\frac{R}{f_T}\right) + \frac{1}{10}\right] = P_1^3 - 1 \qquad (59a)$$

$$P_1^3 = \left(1 - \frac{3}{5}\,\frac{x_{s1} - x_o}{1 - x_o}\right)^{-1} \qquad (59b)$$

$$P_1 \dot{P}_1 = 2\ Ja\ (1-\theta_{s1})\left(\frac{R}{f_T}\right)_1 \qquad (59c)$$

$$P_1 \dot{P}_1 = 2\ Lu\ \frac{x_{s1} - x_o}{1 - x_{s1}} \qquad (59d)$$

$$x_{s1} = \theta_{s1} - (1 - x_\infty) \qquad (59e)$$

While Equations (59) readily give P_1, $\dot{P}_1$, (R/f_T), θ_{s1} and x_{s1} the exact value of time τ_1 can only be obtained from exact integration of Equations (52). An approximate value may, however, be obtained from the solution for small values of time, Equation (55), by extrapolating its validity range to $f_x = R$. The result is

$$\tau_1 \cong \frac{1}{4A_o}\left(\frac{P_1^3 + 2}{P_1} - 3\right) \qquad (60)$$

c. Solution for Intermediate Values of Time ($\tau > \tau_1$)

In this time domain the temperature profile of Equation (34) is unchanged implying that the form of the energy integral remains that given by Equation (52a). Introducing, however, Equation (35b) for the concentration profile, the integral of Equation (44) over all of the gas phase in dimensionless form gives

$$\frac{d}{d\tau}\left\{P^3\left(\tfrac{2}{3}x_c + \tfrac{3}{5}x_s\right)\right\} = \dot{(P^3)} \tag{61}$$

The interface mass balance, Equation (39), accordingly becomes

$$P\dot{P} = 2\,Lu\,\frac{x_s - x_c}{1 - x_s} \tag{62}$$

The nonlinearities of this formulation, Equations (52a), (61), (52c), (62) and (52e), again restrict the solutions that may readily be obtained. With the limitations

$$\left(\frac{R}{f_T}\right) \gg \frac{1}{2} \qquad \text{and} \qquad (1-\varepsilon)\,Ja\,(1-\theta_s) \ll 1 \tag{63}$$

however, Equation (52a) can be integrated despite the time varying θ_s. Integrating also Equation (61) and rearrranging, the five governing equations may be summarized to

$$Ja\,(1-\theta_s)P^3\left(\frac{R}{f_T}\right)^{-1} = P^3 - 1 \tag{64a}$$

$$P^3\left(1 - \tfrac{2}{5}x_c - \tfrac{3}{5}x_s\right) = 1 - x_o \tag{64b}$$

$$P\dot{P} = 2\,Ja\,(1-\theta_s)\left(\frac{R}{f_T}\right) \tag{64c}$$

$$P\dot{P} = 2\,Lu\,\frac{x_s - x_c}{1 - x_s} \tag{64d}$$

$$x_s = \theta_s - (1 - x_{co}) \tag{64e}$$

Eliminating the four variables, (R/f_T), θ_s, x_s and x_c, Equations (64) are reduced to a cubic equation in the variable $U = P\dot{P}/Lu$

$$U^3 + \left(10 - 2\frac{KL^2}{N}\right)U^2 + \left(25 + 20\frac{KLM}{N}\right)U - 50\frac{KM^2}{N} = 0 \qquad (65)$$

where

$$\left.\begin{aligned} K &= Ja^2/Lu \\ L &= 1 - x_\infty \\ M &= (x_\infty - x_o) - (1 - x_o)(1 - 1/P^3) \\ N &= 1 - 1/P^3 \end{aligned}\right\} \qquad (66)$$

A numerical evaluation indicates that over a wide range of values of the four parameter, Ja, Lu, x_∞ and x_o, and variable bubble size P, Equation (65) may be linearized by retaining only its two last terms. As shown in Appendix IV, the criterion for the validity of this approximation may be written

$$\left| \frac{50\frac{KM^2}{N}\left[50\frac{KM^2}{N} + \left(10 - 2\frac{KL^2}{N}\right)\left(25 + 20\frac{KLM}{N}\right)\right]}{\left(25 + 20\frac{KLM}{N}\right)^3} \right| \ll 1 \qquad (67)$$

Because of the complexity of Equation (67) the limination on the variable bubble size P in terms of the governing parameters is not readily obtained explicitely. Instead, the inequality Equation (67) need be checked as the calculations proceed.

Retaining the last two terms of Equation (65) the following differential equation results

$$P\dot{P} = \frac{\left(\frac{1}{P^3} - \frac{1}{P_\infty^3}\right)^2}{\frac{1}{2\,Ja^2\,(1-x_o)^2}\left(1 - \frac{1}{P^3}\right) + \frac{2}{5\,Lu}\,\frac{1}{P_\infty^3}\left(\frac{1}{P^3} - \frac{1}{P_\infty^3}\right)} \tag{68}$$

where for simplicity $P_\infty^3 = (1-x_o)/(1-x_\infty)$ according to Equation (42) has been substituted. Separating variables and integrating from the join point $\tau = \tau_1$ to $\tau > \tau_1$ gives explicitely time as function of the more conveniently chosen bubble size $w = P/P_\infty$ (i.e. $w_o = 1/P_\infty$). Separating the distinct contributions to elapsed time for a given bubble growth from respectively the process of mass and heat transport, the result may be written

$$\tau = \tau_1 + C_H I_H + C_M I_M \tag{69}$$

where

$$C_H = \frac{1}{2\,Ja^2\,(1-x_o)^2\,w_o^8}$$

$$C_M = \frac{2}{5\,Lu\,w_o^2}$$

and

$$I_H = \frac{1}{2}(w^2 - w_1^2) + \frac{1}{3}(1-w_o^3)\left(\frac{w^2}{1-w^3} - \frac{w_1^2}{1-w_1^3}\right)$$

$$- \frac{1}{9}(5-2w_o^3)\left[\ln\left(\sqrt{\frac{1+w+w^2}{1+w_1+w_1^2}}\cdot\frac{1-w_1}{1-w}\right) - \sqrt{3}\left(\operatorname{Arctg}\frac{2w+1}{\sqrt{3}} - \operatorname{Arctg}\frac{2w_1+1}{\sqrt{3}}\right)\right]$$

$$I_M = -\frac{1}{2}(w^2 - w_1^2)$$

$$+\frac{1}{3}\left[\ln\left(\sqrt{\frac{1+w+w^2}{1+w_1+w_1^2}}\cdot\frac{1-w_1}{1-w}\right) - \sqrt{3}\left(\operatorname{Arctg}\frac{2w+1}{\sqrt{3}} - \operatorname{Arctg}\frac{2w_1+1}{\sqrt{3}}\right)\right]$$

Noting that the rate of heat transport depends on Ja and the rate of mass transport depends on Lu , the terms $C_H I_H$ and $C_M I_M$ are recognized to represent the contributions to elapsed time beyond the join point $\tau = \tau_1$ from respectively the heat and mass transport mechanisms. A measure for the relative significance of heat transport to mass transport for retarding bubble growth is therefore obtained in the ratio

$$\frac{C_H I_H}{C_M I_M} = \frac{Lu}{Ja^2}\cdot f(w_o, w_1, w) \qquad (70)$$

The function $f(w_o, w_1, w)$ in Equation (70) is monotonous and increasing as w increases. Hence, the significance of mass transport for the transient decreases and heat transport becomes the controlling factor as the asymptotic stage is approached. The latter observation supports the choice of a quasi-steady model for the asymptotic stage of growth, based on the assumption of uniform composition distribution in the gas phase.

d. Asymptotic Solution

For large values of time the composition distribution in the gas phase approaches uniformity and growth of the bubble is primarily controlled by heat transport in the liquid phase.

The quasisteady model postulated for this time domain assumes a thermally insulated spherical gas phase having uniform composition x, growing at the rate at which the heat of evaporation can be supplied to the bubble interface by heat transport in the liquid phase. The gas phase is ideal as previously assumed, and thermodynamic equilibrium at the bubble interface provides a unique relation between temperature T_s and gas composition x. The average composition, x, is directly related to bubble size, P, and initial composition, x_o,

$$x = 1 - \frac{1 - x_o}{P^3} \tag{71}$$

as seen from continuity considerations or from Equation (64b) for $x_s = x_c = x$. Hence, a unique relationship exists between interface temperature and instantaneous bubble size. From Equations (42), (51), and (71) this relation becomes

$$1 - \theta_s = (1 - x_\infty)\left(\frac{P_{io}^3}{P^3} - 1\right) \tag{72}$$

An approximate solution to the model outlined above is obtained by first formulating the heat transport problem with the aid of the theory of heat sources, and at the bubble interface imposing the condition of Equation (72). Next, this formulation is linearized to facillitate integration.

The formulation of the heat transport problem follows an approach similar to that introduced by Lightfoot (reviewed page 293 of Reference 7)

and used by Forster[18] for the related problem of spherical phase growth in one-component boiling. The approach takes its start in identifying the heat liberated or absorped at the bubble interface, associated with the interface mass transfer, as a uniformly distributed surface source or sink. In the present case, for a bubble of size R growing at a rate $\dot{R}$, the instantaneous spherical source, $\dot{q}$, on its surface has the strength

$$\dot{q} = -(h''_A - h'_A) N_A \, 4\pi R^2 = -4\pi R^2 \dot{R} \rho'' h_{fg} \tag{73}$$

Next, the solution to the equation of linear flow of heat in the domain bounded internally by and insulated at the sphere $r = R$ is written for the case that the domain is at zero temperature prior to the release at $t = 0$ of a unit instantaneous spherical surface source on the sphere $r = R$. The result (Equation XIV-16 of Reference 7) is the Green's function for the problem in question. Evaluating this at $r = R$ the temperature, T_s, of the bubble interface can be written

$$T_s = \frac{1}{4\pi R^2 \sqrt{\alpha' \pi t}} \left[1 - \frac{\sqrt{\alpha' \pi t}}{R} \exp\left(\frac{\alpha' t}{R^2}\right) \operatorname{erfc}\left(\frac{\sqrt{\alpha' t}}{R}\right)\right] \tag{74}$$

The solution for a time varying heat source of strength $\dot{q}(t)$ is obtained by convolution in the time domain,

$$T_s = \int_0^t \frac{\dot{q}(t')/\rho c'}{4\pi R^2 \sqrt{\alpha' \pi (t-t')}} \left\{1 - \frac{\sqrt{\alpha' \pi (t-t')}}{R} \exp\left[\frac{\alpha'(t-t')}{R^2}\right] \operatorname{erfc}\left[\frac{\sqrt{\alpha'(t-t')}}{R}\right]\right\} dt' \tag{75}$$

Forster[19] demonstrated how this result could be extended to account approximately for the interface motion by considering successive differential processes of linear flow of heat (conduction) and radial convection. Thus, resulting from the instantaneous differential heat release, $dq(t')$, at time t', the bubble grows in size from $R(t')$ to $R(t)$ during the time interval t' to t. This sequence of events is then repeated. The corresponding differential change in interface temperature, dT_s, is obtained again from the Green's function for the linear flow of heat, but now accounting for the change in bubble size by selecting an intermediate value of radius, $R(\xi)$ where $t' < \xi < t$. Forster[19] evaluated $R(\xi)$ approximately as

$$R(\xi) = \sqrt{R(t') \cdot R(t)} \tag{76}$$

Summing up the differential contributions over the time interval $(0,t)$, Equation (75) with $R = R(\xi)$ results. As discussed by Forster[19] the second term in the integral of Equation (75) is small when the contribution to the differential change in surface temperature is large. By the time the second term becomes important the contribution to the surface temperature change is small owing to the first factor in the integral. Retaining thus only the first term of Equation (75) and substituting the source term from Equation (73) the result may be written

$$T_\infty - T_s = \int_0^t \frac{\rho'' h_{fg}}{\rho' c'} \frac{R(t') \dot{R}(t')}{\sqrt{\alpha' \pi}\, R(t)} \frac{dt'}{\sqrt{t-t'}} \tag{77}$$

when the inital uniform temperature is T_∞ . Nondimensionalizing according to Equations (50) and using for convenience the notation $*$ for the convolution, Equation (77) becomes

$$2\ Ja\ P(1-\theta_s) = (\dot{P}^2) * \frac{1}{\sqrt{\pi\tau}} \tag{78}$$

Equation (78) is linearized by approximating the left hand side by the form

$$2\ Ja\ P(1-\theta_s) \cong b(a - P^2) \tag{79}$$

where the constants a and b are chosen to satisfy Equation (72) for $P = 1$ and $P = P_\infty$. Hence

$$a = P_\infty^2 \tag{80}$$

$$b = 2\ Ja\ \frac{x_\infty - x_o}{P_\infty^2 - 1} \tag{81}$$

The approximation Equation (79), now written

$$\frac{1-\theta_s}{x_\infty - x_o} \cong \frac{1}{P}\ \frac{P_\infty^2 - P^2}{P_\infty^2 - 1} \tag{82}$$

is compared to the similar form of Equation (72)

$$\frac{1-\theta_s}{x_\infty - x_o} = \frac{1}{P^3}\ \frac{P_\infty^3 - P^3}{P_\infty^3 - 1} \tag{83}$$

in Figure 5 for different values of the parameter P_∞ . Representing

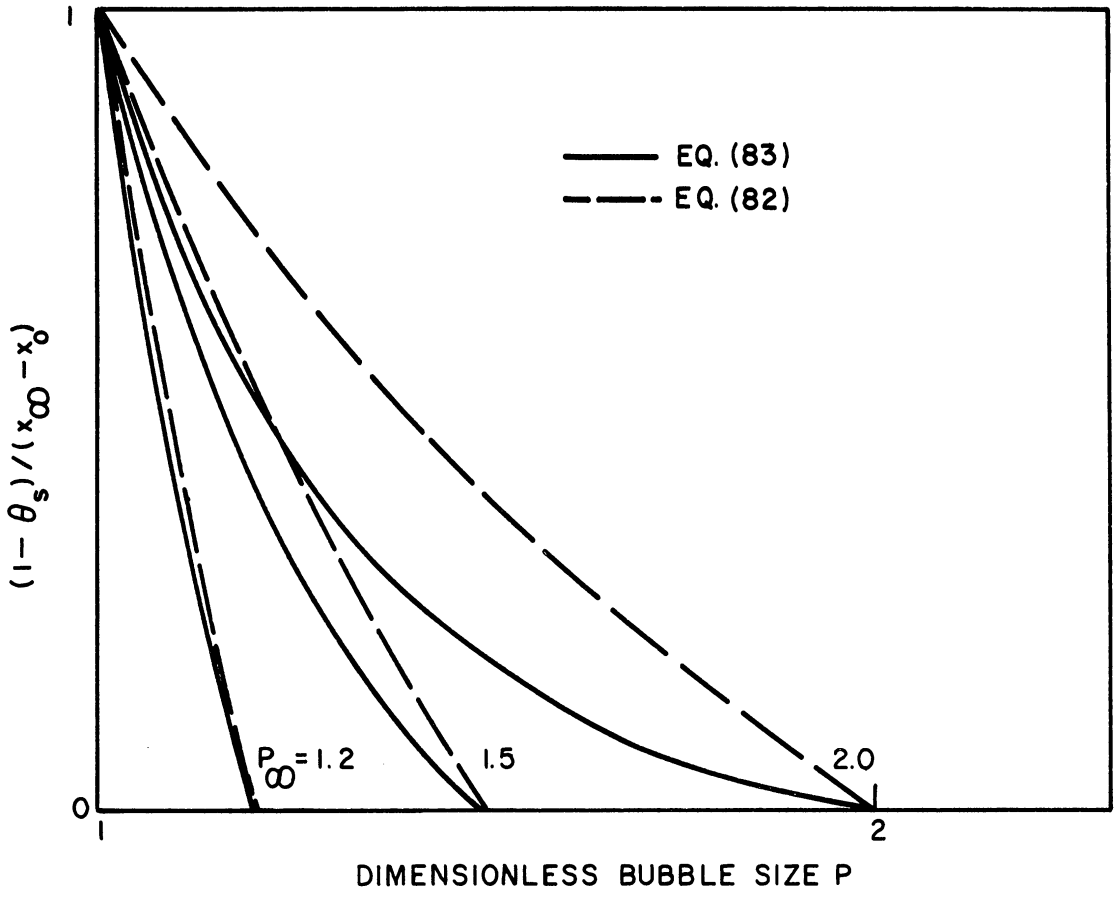

Figure 5. Approximation to Interface Potential for Asymptotic Bubble Growth.

the normalized thermal potential for bubble growth the quantity $(1-\theta_s)/(x_\infty-x_o)$ is seen to approach zero as the bubble size approaches its asymptotic value, P_∞ . The approximation is good in the asymptotic stage, particularly for small values of P_∞ . The linearized form of Equation (78) is operated on by Laplace transformation giving the closed form solution

$$P(\tau) = \sqrt{P_\infty^2 - (P_\infty^2 - 1)\cdot exp\left[b^2(\tau-\tau_o)\right]\cdot erfc\left(b\sqrt{\tau-\tau_o}\right)} \qquad (84)$$

where the hypothetical inital condition, $P(\tau_o) = 1$, is chosen such that Equation (84) satisfies $P(\tau_2) = P_2$ at the join point τ_2 , beyond which this asymptotic solution is valid.

Analogous to the continuation of the solution valid for small values of time at the join point $\tau = \tau_1$, the join point $\tau = \tau_2$ is approximately obtained by extending the intermediate solution to the value P_2 which justifies the use of the quasisteady solution, Equation (84). The criterion for determining P_2 is obtained by comparing the interface composition, x_s , assuming a distributed gas phase, to the average composition, x , given by Equation (71). Although in principle arbitrary, a maximum deviation of 0.5% has been chosen suitable for the criterion, which then gives

$$1 - \frac{x(P_2)}{x_s(P_2)} \leqslant 0.005 \qquad (85)$$

The interface composition x_s for the case of a distributed gas phase is calculated from the intermediate solution, Equations (64a), (64c), and (68),

to

$$x_s = x_\infty - \frac{1 - \frac{P^3}{P_\infty^3}}{\sqrt{1 + \frac{+}{5}\frac{Ja^2}{Lu}\frac{1}{P_\infty^3}\frac{1/P^3 - 1/P_\infty^3}{1 - 1/P^3}}} \frac{1-x_o}{P^3} \qquad (86)$$

which is seen to reduce to Equation (71) for $Lu \to \infty$. Having established P_2 from Equation (85) the corresponding approximate time τ_2 is calculated from Equation (69).

2. Discussion of Analytical Results - Parameter Study

The form of the analytical solution is shown in Figure 6, where the results of Equations (55), (69), and (84) are plotted in terms of relative dimensionless bubble size $Q = (P-1)/(P_\infty-1)$ vs τ for the case $Ja = 100$, $Lu = 100$, $x_\infty = 0.9$ and $x_o = 0$. The graph shows the joining of the solution for small values of time, the intermediate solution and the asymptotic solution at respectively join points τ_1 and τ_2. The solution valid for small times, being less important, is omitted in the subsequent four plots. Figures 7, 8, 9, and 10, respectively show the influence of the parameter Ja, Lu, x_∞ and x_o, while the remining three parameters are kept constant. It is particularly worth noting that for the representation chosen, x_o is a parameter of very weak importance. This observation justifies the omission of x_o from consideration in determining the growth rate. However, decisive in conjuction with x_∞ for the asymptotic bubble size (cf. Equation (42)) x_o remains an important overall parameter.

The effect of initial bubble size, R_o, on the rate of bubble growth is reflected in the dimensionless time parameter τ. As expected

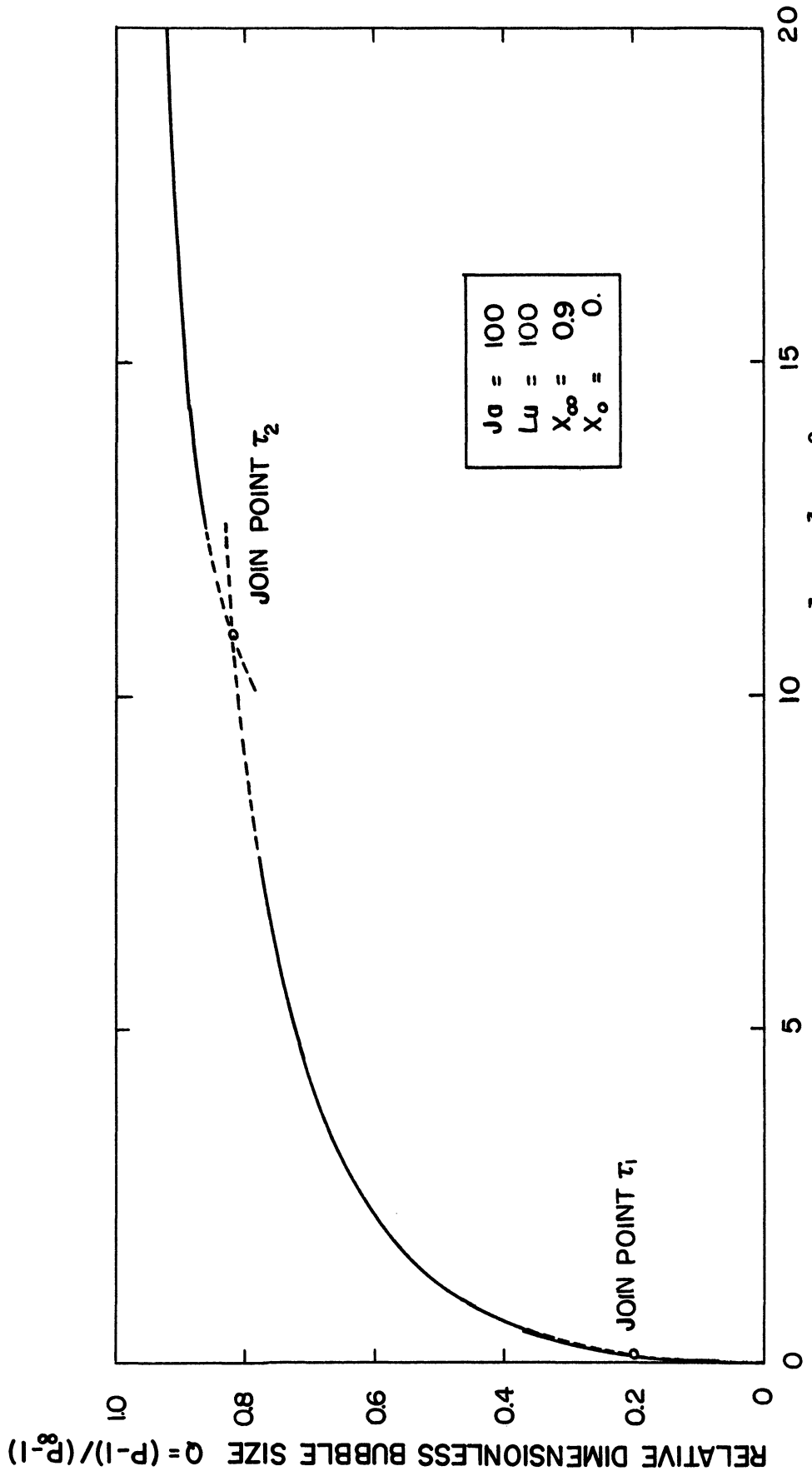

Figure 6. Analytical Solutions for Relative Dimensionless Bubble Growth. Solutions for Small and Intermediate Values of Time and Asymptotic Solution. Nonsoluble Gas Case.

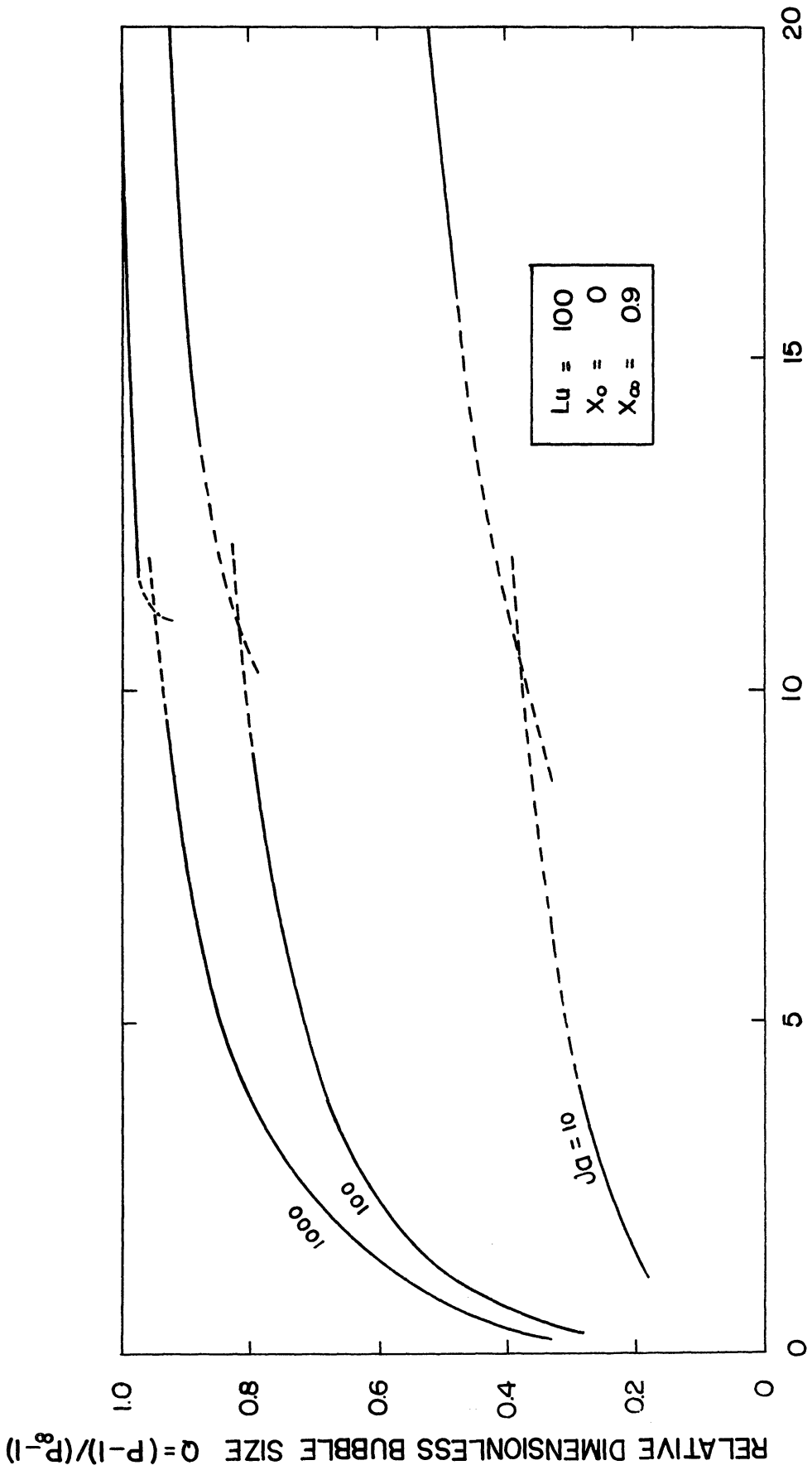

Figure 7. Parameter Study, $Q(Ja,\tau)$. Intermediate and Asymptotic Solutions. Nonsoluble Gas Case.

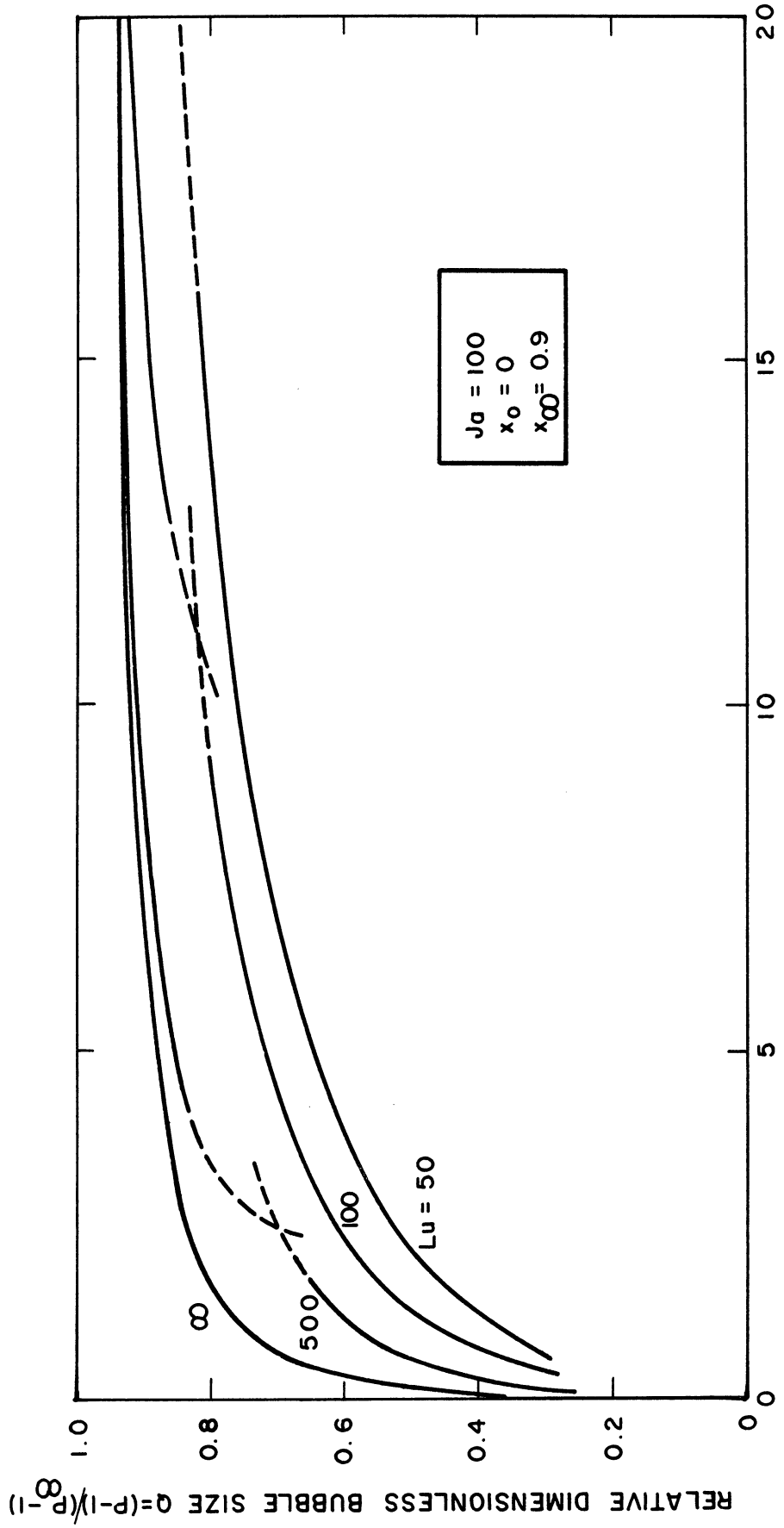

Figure 8. Parameter Study, $Q(Lu,\tau)$. Intermediate and Asymptotic Solutions. Nonsoluble Gas Case.

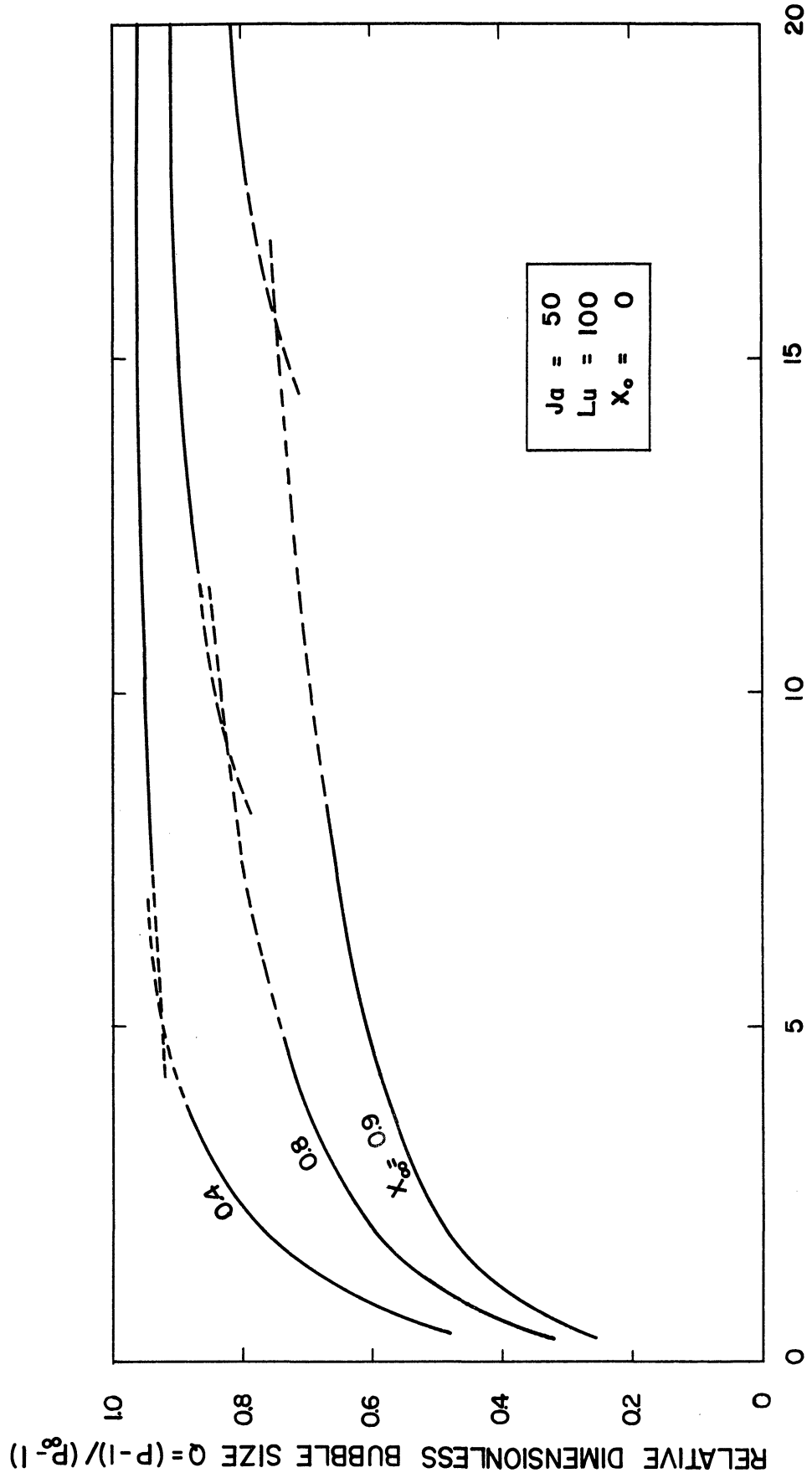

Figure 9. Parameter Study, $Q(x_\infty,\tau)$. Intermediate and Asymptotic Solutions. Nonsoluble Gas Case.

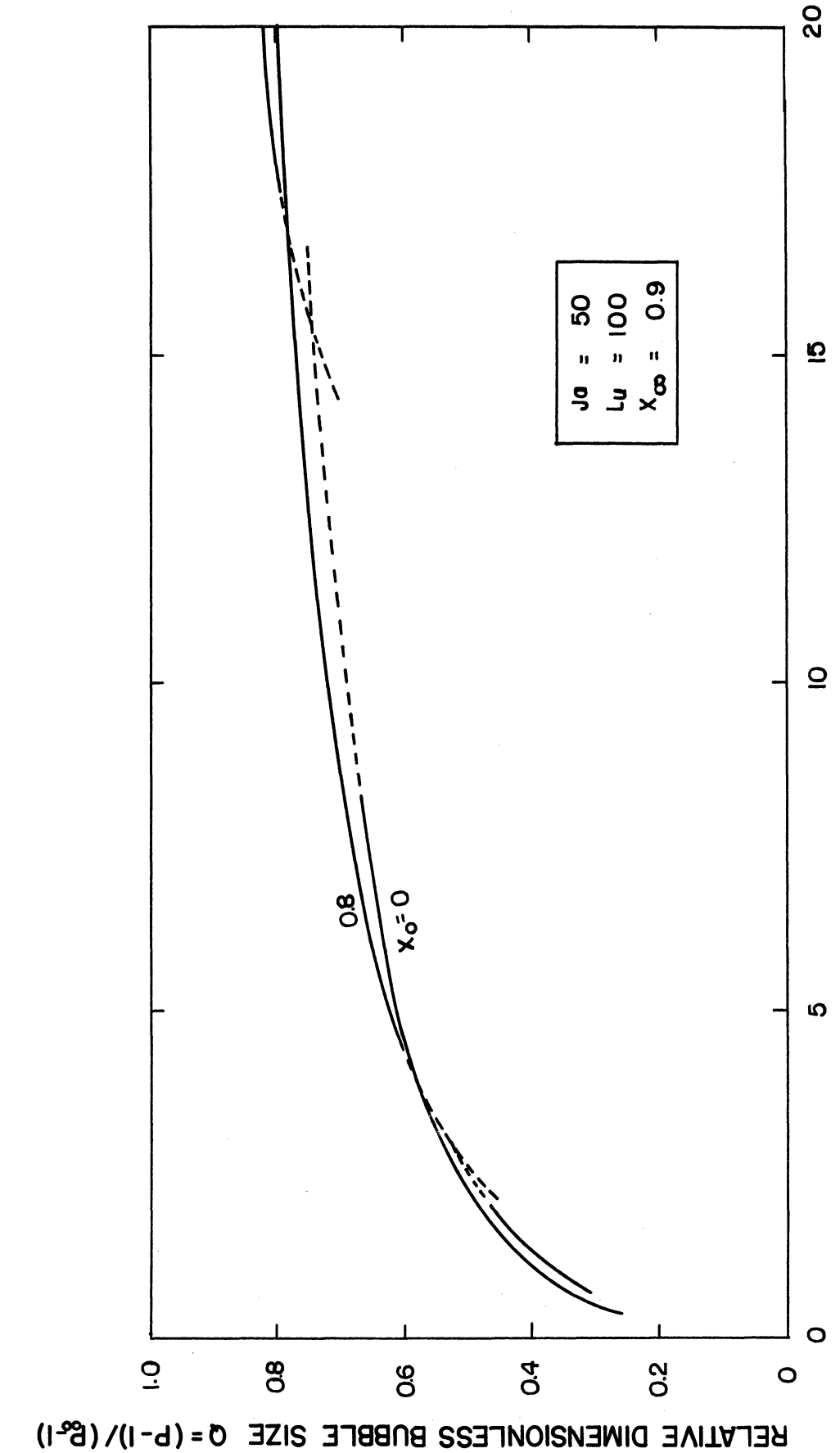

Figure 10. Parameter Study, $Q(x_o,\tau)$. Intermediate and Asymptotic Solutions. Nonsoluble Gas Case.

the growth rate increases as R_o becomes smaller.

As seen from Figures 7 and 8, the effect of increasing the Ja- and Lu-numbers lead to increased growth rates. The case $Lu \to \infty$ is represented by the asymptotic solution throughout. Over the range of parameter values of practical interest the influence of increasing Ja-number is more significant than that of increasing Lu-number, in accordance with the relative significance of these two parameters as expressed by the characteristic group Ja^2/Lu .

For fixed initial gas composition, x_o , as the liquid approaches the saturation state (i.e. x_∞ approaches unity), the rate of relative bubble growth decreases, as shown in Figure 9. The growth rate for the actual bubble radius for constant initial bubble size, however, increases as x_∞ becomes greater, because the normalizing asymptotic bubble size, P_∞ , also becomes greater. The net heat transfer rate from the liquid consequently also increases.

Another useful representation of the transient bubble growth process in terms of a pseudo time constant is shown in Figures 11 and 12. The time for 63.2% (= 1 - 1/e) completion of the relative growth is plotted versus equilibrium composition x_∞ for particular values of the set of significant parameters Ja and Lu, and $x_o = 0$.

In the dimensionless representation of bubble growth derived in this section, the combined property group, Ja^2/Lu, appears whenever the simultaneous processes of heat and mass transport are considered. In the solution for small values of time and for $\epsilon = 1$, as assumed in the subsequent solutions, the initial state at the interface is determined by Ja^2/Lu as seen from Equation (56). As this property group increases, the

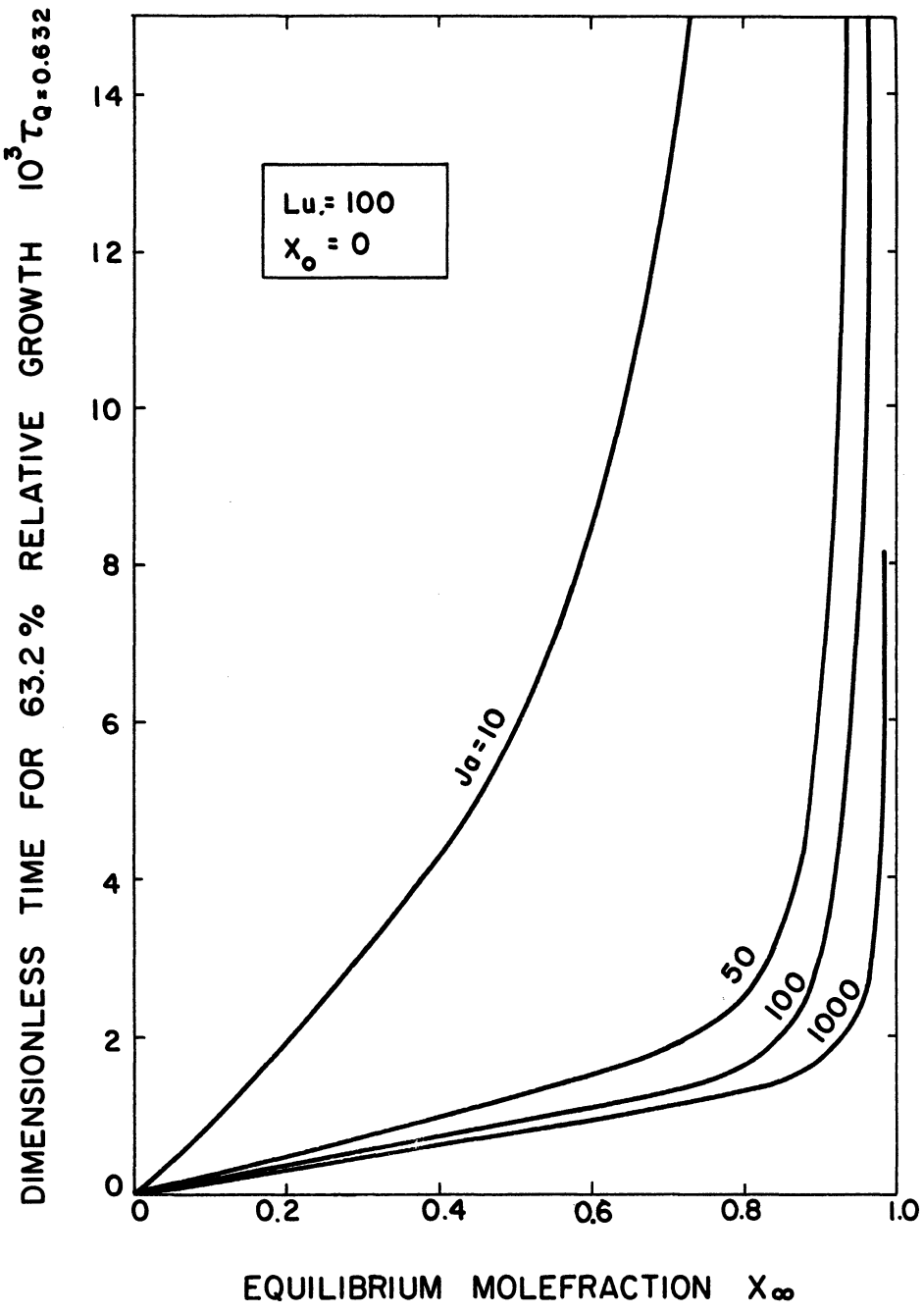

Figure 11. Time Constant for Relative Dimensionless Bubble Growth vs x_∞ and Ja . Nonsoluble Gas Case.

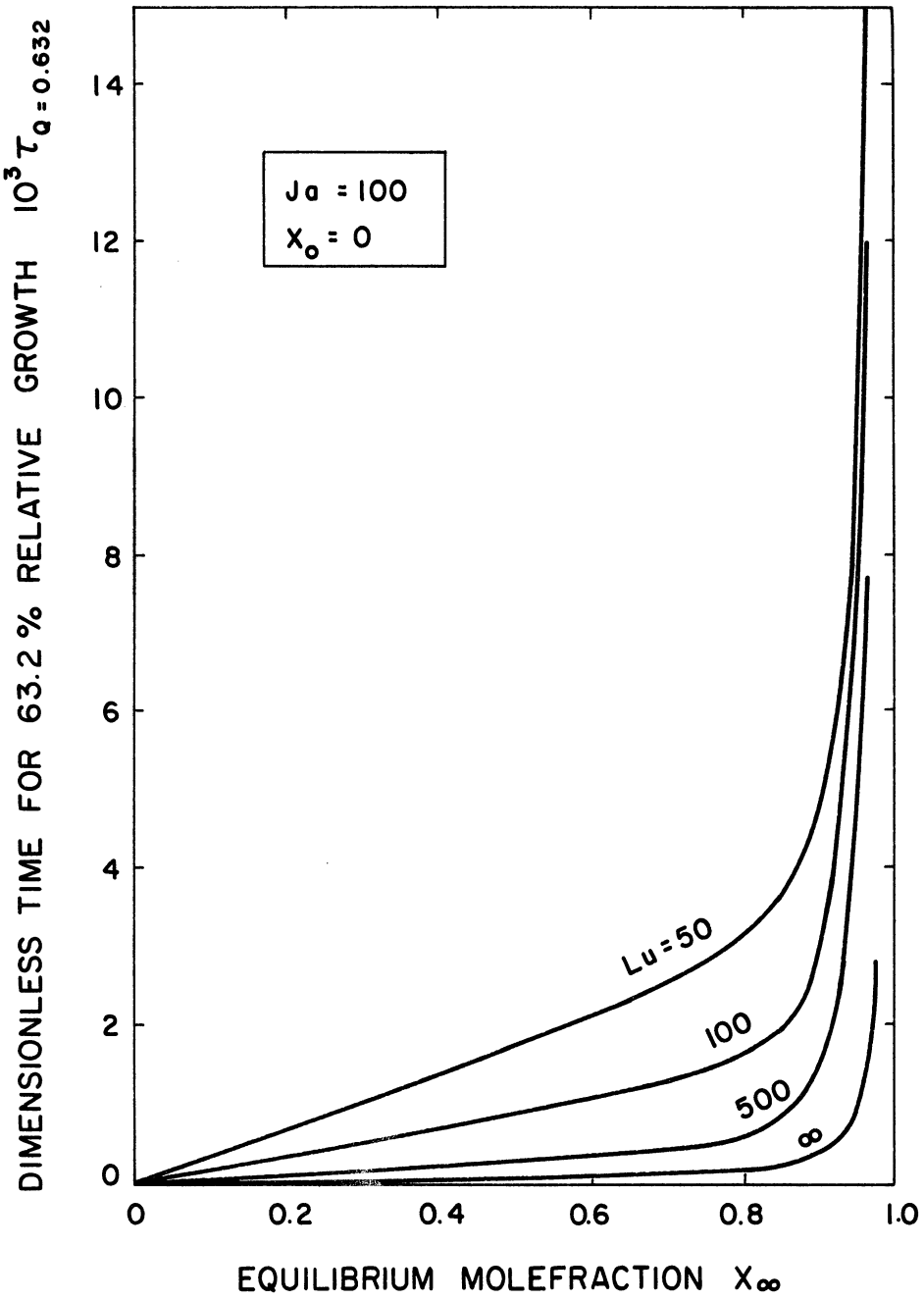

Figure 12. Time Constant for Relative Dimensionless Bubble Growth vs x_∞ and Lu . Nonsoluble Gas Case.

driving potential, $1-\theta_{so}$, for heat transport decreases, while the one for mass transport, $x_{so}-x_o$, increases. The relative significance of the two mechanisms in determining the rate of growth is therefore shifted in favor of the mass diffusion process, although the growth rate increases when either the Ja-number or the Lu-number becomes greater. The same result, now in addition a function of bubble size, was found in the solution for intermediate values of time, as expressed by Equation (70). In the limit as Ja^2/Lu becomes either very large or very small, the growth rate is controlled respectively by mass transport or by heat transport.

E. The Case of a Soluble Gas

The injection of a soluble gas into a volatile liquid -having little application for the injection cooling process- is treated in less detail in the present study. First, the initial behavior of the bubble is predicted by neglecting the curvature and considering the gas and liquid phases as semi-infinite domains. The results predict whether the bubble tends to grow or collapse in the very fist part of the transient. Secondly, by the use of source theory, the approximate solution is derived to the bubble collapse governed alone by heat and mass transport in the liquid phase. This represents the limiting case of a soluble gas bubble in a nonvolatile liquid.

Compared to the case of a nonsoluble gas, the present general case is increased in complexity. Two additional parameters enter the problem, namely the initial liquid composition, x'_∞ , and the property for mass diffusion in the liquid through the dimensionless group, $Lu' = \mathcal{D}'/\alpha'$.

Furthermore, the density deficiency, $\epsilon = 1-\rho''/\rho'$, cannot be taken to unity as for the case of a nonsoluble gas, because this would violate the interface mass balance. The added degrees of freedom are reflected in the possibility for initial growth or collapse, eventually followed by collapse in all cases of a nonsaturated liquid.

1. Solution for Small Values of Time

Neglecting the curvature effect and considering the gas and liquid domains semi-infinite the formulation given by Equation (24), (25), and (26), in terms of the independent space variable, y , measured from the interface in the direction of the liquid phase, becomes

(a) Gas phase:

$$\frac{\partial(x''-x_o'')}{\partial t} + v'' \frac{\partial(x''-x_o'')}{\partial y} = \mathcal{D}'' \frac{\partial^2(x''-x_o'')}{\partial y^2} \tag{87}$$

$$\begin{cases} x''(y,0) - x_o'' = 0 \\ x''(-\infty,t) - x_o'' = 0 \\ x''(0,t) - x_o'' = x_s''-x_o \end{cases}$$

(b) Liquid phase:

$$\frac{\partial(x_\infty'-x')}{\partial t} + v' \frac{\partial(x_\infty'-x')}{\partial y} = \mathcal{D}' \frac{\partial^2(x_\infty'-x')}{\partial y^2} \tag{88}$$

$$\begin{cases} x_\infty' - x'(y,0) = 0 \\ x_\infty' - x'(\infty,t) = 0 \\ x_\infty' - x'(0,t) = x_\infty'-x_s' \end{cases}$$

$$\frac{\partial (T_\infty - T)}{\partial t} + v' \frac{\partial (T_\infty - T)}{\partial y} = \alpha' \frac{\partial^2 (T_\infty - T)}{\partial y^2} \tag{89}$$

$$\begin{cases} T_\infty - T(y,0) = 0 \\ T_\infty - T(\infty,t) = 0 \\ T_\infty - T(0,t) = T_\infty - T_s \end{cases}$$

where the assumption of plane geometry and incompressible fluids imply that the gas and liquid velocities, v" and v' , are spatially independent.

(c) Interface conditions:

The mass balance given by Equations (28), (29), and (30) becomes

$$N_A + N_B = \rho'' v'' = \rho' v' = \frac{\rho'' \mathcal{D}'' \left.\frac{\partial x''}{\partial y}\right|_s - \rho' \mathcal{D}' \left.\frac{\partial x'}{\partial y}\right|_s}{x_s'' - x_s'} \tag{90}$$

where the moleflux to the liquid phase of component A and B expressed in terms of the composition distribution in the gas phase is respectively

$$N_A = \rho'' v'' x_s'' - \rho'' \mathcal{D}'' \left.\frac{\partial x''}{\partial y}\right|_s \tag{91}$$

and

$$N_B = \rho'' v'' (1 - x_s'') + \rho'' \mathcal{D}'' \left.\frac{\partial x''}{\partial y}\right|_s \tag{92}$$

The heat balance, Equation (31), simplifies to

$$N_A h_{fgA} + N_B h_{fgB} = - k' \left.\frac{\partial T}{\partial y}\right|_s \tag{93}$$

Interface equilibrium is given by Equations (22) and (23). Introducing the Henry law constant, $K_B = (1-x')/(1-x'')$, which for dilute solutions of component B may be calculated directly from Equations (22) and (23) to

$$K_B \cong \frac{p_\infty}{p_B^*} \tag{94}$$

the linear phase equilibirum relations become

$$x_S'' = \theta_S - (1-x_\infty'') \tag{95}$$

$$x_S' = 1 - K_B (1-x_S'') \tag{96}$$

where dimensionless temperature, θ , is defined by Equation (50).

The formulation given by Equations (87), (88), and (89) of one-dimensional mass and heat transfer with convection is satisfied by a set of similarity solutions (see Bird, Steward and Lightfoot[5], Example 19.1-1) in such a way that the interface potentials, x_S'' , x_S' and T_S , remain constant during the transient. Each of the partial differential equations is reduced to an integrable ordinary differential equation of second order by introducing the independent similarity variable, $Y = y/\sqrt{\alpha' t}$ and by expressing the gas velocity by

$$v'' = \lambda \sqrt{\frac{\alpha'}{t}} \tag{97}$$

hence by continuity, the liquid velocity by the corresponding form

$$v' = (1-\varepsilon) \lambda \sqrt{\frac{\alpha'}{t}} \tag{98}$$

In Equations (97) and (98) λ is the phase-growth constant, to be determined from the interface conditions. Thus Equation (89), for example, reduces to the form

$$\frac{d^2}{dY^2}\left(\frac{1-\theta}{1-\theta_s}\right) + \left[\frac{Y}{2} - (1-\varepsilon)\lambda\right]\frac{d}{dY}\left(\frac{1-\theta}{1-\theta_s}\right) = 0 \qquad (99)$$

subject to

$$\frac{1-\theta}{1-\theta_s} = 1 \qquad \text{for} \qquad Y = 0$$

$$\frac{1-\theta}{1-\theta_s} = 0 \qquad \text{for} \qquad Y = \infty$$

where dimensionless temperature has been introduced according to Equation (50). Twice integration of Equation (99) gives the solution to the transient temperature distribution in the liquid

$$\frac{1-\theta}{1-\theta_s} = \frac{1 - \operatorname{erf}\left[Y/2 - (1-\varepsilon)\lambda\right]}{1 + \operatorname{erf}\left[(1-\varepsilon)\lambda\right]} \qquad (100)$$

Introducing the remaining dimensionless quantities from Equation (50) with the addition of the Lu-number for mass diffusion in the liquid phase,

$$Lu' = \frac{\mathfrak{D}'}{\alpha'} \qquad (101)$$

Equations (87) and (88) integrate to

$$\frac{x'_\infty - x'}{x'_\infty - x_s} = \frac{1 - \operatorname{erf}\left[\frac{Y/2 - (1-\varepsilon)\lambda}{\sqrt{Lu'}}\right]}{1 + \operatorname{erf}\left[\frac{(1-\varepsilon)\lambda}{\sqrt{Lu'}}\right]} \qquad (102)$$

and

$$\frac{x'' - x_o''}{x_s'' - x_o''} = \frac{1 + \operatorname{erf}\left[\frac{Y/2 - \lambda}{\sqrt{Lu}}\right]}{1 + \operatorname{erf}\left(\frac{\lambda}{\sqrt{Lu}}\right)} \tag{103}$$

Substituting from Equation (100), (102), and (103) into the equations for mass and heat balance, Equations (90) and (93), these become

$$\lambda\sqrt{\pi} = \frac{x_s'' - x_o''}{x_s'' - x_s'} \cdot \frac{\sqrt{Lu}}{\exp\left(\frac{\lambda}{\sqrt{Lu}}\right)^2 \operatorname{erfc}\left(\frac{\lambda}{\sqrt{Lu}}\right)} - \frac{x_\infty' - x_s'}{x_s'' - x_s'} \cdot \frac{\frac{\sqrt{Lu'}}{1-\varepsilon}}{\exp\left[\frac{(1-\varepsilon)\lambda}{\sqrt{Lu'}}\right]^2 \left\{1 + \operatorname{erf}\left[\frac{(1-\varepsilon)\lambda}{\sqrt{Lu'}}\right]\right\}} \tag{104}$$

and

$$\lambda\sqrt{\pi} = \frac{x_s'' - x_o''}{x_s'' + \frac{F}{1-F}} \cdot \frac{\sqrt{Lu}}{\exp\left(\frac{\lambda}{\sqrt{Lu}}\right)^2 \operatorname{erfc}\left(\frac{\lambda}{\sqrt{Lu}}\right)} - \frac{\frac{1-\theta_s}{1-F}}{x_s'' + \frac{F}{1-F}} \cdot \frac{Ja}{\exp\left[(1-\varepsilon)\lambda\right]^2 \left\{1 + \operatorname{erf}\left[(1-\varepsilon)\lambda\right]\right\}} \tag{105}$$

where the ratio of heats of phase transition is given by $F = h_{fgB}/h_{fgA}$. Equations (104) and (105) in conjunction with the condition of phase-equilibrium at the interface determines the growth constant λ and the state at the interface. Introducing the linear approximations to phase-equilibrium, Equations (95) and (96), and eliminating x_s', x_s'' and θ_s a single implicite equation in λ results,

$$\left[\sqrt{\pi}(1-K_B) - \frac{1}{\frac{\lambda}{\sqrt{Lu}} E\left\{\frac{\lambda}{\sqrt{Lu}}\right\}} - \frac{K_B}{\frac{(1-\varepsilon)\lambda}{\sqrt{Lu'}} E\left\{-\frac{(1-\varepsilon)\lambda}{\sqrt{Lu'}}\right\}}\right] \cdot \left[\sqrt{\pi} F + \frac{(1-F)\, x_o''}{\frac{\lambda}{\sqrt{Lu}} E\left\{\frac{\lambda}{\sqrt{Lu}}\right\}} + \frac{x_\infty''}{\frac{\lambda}{Ja} E\left\{-(1-\varepsilon)\lambda\right\}}\right] \tag{106}$$

$$+ \left[\sqrt{\pi}(1-K_B) - \frac{x_o''}{\frac{\lambda}{\sqrt{Lu}} E\left\{\frac{\lambda}{\sqrt{Lu}}\right\}} + \frac{1 - x_\infty' - K_B}{\frac{(1-\varepsilon)\lambda}{\sqrt{Lu'}} E\left\{-\frac{(1-\varepsilon)\lambda}{\sqrt{Lu'}}\right\}}\right] \cdot \left[\sqrt{\pi}(1-F) - \frac{1-F}{\frac{\lambda}{\sqrt{Lu}} E\left\{\frac{\lambda}{\sqrt{Lu}}\right\}} - \frac{1}{\frac{\lambda}{Ja} E\left\{-(1-\varepsilon)\lambda\right\}}\right] = 0$$

where for simplicity the functional notation, $E() = \exp()^2 \cdot \operatorname{erfc}()$, is used. The interface temperature is accordingly given by

$$\theta_s = \frac{\sqrt{\pi}\left(1-x''_\infty-\frac{F}{1-F}\right) - \frac{1-x''_\infty+x''_o}{\frac{\lambda}{\sqrt{Lu}}E\left\{\frac{\lambda}{\sqrt{Lu}}\right\}} - \frac{\frac{1}{1-F}}{\frac{\lambda}{Ja}E\left\{-(1-\varepsilon)\lambda\right\}}}{\sqrt{\pi} - \frac{1}{\frac{\lambda}{\sqrt{Lu}}E\left\{\frac{\lambda}{\sqrt{Lu}}\right\}} - \frac{\frac{F}{1-F}}{\frac{\lambda}{Ja}E\left\{-(1-\varepsilon)\lambda\right\}}} \tag{107}$$

and the corresponding interface compositions are subsequently obtained from Equations (95) and (96).

As seen from the definition of the phase-growth constant λ by Equation (97), $\lambda > 0$ implies initial bubble collapse, while $\lambda < 0$ conversely indicates a net flow of gas away from the interface, hence growth of the gas phase. Applying the equation of continuity to the incompressible gas phase of a bubble, its dynamic behavior for small values of time may be approximated by

$$P(\tau) = 1 - 2\lambda\sqrt{\tau} \tag{108}$$

That λ may take either positive or negative values is seen from Equations (104) and (105). Thus for large values of Ja^2/Lu and $\frac{1}{1-\epsilon}\sqrt{Lu'/Lu}$, initial growth may be anticipated.

Setting the growth parameter in relation to the Ja-number by introducing the ratio λ/Ja into Equations (106) and (107), the Lu-numbers always appear in the significant groups, Ja^2/Lu and Ja^2/Lu'. As found for the case of a nonsoluble gas, the simultaneous processes of mass and heat transport are governed by these characteristic property groups, giving the relative significance of the two mechanisms in determining the rate of phase change. Figure 13 shows a plot of λ/Ja vs $Ja/\sqrt{Lu}$ for $Ja/\sqrt{Lu'} = 1000$ and $Ja/\sqrt{Lu'} = 100$ with x''_∞ as parameter, obtained from Equation (106) for a representative set of values of the remaining para-

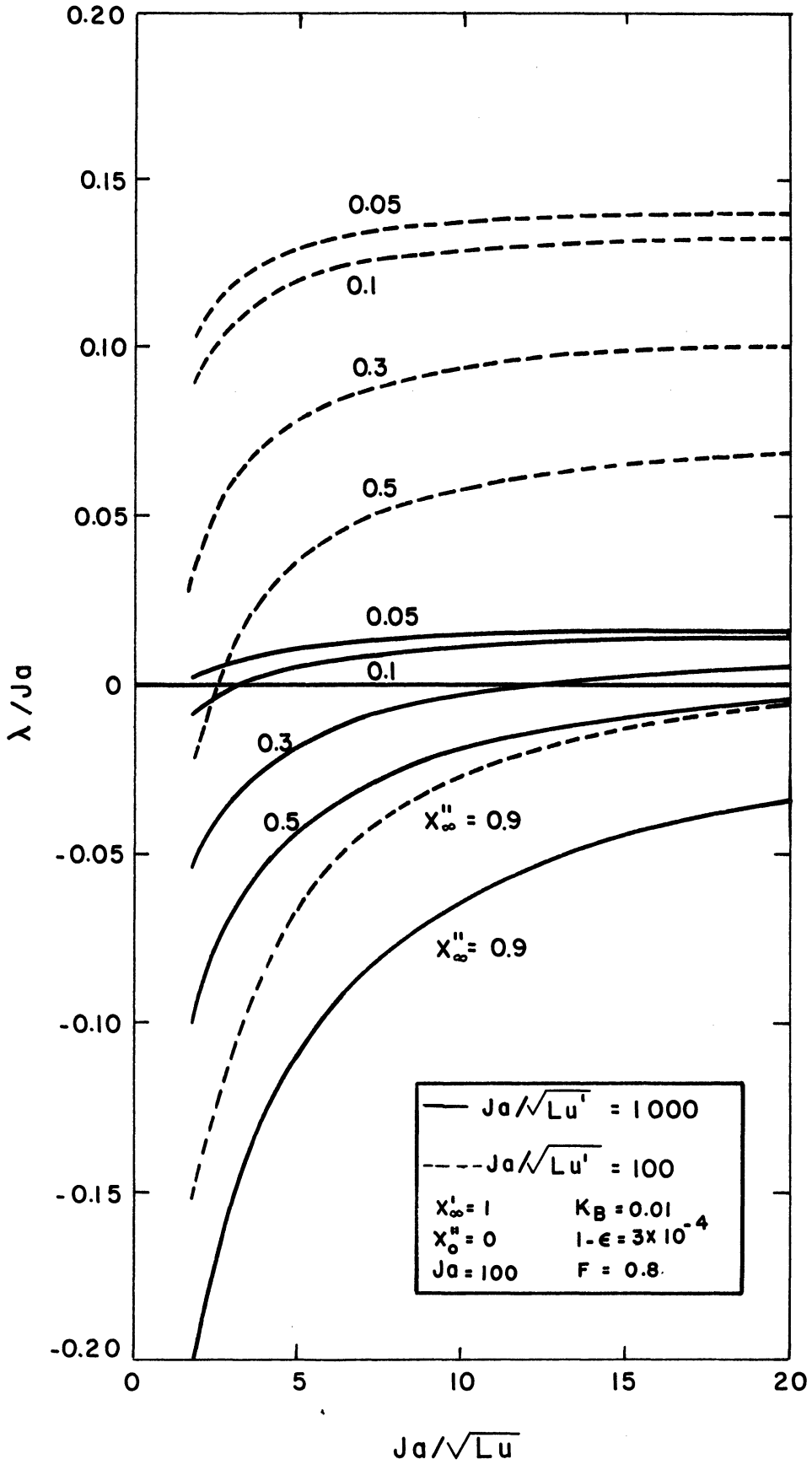

Figure 13. Parameter Study of Phase-growth, λ/Ja vs $Ja/\sqrt{Lu}$. Soluble Gas Case.

meters as follows

$$x''_o = 0 \qquad 1-\epsilon = 0.0003$$

$$x''_\infty = 1 \qquad K_B = 0.01$$

$$Ja = 100 \qquad F = 0.8$$

Because the Ja-number only appears in Equation (106) with the small factor $(1-\epsilon)\lambda/Ja$ in the argument of the exponential and error functions the representation of Figure 13 is practically independent of the Ja-number when this is less than about 200. As x''_∞ increases, the liquid component A becomes more volatile and initial growth, rather than collapse, is obtained at lower values of the parameter $Ja/\sqrt{Lu}$. A one hundred fold increase of the mass diffusivity in the liquid phase, appearing as a ten fold decrease of the parameter $Ja/\sqrt{Lu'}$, results, as shown in Figure 13, in a shift of λ/Ja towards greater values, implying a higher tendency to collapse of the gas phase, other parameters being unchanged.

2. Solution to Bubble Collapse in a Nonvolatile Liquid

For the special case of a nonvolatile liquid, the collapse of a bubble containing only component B is governed by heat and mass transport in the liquid phase.

The method of source theory, as discussed in detail in Section D, part 1.d., is now applied to the spherical domain, $r \geq R$, for the simultaneous processes of mass and heat diffusion. This approach has been used by Yang[64] in predicting approximate bubble growth rates in boiling binary mixtures. Analogous to identifying the liberation of heat of phase transition as a spherical heat source, Equation (73), the instantaneous mass flux,

N_B , entering into liquid solution at the bubble interface is identified as a spherical mass source of strength

$$\dot{q}_M = 4\pi R^2 N_B = -\rho'' 4\pi R^2 \dot{R} \tag{109}$$

Introducing Equation (109) into the analogous form of Equation (74) for mass diffusion and integrating, there results

$$-(x'_\infty - x'_s) = \frac{\rho''}{\rho'} \frac{1}{\sqrt{\pi \mathcal{D}}} \int_0^t \frac{R(t')\,\dot{R}(t')}{R(t)\,\sqrt{t-t'}}\, dt' \tag{110}$$

Dimensionless quantities are next introduced from Equations (50) and (101), now, however, basing the Ja-number and the reference temperature used in nondimensionalizing T on the properties of component B , such that

$$Ja' = \left(\frac{\partial T}{\partial x'}\right)_{p_\infty T_\infty} \frac{\rho' c'}{\rho'' h_{fgB}} \cong \frac{p_B^*(T_\infty)}{K_B} \left(\frac{dT}{dp}\right)^*_{B,T_\infty} \frac{\rho' c'}{\rho' h_{fgB}} \tag{111}$$

and

$$\theta' = 1 - \frac{T_\infty - T}{\frac{p_B^*(T_\infty)}{K_B} \left(\frac{dT}{dp}\right)^*_{B,T_\infty}} \tag{112}$$

where K_B is given by Equation (94) for $p_B^* \gg p_A^*$. Using the notation * for the convolution, Equations (110) and (77) for mass and heat transport become

$$-2 \frac{\sqrt{Lu'}}{1-\varepsilon} (x'_\infty - x'_s)\, P = \left(\dot{P}^2\right) * \frac{1}{\sqrt{\pi \tau}} \tag{113}$$

$$2\, Ja'\, (1-\theta'_s)\, P = \left(\dot{P}^2\right) * \frac{1}{\sqrt{\pi \tau}} \tag{114}$$

The similarity of the two processes, as evidenced by the analogous form of Equations (113) and (114), implies that during the collapse, interface temperature and composition remain constant, as given by

$$- \frac{x'_\infty - x'_s}{1 - \theta'_s} = (1-\varepsilon) \frac{Ja'}{\sqrt{Lu'}} \tag{115}$$

subject to the phase equilibrium relation, which from Equations (22) and (23) for the case component A is nonvolatile becomes

$$x'_s = \theta'_s - (1 - x^*) \tag{116}$$

where x^* is the liquid equilibrium composition at T_∞ (see Figure 2).

The nonlinear integral equation, Equation (113), is linearized by the approximation

$$- 2 \frac{\sqrt{Lu'}}{1-\varepsilon} (x'_\infty - x'_s) \phi(P) = (\dot{P}^2) * \frac{1}{\sqrt{\pi\tau}} \tag{117}$$

where the function $\phi(P)$ has the form

$$\phi(P) = a + (1-a) P^2 \tag{118}$$

and a is a constant. Operating by Laplace transformation on Equation (117), subject to the initial condition $P(0) = 1$, the solution for bubble collapse becomes

$$P(\tau) = \sqrt{\frac{1}{1-a} \exp\left[C^2(1-a)^2\tau\right] \operatorname{erfc}\left[C(1-a)\sqrt{\tau}\right] - \frac{a}{1-a}} \tag{119}$$

where

$$C = 2 \frac{\sqrt{Lu'}}{1-\varepsilon} (x'_\infty - x'_s)$$

For $a \neq 0$ the collapse time, τ_c, is given by the implicite equation

$$\exp\left[C^2(1-a)^2\tau_c\right] \cdot \operatorname{erfc}\left[C(1-a)\sqrt{\tau_c}\right] = a \qquad (120)$$

while the case $a = 0$ implies asymptotic collapse.

With reference to the plot of $\phi(P)$ vs P in Figure 14 the choice of $a = 0.4$ indicates that the function $\phi(P)$ of Equation (118) closely represents the relation $\phi(P) = P$, which it approximates, over the first half of the bubble collapse. The resulting solution

$$P(\tau) = \sqrt{\tfrac{5}{3}\exp\left(\tfrac{9}{25}C^2\tau\right) \cdot \operatorname{erfc}\left(\tfrac{3}{5}C\sqrt{\tau}\right) - \tfrac{2}{3}} \qquad (121)$$

shown in Figure 15, thus closely approximates the actual bubble collapse over the interval $1 \geq P > 0.5$ while for $P < 0.5$ it indicates too rapid a collapse because $\phi(P)$ exceeds P in this region. This solution represents a lower limit for the transient. For comparison the case $a=0$ for which $\phi(P)$ satisfies both initial and terminal conditions of $\phi(P)=P$, is also included in Figures 14 and 15. Because of the inadequate approximation obtained in this case over most of the interval $1 > P > 0$, as seen from Figure 14, the resulting asymptotic bubble collapse represents a very conservative upper limit.

As for the previous solutions, the characteristic group, Ja'^2/Lu', determines the state at the interface through Equation (115) and thus the relative significance of mass to heat transport for the rate of the process.

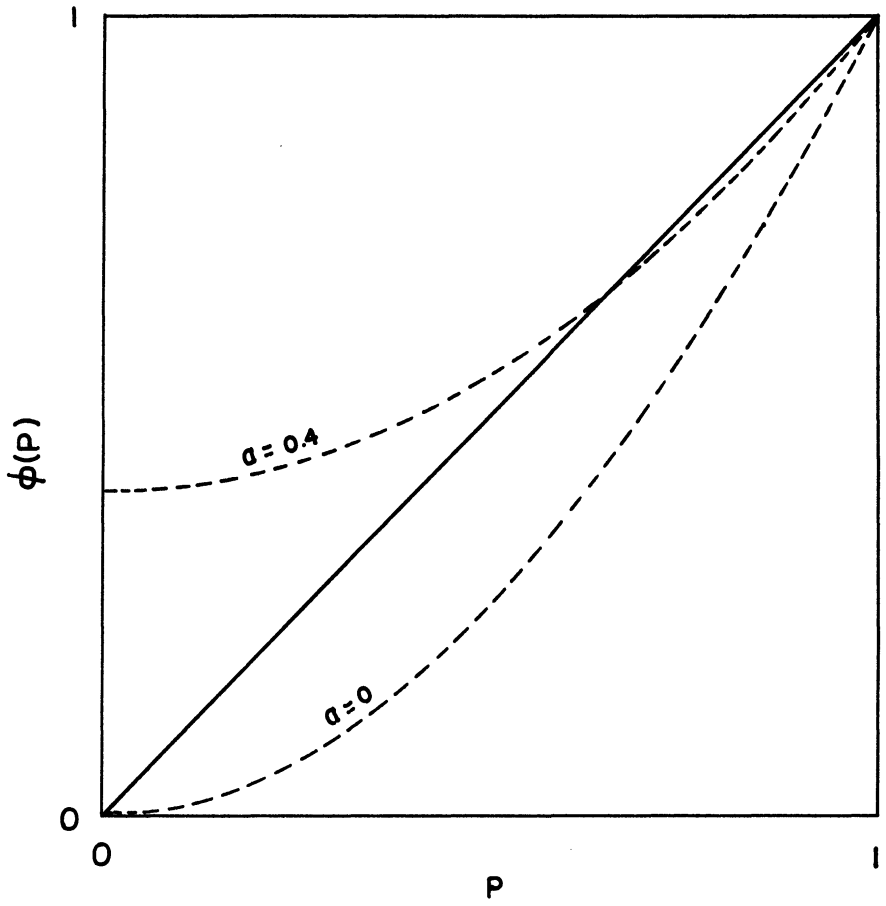

Figure 14. Approximating Function $\phi(P)$, Equation (118).

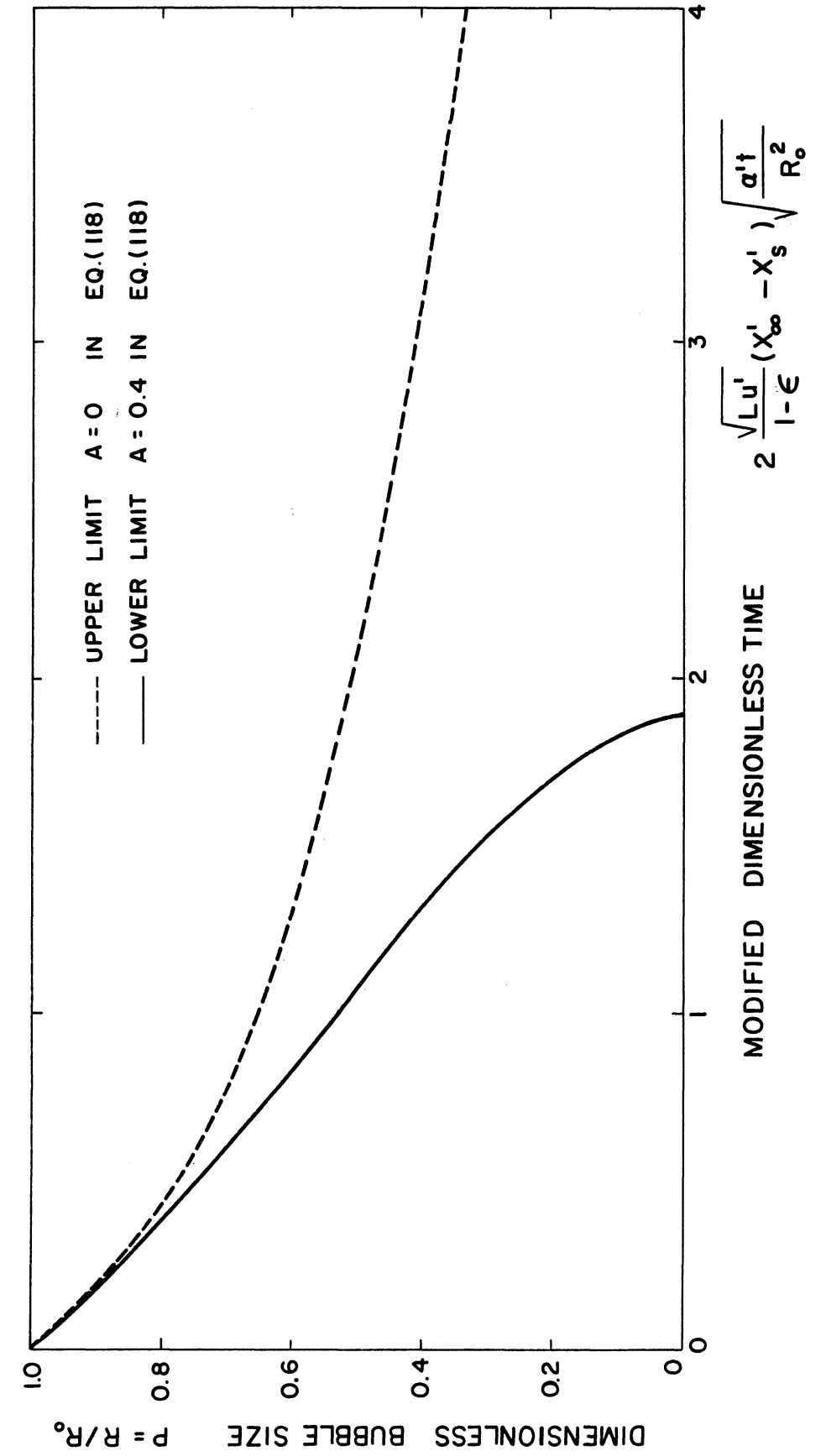

Figure 15. Dimensionless Bubble Collapse in Nonvolatile Liquid.

For very large values of $(1-\epsilon)^2 Ja'^2/Lu'$ bubble collapse becomes mass diffusion controlled and the processes can be considered isothermal. In this case $\theta_s' = 1$, and Equations (115) and (116) reduce to $x_s' = x^*$. For this case the collapse time, τ_c, which according to Figure 15 is given approximately by $\sqrt{\tau_c} \cong 2/C$, may be compared to the quasisteady solution obtained by Clark et al.[9]. Considering mass diffusion rather than heat diffusion in their model, which neglects radial convection and assumes the initial interface area, $4\pi R_o^2$, to be available for mass transfer throughout the process, the collapse time is given by $\sqrt{\tau_c} + (\sqrt{\pi Lu'}/2)\tau_c = \sqrt{\pi}/3C$. For small values of $\sqrt{Lu'}$ and τ_c this result is approximately written $\sqrt{\tau_c} = \sqrt{\pi}/3C$, indicating collapse times a factor $36/\pi$ smaller than those predicted by the present study.

CHAPTER III

EXPERIMENT

A. Introduction

This chapter describes the experimental study of gas-vapor bubble dynamics for stationary bubbles initially containing both a nonsoluble gas and a gas of high solubility. In addition, results for the case in which the bubble is permitted to detach and rise through the liquid are included to show the effect of translatory bubble motion on the dynamic bubble growth.

Water was used as the volatile liquid component in all cases. The gas to be injected was respectively nitrogen, helium and ammonia.

While the actual process of gas injection into a liquid is simple to repeat experimentally, the analytical idealization of the stationary bubble with its initial non-equilibrium conditions cannot be duplicated exactly by experiment. The analytical model may, however, be approached closely, a main objective in the design of the experiment. The key features of the experiment are, firstly, to introduce the gas phase into the liquid in a time very short compared to the time for appreciable bubble growth, secondly, to maintain the bubble stationary in the liquid. This has been accomplished by a specially designed bubble injector. The bubble is formed and maintained attached to the 1.5 mm I.D. tip of the injector during its transient growth. The injector tip may face downward and upward in the liquid during the experiment. In the downward position the static equilibrium shape of the formed bubble deviates from the sphere in being slightly

oblate. When the injector tip faces upward the static shape is oblong. The latter configuration being less stable was almost exclusively used for the study of the bubble having translatory motion, by injecting a sufficient amount of gas to facilitate departure from the tip.

B. Apparatus

The general view of the experimental apparatus in Figure 16 shows from left to right, gas cylinder, instrument panel, cameras, insulated view tank (test section proper) and instrument table. The close-up of the view tank in Figure 17 shows its 3 inch styrofoam insulation, the 1 kw immersion heater, bubble injector, gas preheater coil, thermocouples, and connections for gas flow and pressure regulation.

The diagram for gas flow, pressure control and instrumentation is shown schematically in Figure 18. The gas used in the experiment is first passed from the cylinder equipped with pressure regulator through two silica gel absorbers in series to remove possible traces of water vapor. Before entering the bubble injector the gas is preheated essentially to the liquid temperature in a 1/8 inch stainless steel tube coil submerged in the liquid. The gas pressure in the bubble injector is measured with a standard 30 inch mercury manometer connected to the return line from the injector. To ensure purity and constant pressure of the gas, a small steady flow of about 0.2 - 0.5 liters/min is permitted to pass through the injector by bleeding the manometer line to the atmosphere through the sample valve, a flowmeter and a needle valve. The three-way sample valve also permits the gas flow upstream of the injector to be vented through the flowmeter, which can be connected to a sampling tube

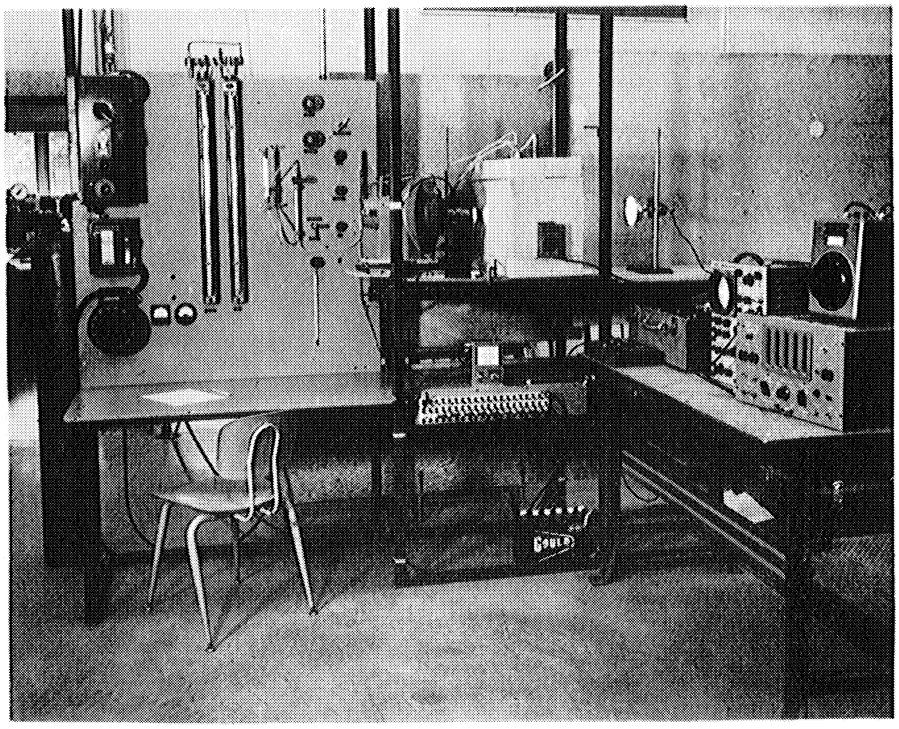

Figure 16. Experimental Apparatus. General View.

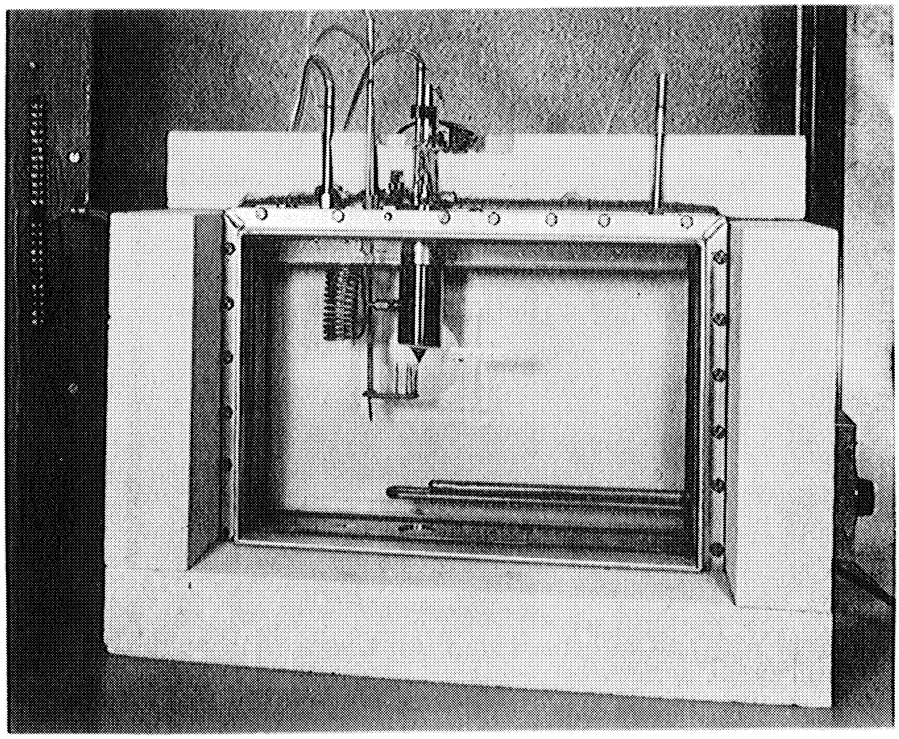

Figure 17. View Tank with Bubble Injector.

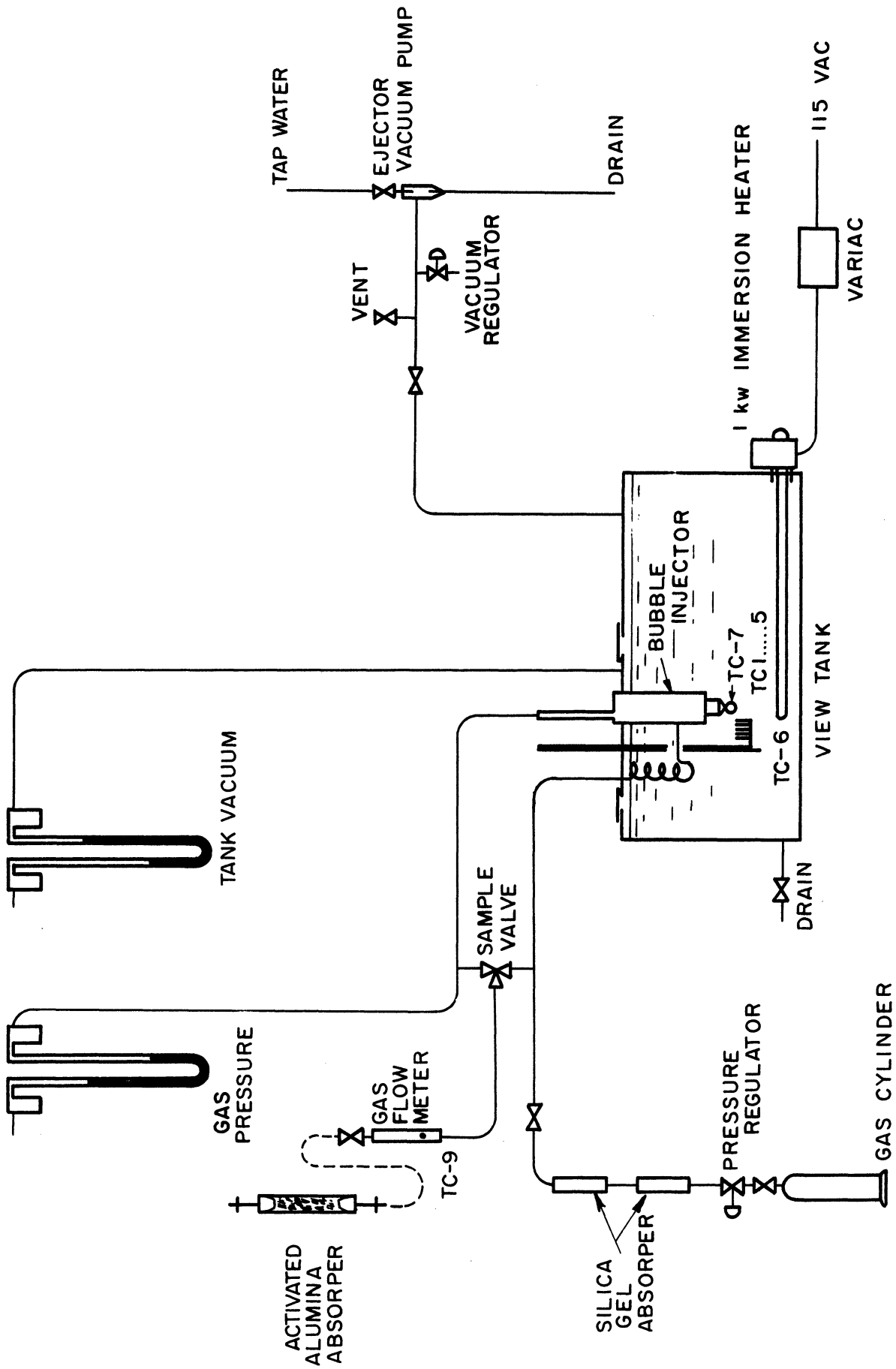

Figure 18. Schematic Diagram for Gas Flow, Pressure Control and Instrumentation.

containing activated alumina. In this way the content of water vapor of the gas respectively upstream and downstream of the injector may be obtained by accurate weighings of the sample tube, hereby checking for possible leaks around the injector valve causing diffusion of water vapor into the gas.

The tank pressure is adjustable between atmosphere pressure and about 20-25 inch mercury of vacuum by means of an ejector pump driven by tap water. The pump suction line is connected to the vapor space of the closed view tank through a shut-off valve and can be vented either directly from the atmosphere through another shut-off valve or through a conventional inverted pressure regulator. The tank pressure is measured with a standard 30 inch mercury manometer connected to the vapor space.

The view tank and bubble injector, being components designed specifically for the experiment, will be described in detail. The 17x11x2-1/8 inch view tank, holding the experimental liquid, is constructed from 2-1/8 inch stainless steel channels welded into a frame, sandwiched between the 1/2 inch Pyrex glass sides by two 1-1/2 inch welded angle frames bolted together. The tank lid, which closes a 6x1-3/4 inch opening in the tank top, serves as mounting plate for the bubble injector, gas preheater coil and thermocouple support. The bubble injector is shown disassembled in Figure 19 and in section in Figure 20. A 6 volt, D.C., 24-oz. solenoid L with adjustable core stop K for the plunger M , is mounted on the top plug E in the cylindrical 1-3/4 inch O.D. casing H . The solenoid plunger M is connected to the valve, P , which forms a 60° conical seat near the tip of the 1.5 mm I.D. nozzle R by means of the Spring, S .

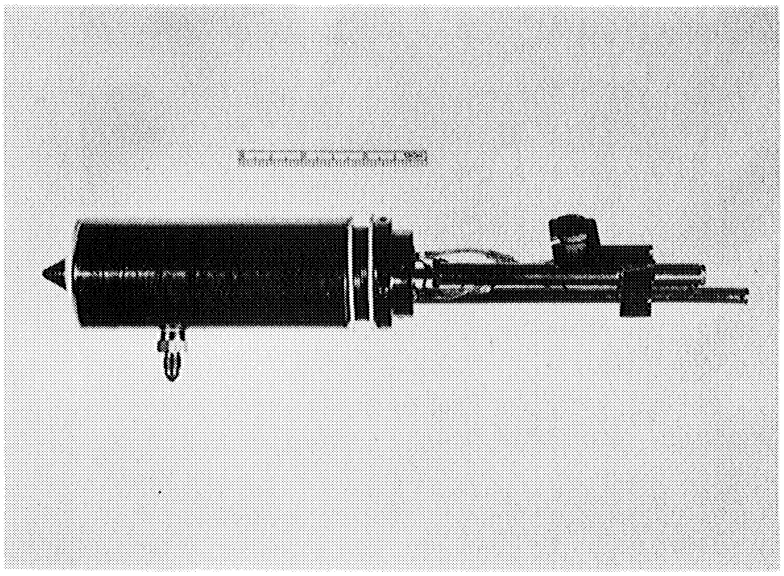

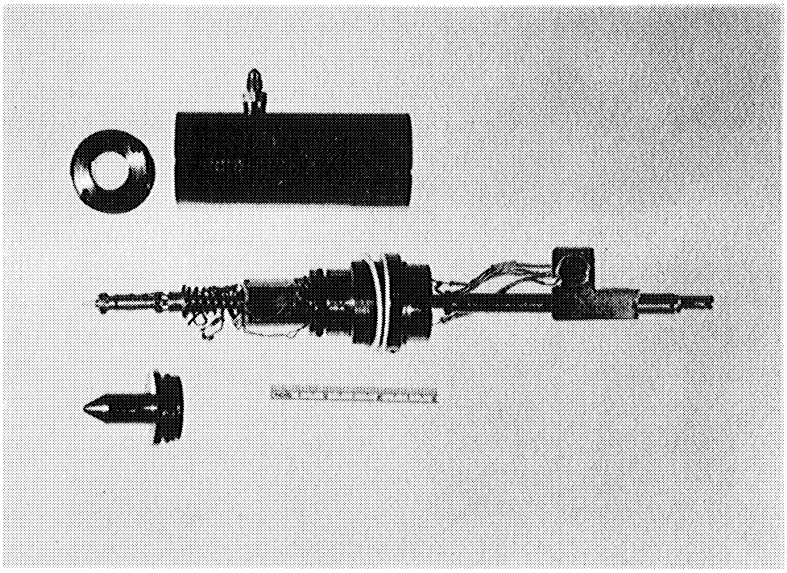

Figure 19. Bubble Injector (Assembled and Disassembled).

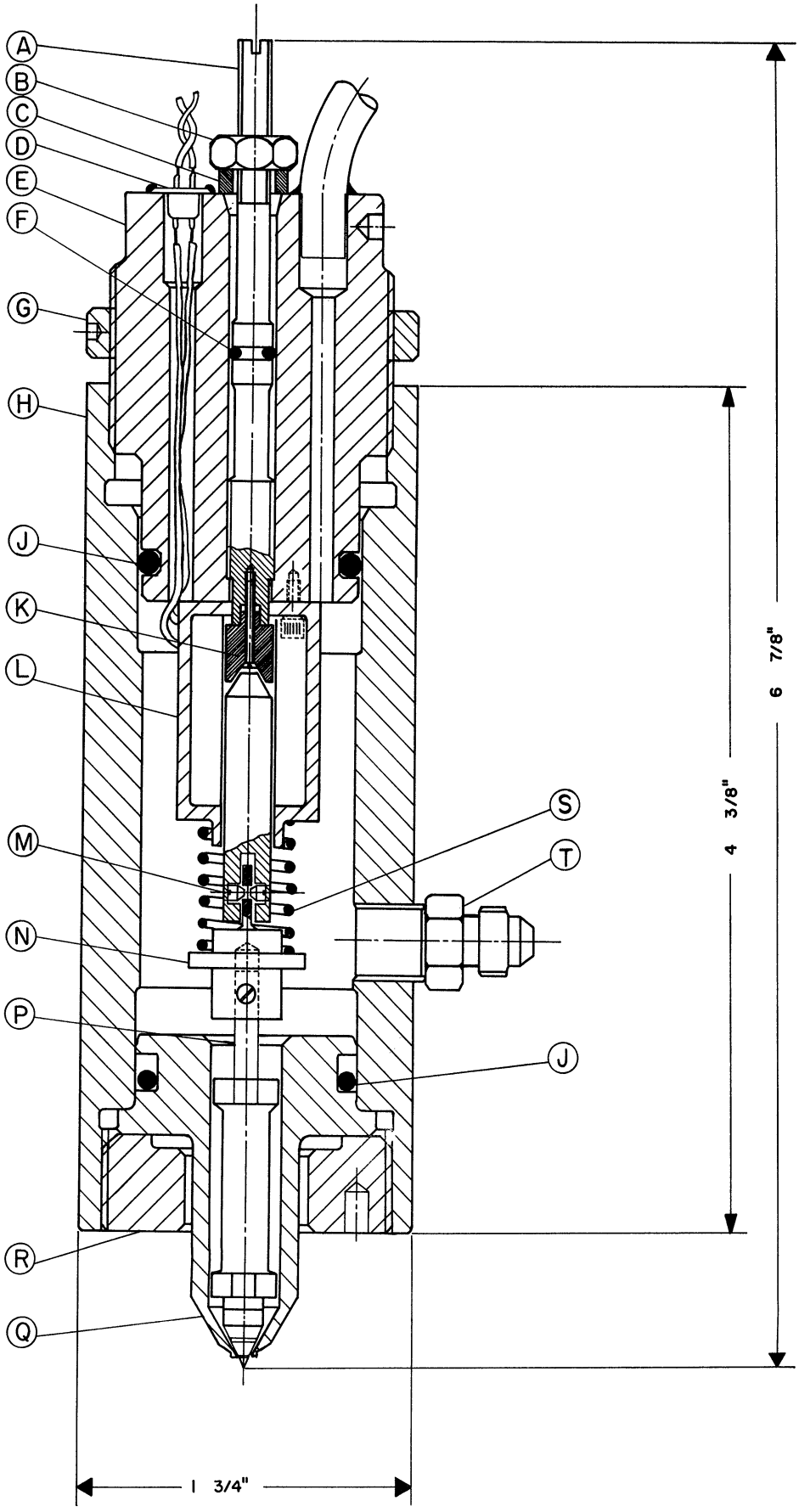

Figure 20. Section of Bubble Injector.

Gas from the preheater coil is supplied at the fitting, T, to the inside of the casing, which is sealed at all joints with O-rings. The 1/4 inch bleed-off line is soldered to the top plug E through which leads for thermocouples and solenoid power enters by means of insulated glass seals. The valve stroke is adjustable from outside the injector by the screw A sealed in the center hole of the top plug by an O-ring. The moving parts, N and P, are machined from aluminum to reduce the mechanical time constant of the spring-valve system. A teflon valve tip, attached to the valve stem with a press fit, is used to prevent damage to the valve seat and to ensure a perfect seal. The remaining parts are machined from brass and finished with a chrome plating. The nozzle is designed to minimize the residual gas volume exposed to the liquid prior to bubble formation by placing the valve seat as close as structurally possible to the end of the nozzle tip. In addition, it was desirable to keep the bubble far removed from the main body of the injector. Bubble formation is accomplished by energizing for a short period of time the solenoid, giving a valve lift sufficient for a flow of gas needed to form a single bubble. Adjustment of valve stroke, energizing time and voltage of the solenoid, spring tension, and gas pressure permits the desired initial bubble size to be attained.

All temperature measurements were carried out using 22 gauge copper-constantan thermocouples each having separate cold junction at the ice-point. The EMF is measured with a Leeds & Northrup Model 8662 portable precision potentiometer. The liquid temperature and its distribution is measured with six thermocouples (TC-1 ... TC-6), positioned as shown in

Figure 18. The thermocouples are suspended from a 3/16 inch stainless steel tube entering the tank lid through a conax fitting with teflon seal, and are embedded in epoxy which also serves as seal. To prevent direct contact of the junction with the water, the thermocouple ends were coated with thermal hardened heat resistant paint. The temperature of the gas to be injected is recorded with thermocouple TC-7 which is installed in the gas space just above the valve seat inside the bubble injector. Thermocouple TC-9 is installed in the bleed line at the flowmeter inlet to allow for temperature corrections on the flowmeter readings.

For heating and temperature control of the liquid, the view tank is fitted with a 1 kw immersion heater with stainless steel blades and thermostat. The heater power is adjusted with a variac.

The transient bubble size was recorded as shown in close-up in Figure 21 with a Beckman and Whitley DYNAFAX Model 326 high-speed camera timed with the bubble injection moment to give the beginning and major part of the event. The film length in the camera being limited to 36 inches of 35 mm film, equivalent to a total of 224 successive frames, limits either the resolution (time interval between frames) or the total writing time. The film speed is adjustable between 200 and 26,000 fps (frames per second), and remains constant during a recording at a value which can be read accurately on an electronic counter connected to the magnetic camera pick-up. Depending on the particular conditions for the experiment the main part of the bubble growth event lasts 50 - 200 ms (milliseconds) and the film speed is accordingly chosen to 4,000 - 1,000 fps. This record of the transient was supplemented for greater values of

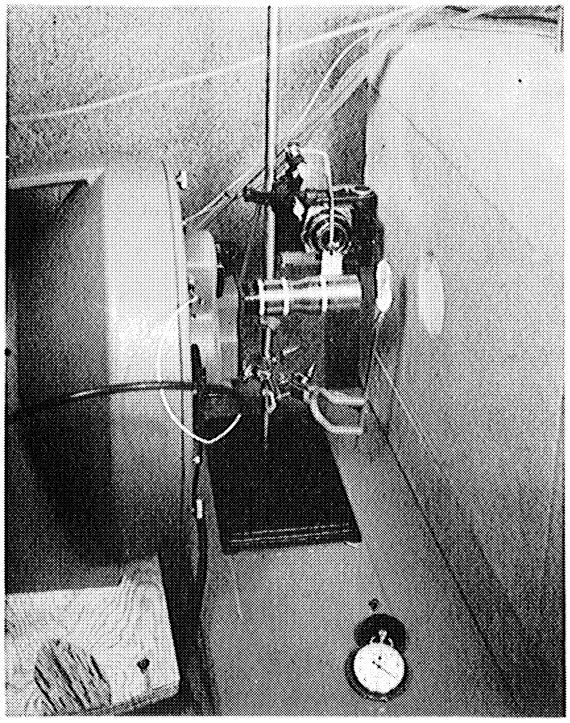

Figure 21. Close-up of Dynafax Camera in Position for High Speed Film Recording.

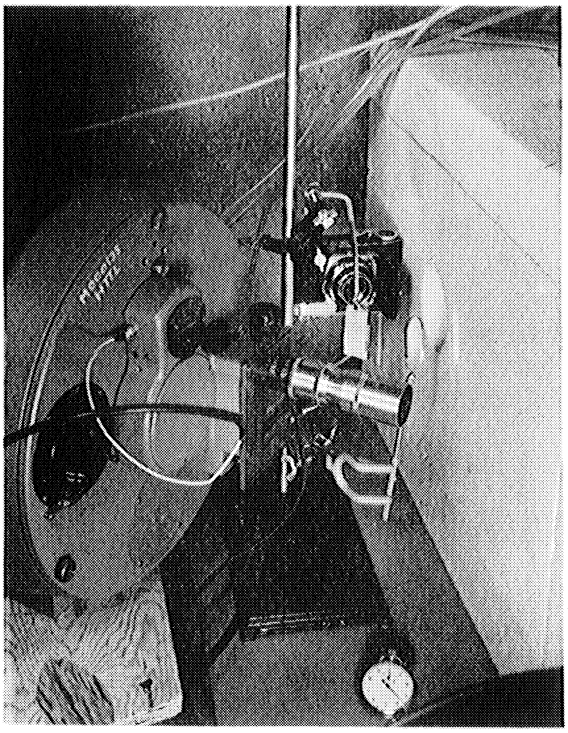

Figure 22. Close-up of 35-mm Camera in Position for Recording of Single Frames.

time by taking one or several still pictures with a single frame 35 mm camera, shown in position in Figure 22. A representative photographic record for a single experiment (Run 523) is reproduced in Figure 23, showing the negatives every second frame of the high speed film and a single exposure from the 35 mm camera. Each frame shows the downward facing tip of the bubble injector on which the bubble is formed, and the hot junction of two of the upward pointing thermocouples positioned in a plane behind the axis of the injector. Frame number 0 of the high speed film shows the injector tip prior to gas injection which is completed between frame numbers 3 and 4.

The wiring for the high speed camera and the optical characteristics of the system is shown in the schematic Figure 24. As evidenced from Figure 17, the view tank was completely surrounded with pieces of expanded polyethylene plate and open to the ambient only through two circular holes, one in each side, serving respectively as observation and light port. The latter was covered with a ground glass plate which made the back lighting from the 150 watt flood light uniformly diffuse. The closed tank in conjunction with the diffuse backlighting gives ideal conditions for a clear and contrasty picture of the bubble. The center portion of the bubble will transmit light while more and more is reflected as the perifery is approached. Total reflection occurs when the angle between bubble interface and line of sight exceeds Arcsin (n'/n"), where n' and n" are the indices of refraction for respectively the liquid and the gas phase. Because side light is excluded a perfectly sharp black edge of the bubble perifery is obtained. In addition these optical characteristics aid in visualizing the approximate bubble shape when this departs from that of a sphere.

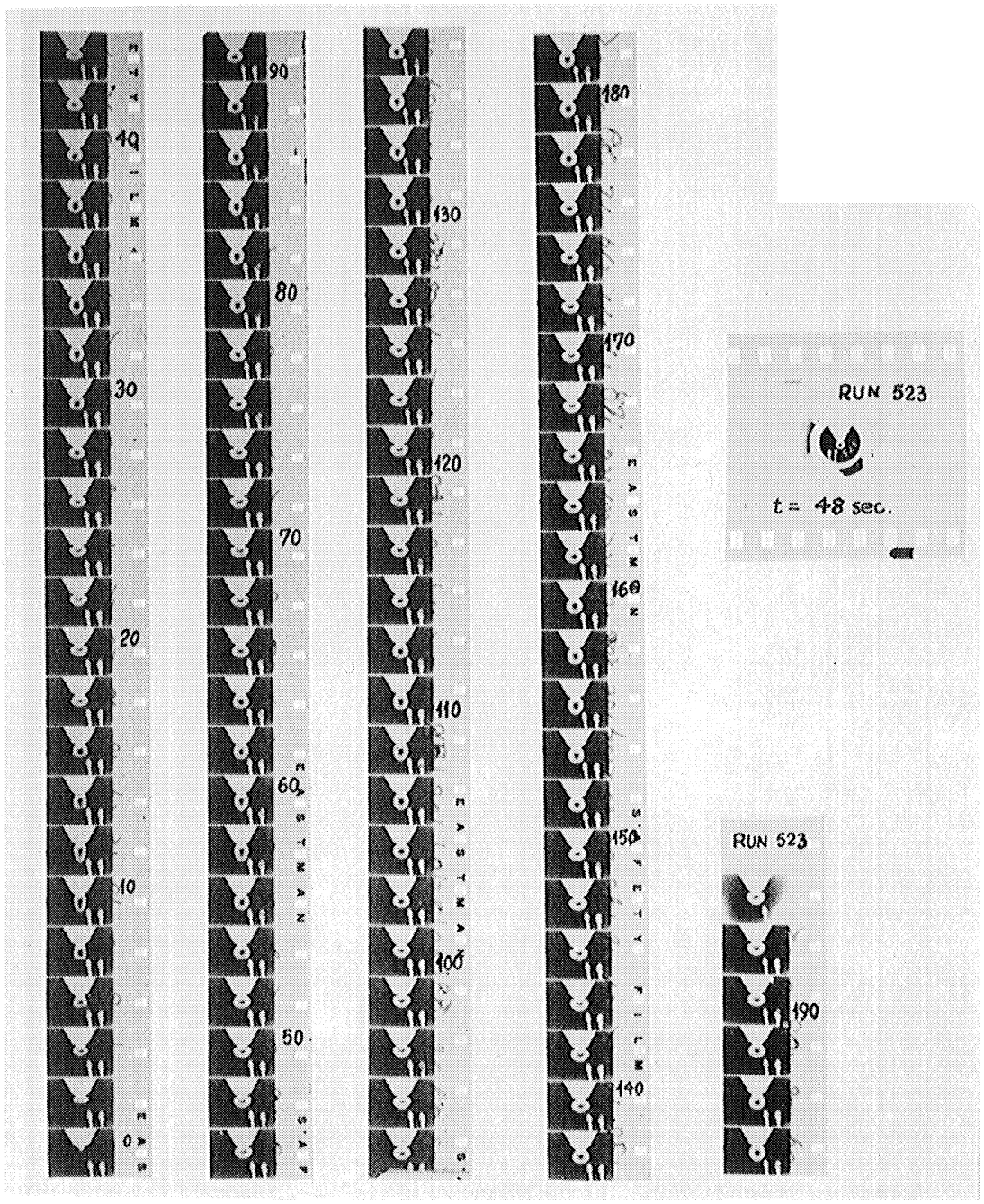

Figure 23. High Speed Film Record and Single Frame from Run 523. One Half of the High Speed Film is Reproduced, Showing Every Second Frame. Film Speed: 1008 fps.

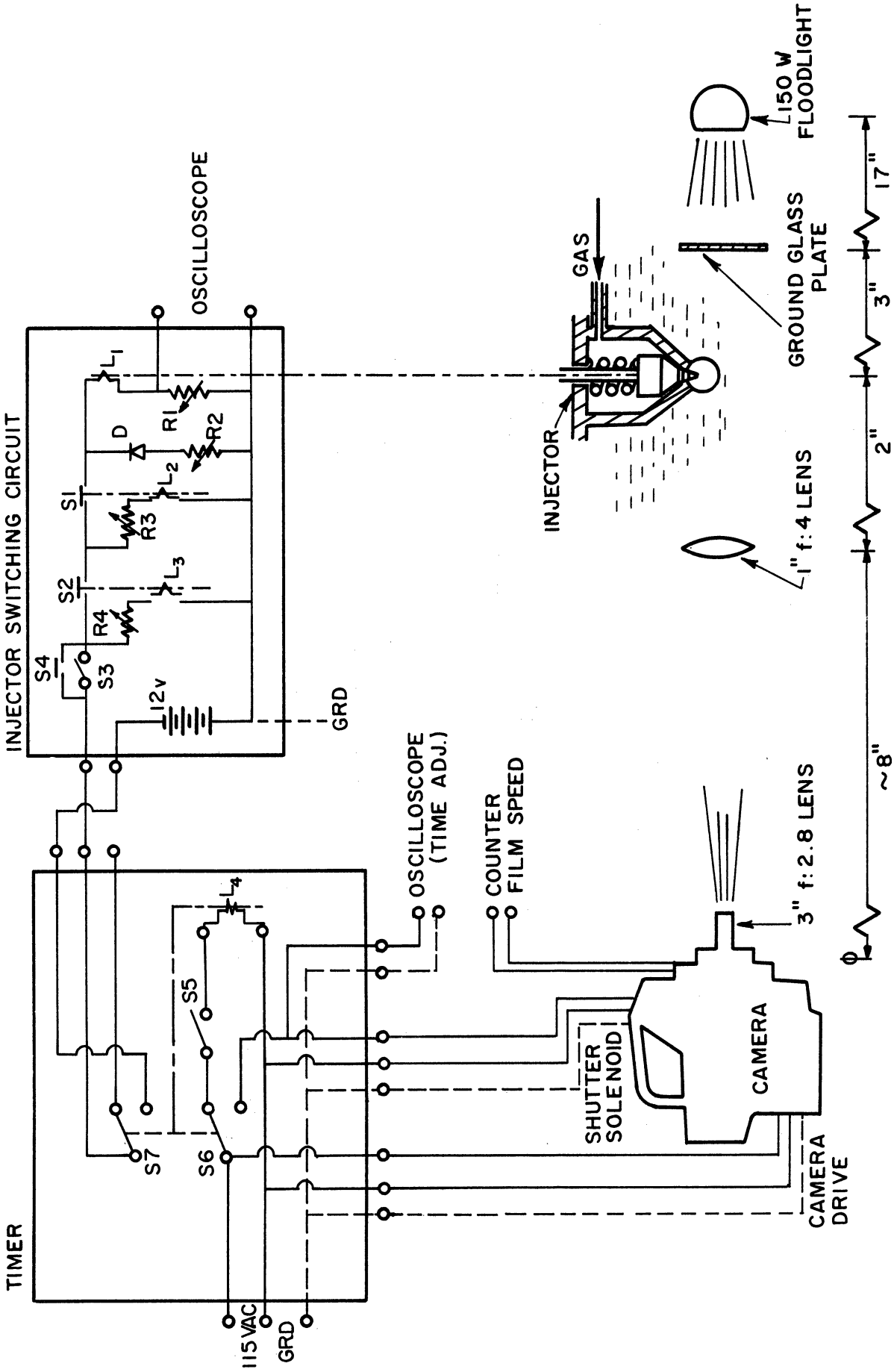

Figure 24. Schematic for Wiring of Camera, Timer and Injector Circuit.

The electrical circuits for bubble formation and camera shutter control are shown in the schematic in Figure 24. Because the built-in timer in the high-speed camera shutter had an upper exposure time limit of 60 ms it was necessary to use an external timer for film speeds below 4000 fps. The circuit for the timer, built for this purpose, is shown in Figure 24, where L4 is the solenoid of a double pole, double throw type NE-22 Agastat adjustable time delay relay. When the manual switch S5 is closed momentarily the solenoid L4 throws S6 and S7 to the opposite positions of those shown, which are held for the adjusted time delay before again released. Switch S6 connects the shutter solenoid to 115 VAC while S7 puts the 12 V battery voltage on the injector switching circuit where S3 is in closed position. The subsequent sequence of events with approximate delay times relative to the moment of initiation are as follows. The shutter is released by the solenoid after 3 - 6 ms and reaches fully open position after 24 - 27 ms. Switch S2, normally open, closes after 15 - 25 ms starting the current through relay coil L2 and injector solenoid L1, which starts the opening of the valve at 30 - 35 ms. At 33 - 38 ms solenoid L2 opens the normally closed switch S1 whereby L1 is de-energized and the valve is again in closed position at 34 - 39 ms. With the shutter timer of the camera in position B, the film is exposed till the shutter solenoid is de-energized at the end of the time delay set by the external timer, namely when S6 and S7 return to their normal positions. It should be recalled that S5 was only closed momentarily to initiate the sequence of events and is thus open when S6 closes, preventing a repetition of the cycle. The sequence of events is shown schematically in Figure 25. When

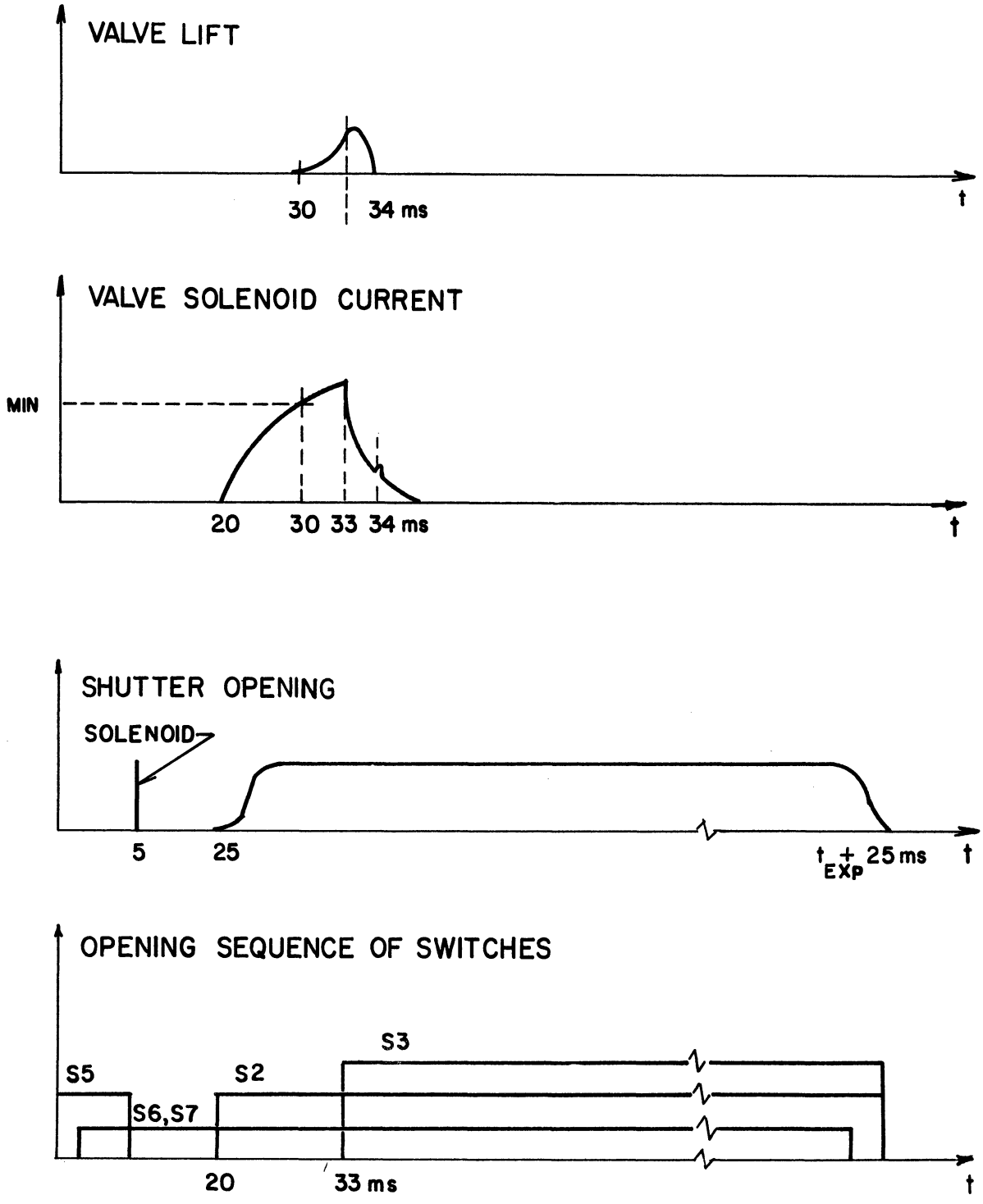

Figure 25. Schematic of Syncronization of Film Exposure and Bubble Formation.

the built-in timer in the camera shutter is used, its setting determines the exposure time, and the same circuitry is used.

The desired syncronization of the events is achieved by proper adjustment of timer delay and resistors R1, R2, R3 and R4, determining the respective time constants for the R-L circuits. The effective time for the flow of gas through the valve, from its motion starts till again fully closed, may be obtained from an oscilloscope record of the voltage drop over resistor R1, representing the solenoid current. Actual recordings of this voltage as taken of the oscilloscope with a Polaroid camera are shown in Figure 26. Referring to the schematic Figure 25 the beginning of the valve motion is identified by a minimum current, i_{min}, measured once for all for a given spring tension as the current necessary for starting valve motion. The mechanical impact at the closing of the valve manifests itself in a small blip of induced current super-imposed the exponential decay. The bubble formation time obtained this way is 3 - 4 ms which is in agreement with film recordings of bubble formation in case of no growth, as discussed below.

C. Experimental Procedure

In preparation for a series of experiments for the case of a non-soluble gas the electrical resistivity of the liquid (single distilled water in all cases) was checked to exceed 200,000 ohm-cm. For the case of a soluble gas the resistivity was read subsequent to each experimental run. Careful degassing was carried out at atmospheric pressure or below, depending on the conditions desired later. Before and after a series of experiments sampling for water vapor in the gas stream vented before and after

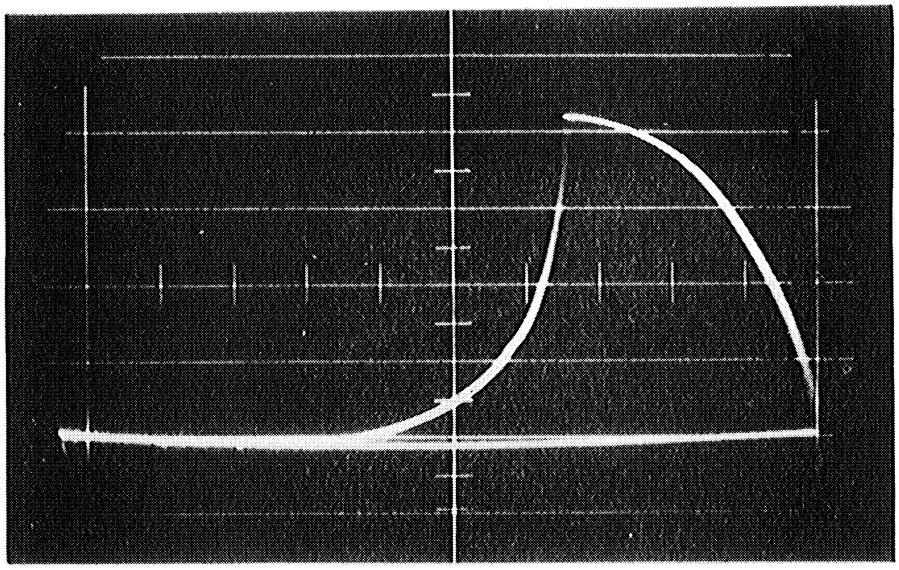

(a)

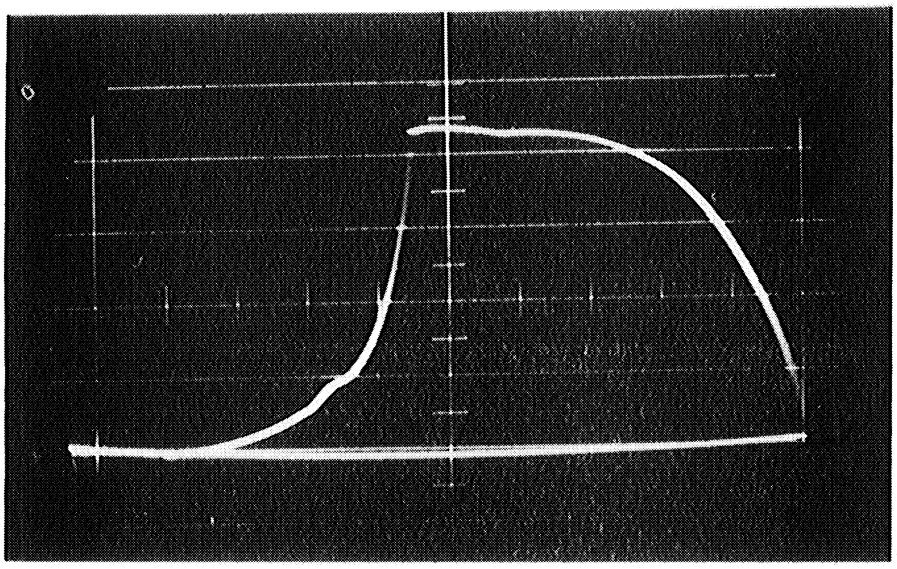

(b)

time (2ms/unit of scale)

(Necessary current for valve motion, $i_{min} \cong 8.2$ units on ordinate scale)

Figure 26. Oscilloscope Record of Solenoid Current During Bubble Formation.

a. Energizing time adjusted for bubble formation without departure. Impact, when valve seats, visible as small blip as current decays.

b. Energizing time increased for the formation of a large departing bubble. Impact when valve reaches fully open and fully closed position visible as blip on respectively curve for current rise and decay.

the bubble injector was done by means of the activated alumina sampling tube. The mass of gas sampled was determined from the time of sampling and from gas flow meter readings, corrected for type of gas, pressure and temperature. The mass of absorbed water vapor was obtained from successive weighings of the sampling tube on a micro-balance to 0.5 mg accuracy. In all cases of a nonsoluble gas the content of water vapor was found less than 100 pm, or in terms of molefraction, less than 10^{-4}. This is less than the uncertainty in determination of the initial composition in the bubble and in the order of magnitude of the maximum gas impurity, which according to the manufacture's catalog was respectively 0.3% and 0.01% for the nitrogen and helium used. For the present purpose the gases were therefore assumed to be pure. Comparing samples before and after the injector, no increase in water vapor content could be detected and it was concluded that the injector valve seat was leak proof for diffusion of water vapor into the gas. Leaks in the opposite direction, readily detectable visually, were not encountered.

Prior to a specific run the temperature and pressure were adjusted to and kept at their desired values for a sufficient period of time to insure uniform temperature of liquid, tank and bubble injector. After the heater was shut off the system was left for several minutes to permit convective currents to decay. The drift in temperature owing to the small heat flow to the ambient amounted ot 0.1 - 0.4°F/min. The lateral temperature variation as checked with the five upper thermocouples (TC-1 ... 5 of Figure 18) did not exceed 0.1°F/cm, and the vertical thermal gradient obtained from TC-1 and the lower thermocouple TC-6, was no greater

than 0.15°F/cm, when an experiment was carried out. For the case of a soluble gas the liquid was thoroughly stirred prior to heater shut-off to ensure uniform composition throughout. With the high speed camera at the desired speed as read on the counter and the back light switches on, the event was triggered by momentarily closing switch S5 of the timer unit (see Figure 24). At the same time a stop-watch was started to fix the time for the single frames taken with the 35 mm camera. The high intensity floodlight, not needed for the single frame exposures, was only switches on during the high speed film recording to prevent heating of the liquid. From readings of the thermocouples in the liquid no temperature change could be traced to result from the use of the flood light over periods of time up to one minute, the maximum time this light was on during an experiment. Immediately following the event, tank vacuum, hydrostatic pressure, barometer and temperature readings were made.

After every other run the high-speed films and corresponding single frames were developed. For both cameras it was found satisfactory to use Kodak Plus-X negative film, normally developed and fixed. For the high speed camera triple perforated 35 mm film was used to enable subsequent slitting of the film into two 16 mm single perforated strips, suited for conventional movie projection.

C. Reduction of Data

1. Properties

The state of the bulk liquid is defined by its temperature, T_∞, pressure, p_∞, and composition x'_∞. The temperature was obtained as the mean value of TC-1 ... TC-3, the three thermocouples closest to the bubble,

corrected according to the calibration for the particular gauge 22 copper-constantan wire used. The calibration curve was based on the ice-, steam- and tin-point. The liquid pressure at the location of the bubble was obtained from barometer readings corrected for temperature, the reading of tank vacuum and hydrostatic head of the liquid in the tank corrected for its temperature. The equilibrium gas composition, x_∞ at T_∞, was calculated from steam tables[30] according to Equation (22). For the case of a non-soluble gas the liquid was considered pure water when the electrical resistivity exceeded 200,000 ohm-cm. In the course of the sequential injection of several bubbles of the soluble gas, the liquid composition deviated slightly from that of pure water, $x'_\infty = 1.0$. The measured resistivity was related directly to composition with the use of the standard curve shown in Figure 27, obtained from resistivity measurements of solutions of ammoniahydroxide of known concentration. As seen from Figure 27 the resistivity was found not to change with temperature over the range 26-37°C, in which the measurements of liquid samples were also conducted. In all experiments using ammonia as the gas, the mole fraction of ammonia, $1 - x'_\infty$, was in the range 10^{-5}-10^{-4}.

The thermal diffusivity $\alpha'(T_\infty)$ is obtained from Jakob and Hawkins[28] and the two important dimensionless property groups, Ja and Lu, are evaluated at T_∞ from the graphs shown in Figures 28 and 29. The plot of Ja-numbers vs temperature for water was prepared from steam tables[30] according to the definition of Equation (50). The Lu-number for the diffusion of water vapor through respectively nitrogen, helium and ammonia was evaluated from Gilliland's equation[1]

---

[1] For the pressure and temperature range investigated in the present study, Equation (122) gives values of the mass diffusivity consistent with those determined when using the more accurate Chapman-Enskog formula (see Reference 5 p. 510 ff).

$$\mathcal{D}''_{AB} = 0.0043 \frac{T^{3/2}}{p\left(V_A^{1/3} + V_B^{1/3}\right)^2} \sqrt{\frac{1}{M_A} + \frac{1}{M_B}} \qquad \left[\frac{cm^2}{sec}\right] \qquad (122)$$

where T is the absolute temperature in °K, p the total pressure in atm, M the molecular weight, V the molecular volumes (cm^3/gmole) at the normal boiling point obtained from Reference 59. In forming the Lu-number according to the definition of Equation (50), the thermal diffusivity for water was again obtained from Reference 28. The Lu-number for the diffusion of ammonia through water was calculated according to the definition of Equation (101) using the constant value[43] $\mathcal{D}' = 1.5 \times 10^{-5}$ cm^2/sec for the mass diffusivity, which is little affected by pressure and temperature.

The assumption of ideality of the binary system, prompted by the analysis, is only partly approximated by the ammonia-water system chosen for the soluble gas case. While equilibrium gas compositions calculated according to Equation (22) were found to be consistent with data summarized by Perry[43], the heat of evaporation of mixtures indicated some non-ideality. However, a value of $F = h_{fgB}/h_{fgA} = 0.8$, based on the gas composition, was found to adequately approximate the data of Reference 43 for 1 atm over the range $0.6 < x'' < 1$, and was used in the calculations. The Henry law constant K_B calculated based on vapor pressure data[30, 43] using Equation (94), is valid only for very dilute solutions. A more accurate value, used in the calculations, was obtained from the definition, $K_B = (1-x^*)/(1-x''_\infty)$, by employing the experimentally determined equilibrium molefraction x^* at T_∞, as taken from Table 24, Section 3 of Reference 43.

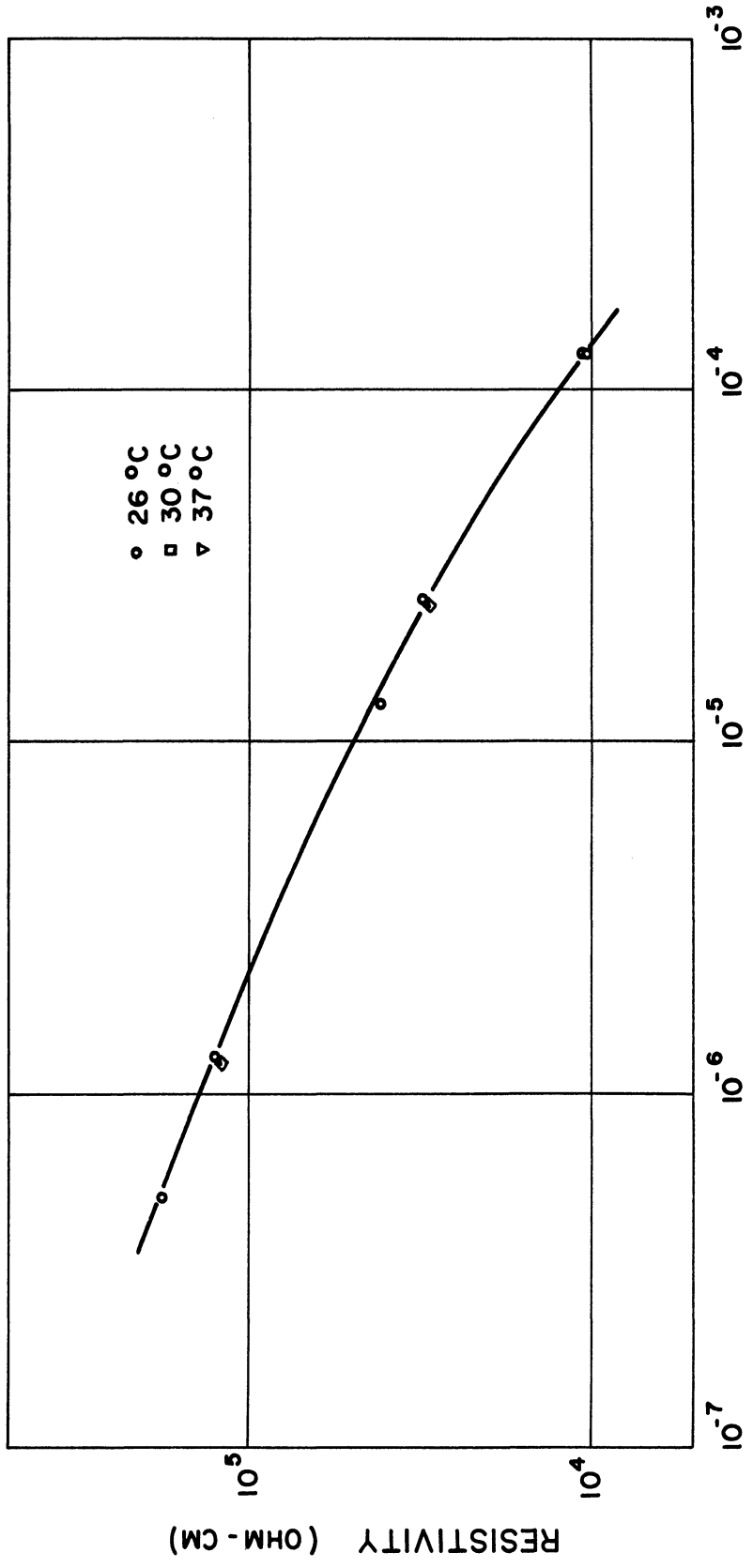

Figure 27. Calibration Curve for the Electrical Resistivity of NH_3-Solutions.

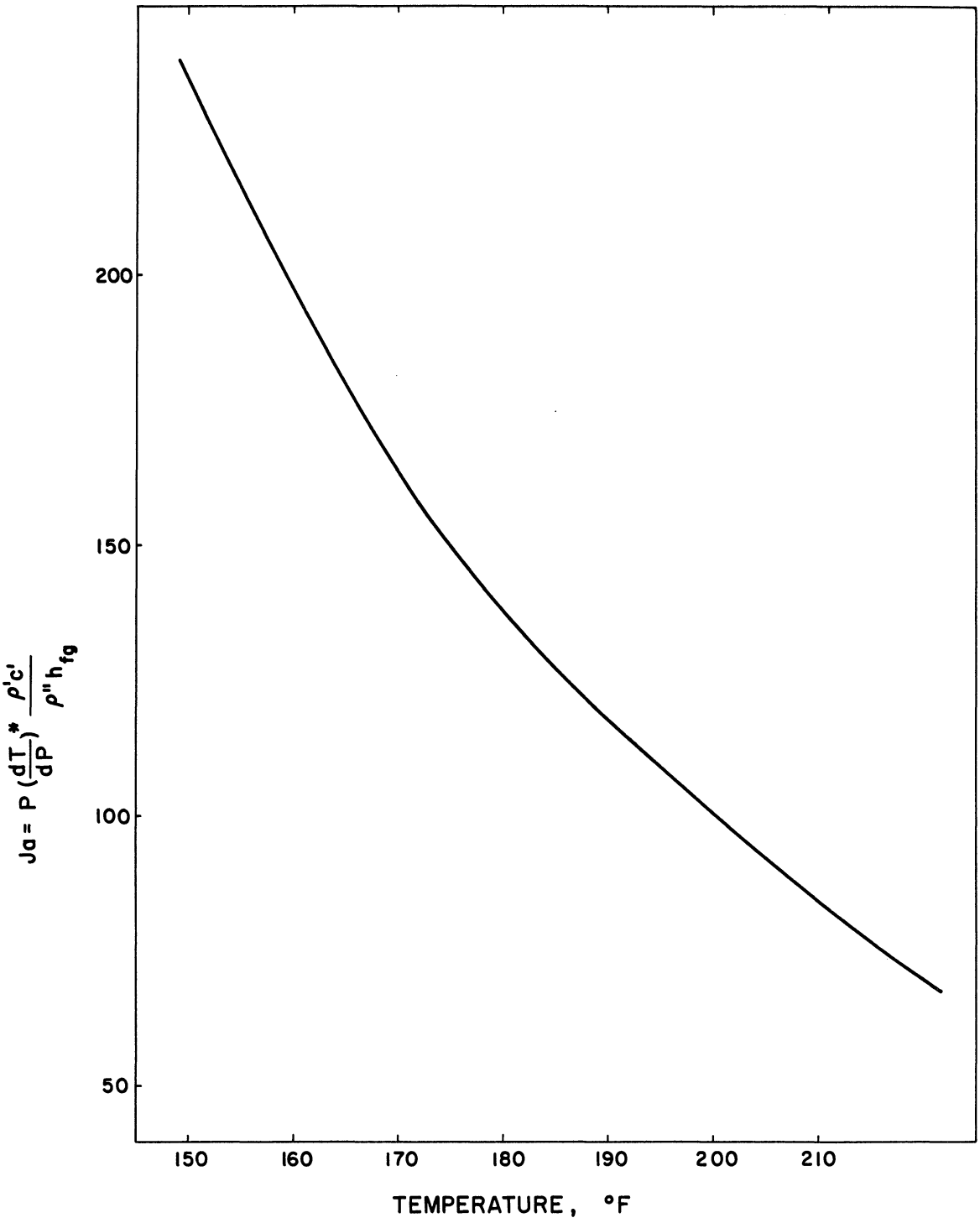

Figure 28. Ja-number vs Saturation Temperature for Water.

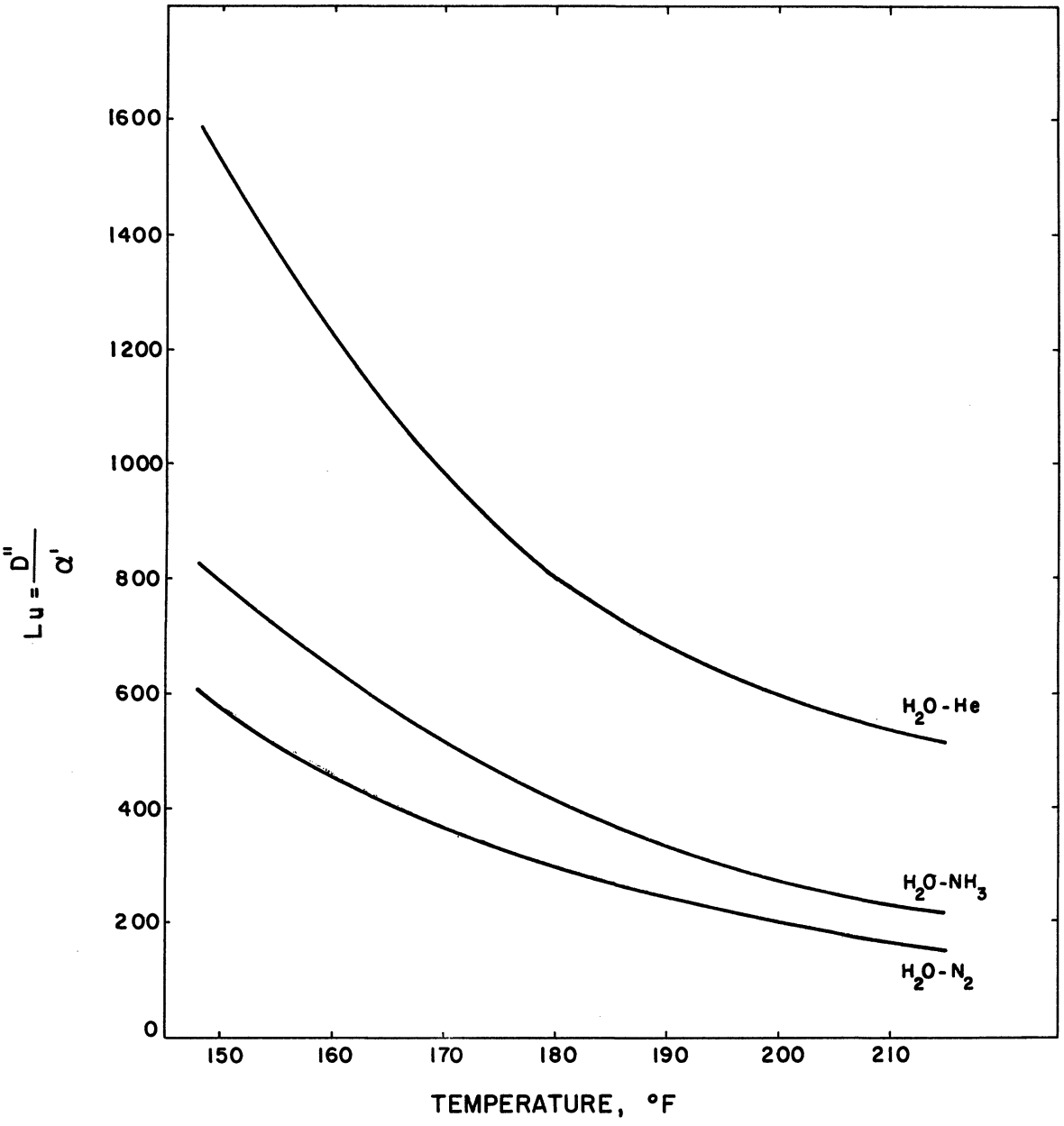

Figure 29. Lu-number vs Saturation Temperature for Water-Nitrogen, Water-Helium and Water-Ammonia.

2. Transient Bubble Size

The remaining data, in essence equivalent mean bubble radius as function of time, is obtained from the high speed film and the single frames exposed during the transient process. The approach followed in getting the initial bubble size, and composition, x_o , being important for the interpretation of the data, is subsequently explained in detail for the case of a nonsoluble gas.

The spherical symmetry in the liquid is experimentally rather undisturbed by the method of suspending the bubble from the injector tip, whereby part of its surface is left unexposed to the liquid, provided the sector taken up by the injector may be considered adiabatic. The approach to symmetry also in the gas phase calls for the displacement of the volume of the spherical sector subtended to the unexposed area of the bubble surface. Although the bubble undergoes growth this correction to the system geometry is approximately accomplished by a constant sector of 60° top angle, formed by an extension of the teflon valve tip as shown in Figure 30(a). The resulting system geometry, as shown during the growth process in Figure 30(c) and (d), simulates the analytical idealization of spherical symmetry in the two phases. The equivalent mean bubble radius is thus determined as the radius of a sphere having a volume equal to the volume displaced in the liquid, V(I) in Figure 30(c). Because of its smallness and the nonwetting nature of teflon, the ring shaped volume V_{ring} in Figure 36(a) will not be filled with liquid when a bubble has departed from the tip, but it will contain a mixture of water vapor and gas of the equilibrium composition, x_∞ . The same applies to any small cavity left

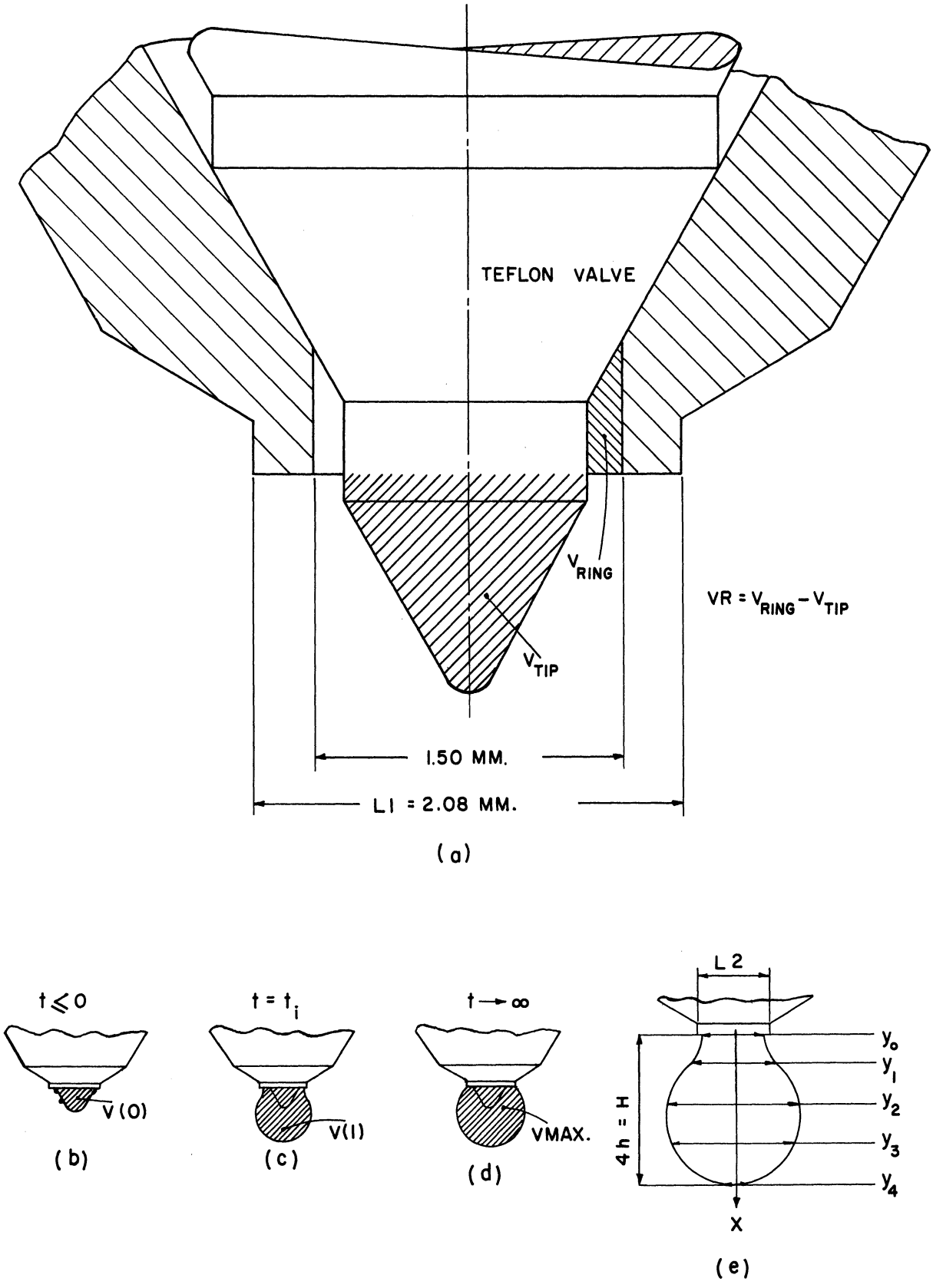

Figure 30. Characteristic Dimensions of Injector Tip and Bubbles.

on the teflon tip and visible on the film prior to the injection moment. The water vapor existing in these cavities will be present in the initial bubble formed on the injector tip and constitutes the only contribution to an initial non-zero gas composition x_o . Owing to the supposed well mixing taking place during the injection, x_o is assumed uniformly distributed and is calculated in the following way,

$$x_o = x_\infty \frac{VR + V(0)}{V0} \tag{123}$$

where

$$V0 = (VMAX + VR)(1 - x_\infty) + [V(0) + VR] x_\infty \tag{124}$$

since

$$P_\infty^3 = \frac{1 - x_o}{1 - x_\infty} = \frac{VMAX}{V0} \tag{125}$$

Here, referring to Figure 30(a), (b) and (d), VR is the difference between the ring shaped volume, V_{ring} , and the tip volume V_{tip} , V(0) is the visible volume prior to bubble formation, i.e., that of the tip plus any possible remanent cavities on this, and VMAX is the asymptotic bubble volume of the equilibrium composition x_∞ . As seen from Equation (124) the initial bubble volume, V0 , is calculated from the measured volumes V(0) , VR and VMAX and the gas composition x_∞ previously determined. This is a necessary procedure because V0 is in fact not observable but represents an idealization. Although the injection of the gas to form the initial bubble volume V0 is very rapid ($\sim$ 3 ms) the growth process is already in progress when this has been accomplished. V0 can therefore not

be obtained from the film, even if the exact formation time was known. The asymptotic bubble volume, VMAX, being a critical quantity, was obtained as follows. Starting from frame number I1, chosen about 20 frames from the end of the high speed film, the first local maximum in bubble volume was located. The arithmetic mean of the volumes on subsequent frames including the next local maximum was then determined. This mean value was taken to be VMAX unless the volume on the first still picture, recorded 30-50 sec after the introduction of the bubble, exceeded this in which case the volume from the still picture was used.

Bubble volumes were obtained in the following way from the two-dimensional picture appearing on the films. The measurements were carried out on a 30-40 times magnified picture of the negative film frame, back projected onto an opaque glass screen in a specially designed film analyzer. With a ruler system designed for the purpose the characteristic lengths as shown in Figure 30(e) were measured. Bubble length H along the axis of assumed symmetry, five diameters $y_0 \ldots y_4$ with an even spacing of H/4 along the axis, and the tip diameter L2 of the injector as reference length. Expressing the diameter variation $y(x)$ as a fourth order polynomial through the five diameters $y_0(0) \ldots y_4(4 \cdot H/4)$, a close approximation to the actual volume is obtained from

$$V(I) = \left(\frac{L1}{L2}\right)^3 \frac{\pi}{4} \int_0^H y(x)^2 \, dx = \left(\frac{L1}{L2}\right)^3 \cdot H^3 \cdot \frac{\pi}{4} \cdot INT \tag{126}$$

where

$$INT = \int_0^1 \left(\frac{y(x)}{H}\right)^2 d\left(\frac{x}{H}\right) \tag{127}$$

L1 is the true value in desired units of the reference length L2 appearing in the magnified picture. The integral INT of Equation (127) is obtained by analytical integration of the square of the approximating polynomial, $y(x)$, as obtained by Newton's interpolation formula for a polynomial of fourth order. The explicit form of INT appears in part (1) of the computer program, Appendix V-1. The equivalent mean radius, $R(I)$, of the bubble having the volume $V(I)$ is then calculated from

$$R(I) = \sqrt[3]{\frac{3}{4\pi} V(I)} \tag{128}$$

3. Computer Program

Because of the extend of arithmetic manipulation needed for the reduction of data following the above procedure, a program was prepared for the processing to be carried out on an IBM 7090 digital computer.

The computer program for the case of a nonsoluble gas comprises three main parts: reduction of experimental data, calculation of the analytical solution for the particular conditions of the experiment, and plotting of both theoretical and experimental points. The actual program written in the MAD (Michigan Algorithm Decoder) language and utilizing the subroutine library MESS (Michigan Executive System Subroutines) is reproduced in Appendix V-1. The nomenclature for the program is listed in Appendix V-2, followed in Appendix V-3 by a typical sample of the data input for a single run (RUN 523). Subsequent to general input data comes, in format, the data from each picture successively. In the process of measuring the characteristic dimensions of a bubble in the film analyser

these data cards were directly punches by the operator, made possible by locating the film analyzer, next to a conventional key-punch machine.

To illustrate the results of the digital computer program, the print-out, likewise from run 523, has been included in Appendix V-4. First, in Part 1(a) of this a complete table of the input from the bubble measurements is printed, giving frame number und characteristic lengths. Then follows in Part 1(b) the reduced experimental data in the form of initial and asymptotic conditions and a table of dimensional and dimensionless bubble growth. Next, in Part 2, the analytical solutions to dimensionless bubble growth are given: (a) for small values of time, (b) at the join point τ_1 , (c) for intermediate values of time, (d) at the join point τ_2 , and (e) for large values of time. Part 3 gives the symbols used in the plots and the dimensionless time, TAUMS , corresponding to one millisecond, and the print-out is completed by plots of respectively P vs τ and Q vs τ , in which the titles list the parameter values and substances for the experiment.

The analytical Part (2) of the computer program was used for the parameter study reported in Chapter II-D.

For the case of a soluble gas a computer program was written to include three parts, reduction of experimental data, plot of these and calculation of the initial bubble behavior according to the analysis, Equation (106). The latter part also provided numerical results from which the parameter study of Figure 13 was prepared.

E. Results

In this section the experimental results are presented and discussed, and the uncertainty of the results is illustrated by a sample calculation.

Because of the nature of the process under study -an initial value, transient problem depending on many parameters- the experimental program was planned to cover a number of particular conditions for which in each case the analytical solutions were compared to experiment. In the range of agreement between experiment and theory the results can thus conveniently be presented by the parameter study based on the analysis.

1. Discussion of Experimental Results

a. Case of a Nonsoluble Gas

In comparing experiment with theory two nondimensional representations are used, namely

$$P(\tau) = f(Ja, Lu, x_\infty, x_o)$$

and

$$Q(\tau) = (P-1)/(P_\infty-1) = f(Ja, Lu, x_\infty, x_o)$$

In nondimensionalizing time to $\tau = \alpha' t/R_o^2$, one of the five parameters, R_o, has been accommodated. The relative nondimensional bubble size, Q, normalizes growth to the interval $0 \leq Q < 1$, and was found most useful in the representation of the data.

For the case of a nonsoluble gas, the range of parameter values subject to study in the experiments reported here, using nitrogen and helium as gas and water as the volatile liquid, are summarized in Table II.

TABLE II

PARAMETER RANGE IN EXPERIMENTS FOR THE NONSOLUBLE GAS CASE

System	Ja	Lu	x_o	x_∞	R_o(mm)
H_2O-N_2	90-235	170-570	> 0.15 < 0.4	> 0.03 < 0.94	0.65-1.5
H O-He		540-1530			

The values of the Ja- and Lu-numbers are based on a system temperature range of T_∞ = 206-150°F with corresponding saturation pressures of p^* = 26.5-7.6 inch Hg abs. The presence of remanent gas prior to bubble injection sets a lower limit for x_o. The upper limit for x_∞ corresponds to a compromise between the desires for: considerable bubble growth (P_∞ = 1.8-2.4) reasonable initial size (R_o = 0.65-1.5 mm) and the bubble to stay on the injector tip when growth terminates ($R_\infty \sim$ 1.6-1.8 mm).

A summary of the experimental runs conducted is tabulated in Appendix VI-1 giving the conditions for each run. Plots of experimental data and calculated analytical solutions for a number of runs are shown in Figures 31-40, directly reproduced from the print-out obtained from the IBM 7090 digital computer according to the program shown in Appendix V-1. To clearly identify the sequence of the experimental points in the

plots a solid line has been drawn through successive points. In addition, the intermediate and asymptotic solutions joined at point τ_2 are included. The characteristic parameters for each run appears in the title of the graph, where $A(mm^2/sec)$ is the thermal diffusivity and $RO(mm)$ the initial bubble radius.

Figure 31 for Run 511, shows the bubble formation $P(\tau)$ representative for a number of runs made under conditions where no growth occurred. As seen from the title of the graph, $P_\infty = 1.009$, hence the formation size R_o, is practically identical to the asymptotic size, R_∞, and the plot shows how the equivalent bubble radius approaches its initial value in the course of 3-4 ms. The oscillations in bubble shape, being associated with a volume oscillation as discussed in Appendix II, appears clearly in the plot. Taking these into account the actual gas injection is seen to have been terminated in less than 3 ms. Because the initial bubble size is chosen considerably smaller in the cases where growth occur, by reducing the activation time of the injector valve, it can be concluded that a formation time of 3 ms was in no case exceeded, which is in agreement with the less accurate oscilloscope measurements of injector solenoid current discussed in Section III-B.

Next, relative dimensionless bubble growth $Q(\tau)$ for nitrogen in water is presented in Figures 32-37. The first three graphs, Runs 523, 504 and 702, show bubble growth under practically identical values of the governing parameters, Ja , Lu , x_∞ , x_o , but with a considerable difference in the randomly introduced initial disturbance responsible for the subsequent oscillations superimposed the transient growth. A particularly large

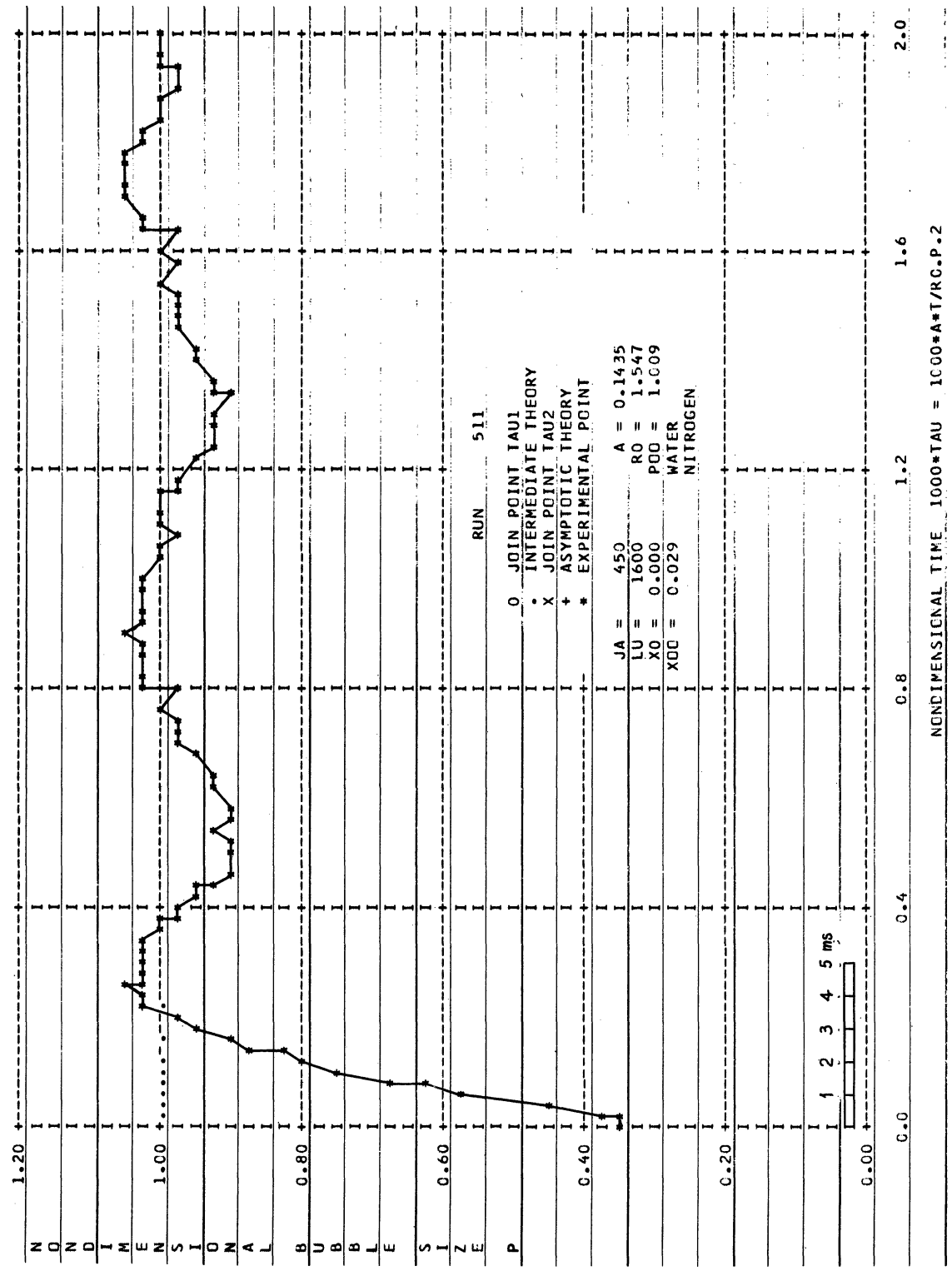

Figure 31. Bubble Formation, Run 511, P vs τ .

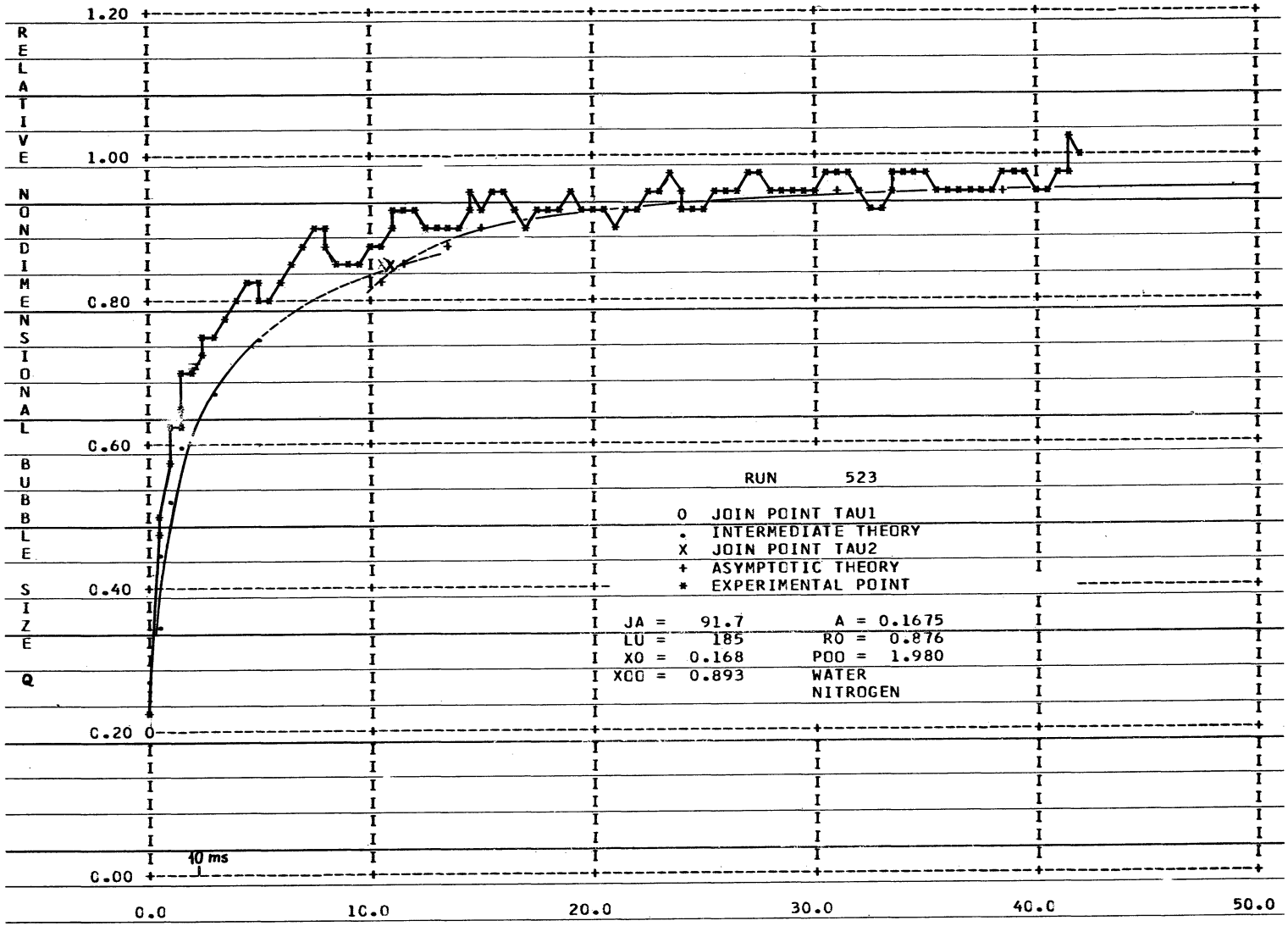

Figure 32. Bubble Growth, Run 523, Q vs τ .

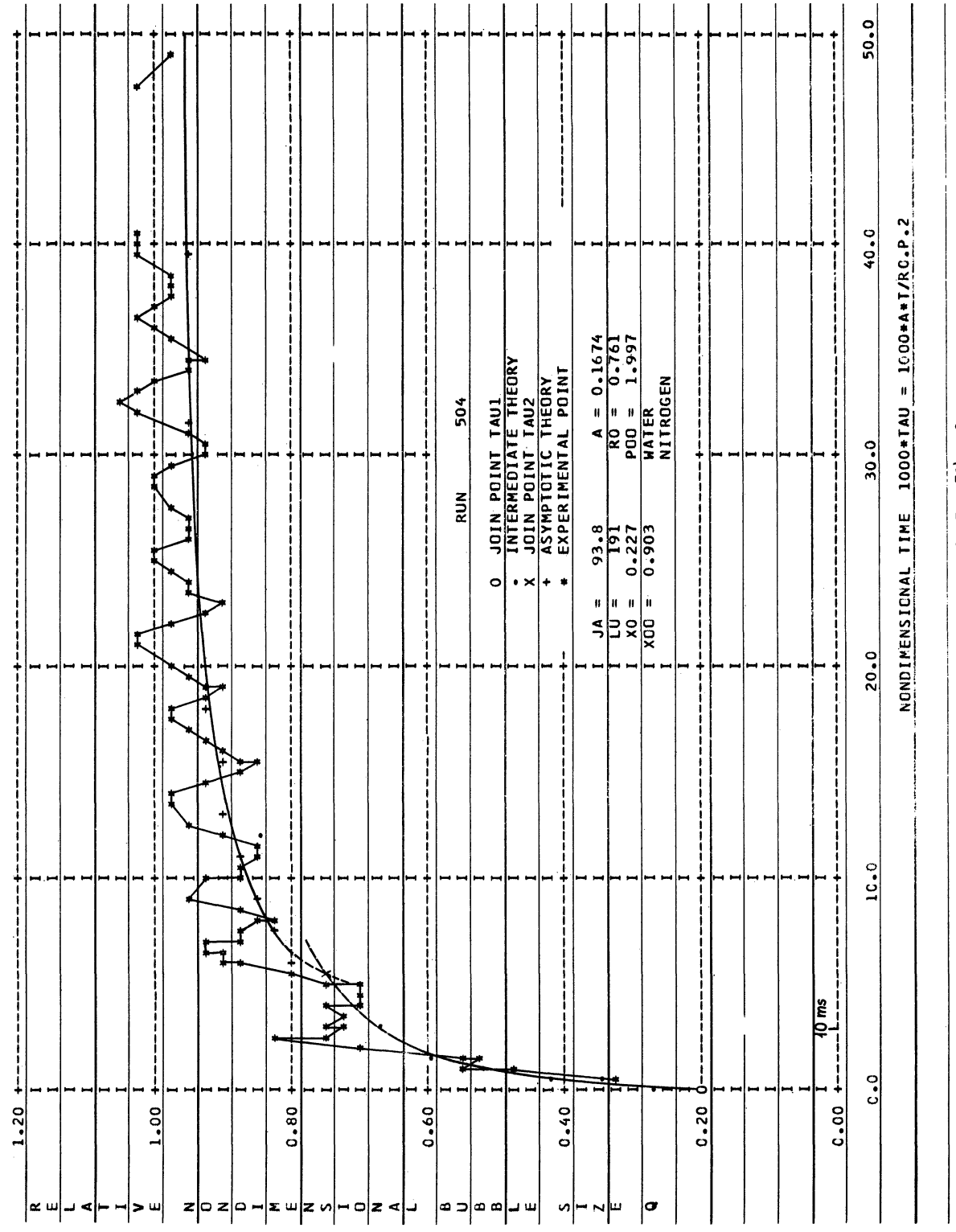

Figure 33. Bubble Growth, Run 504, Q vs τ .

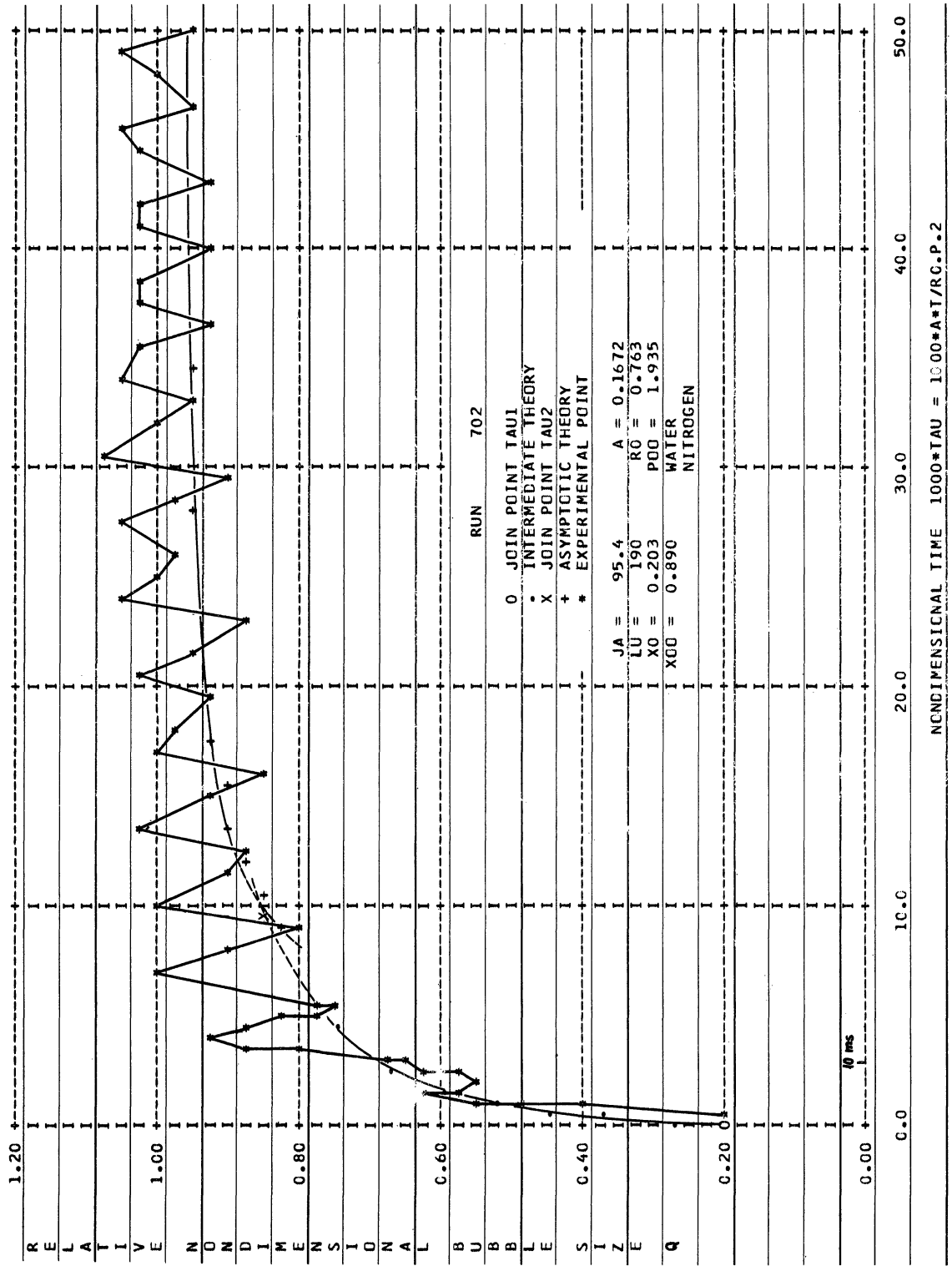

Figure 34. Bubble Growth, Run 702, Q vs τ .

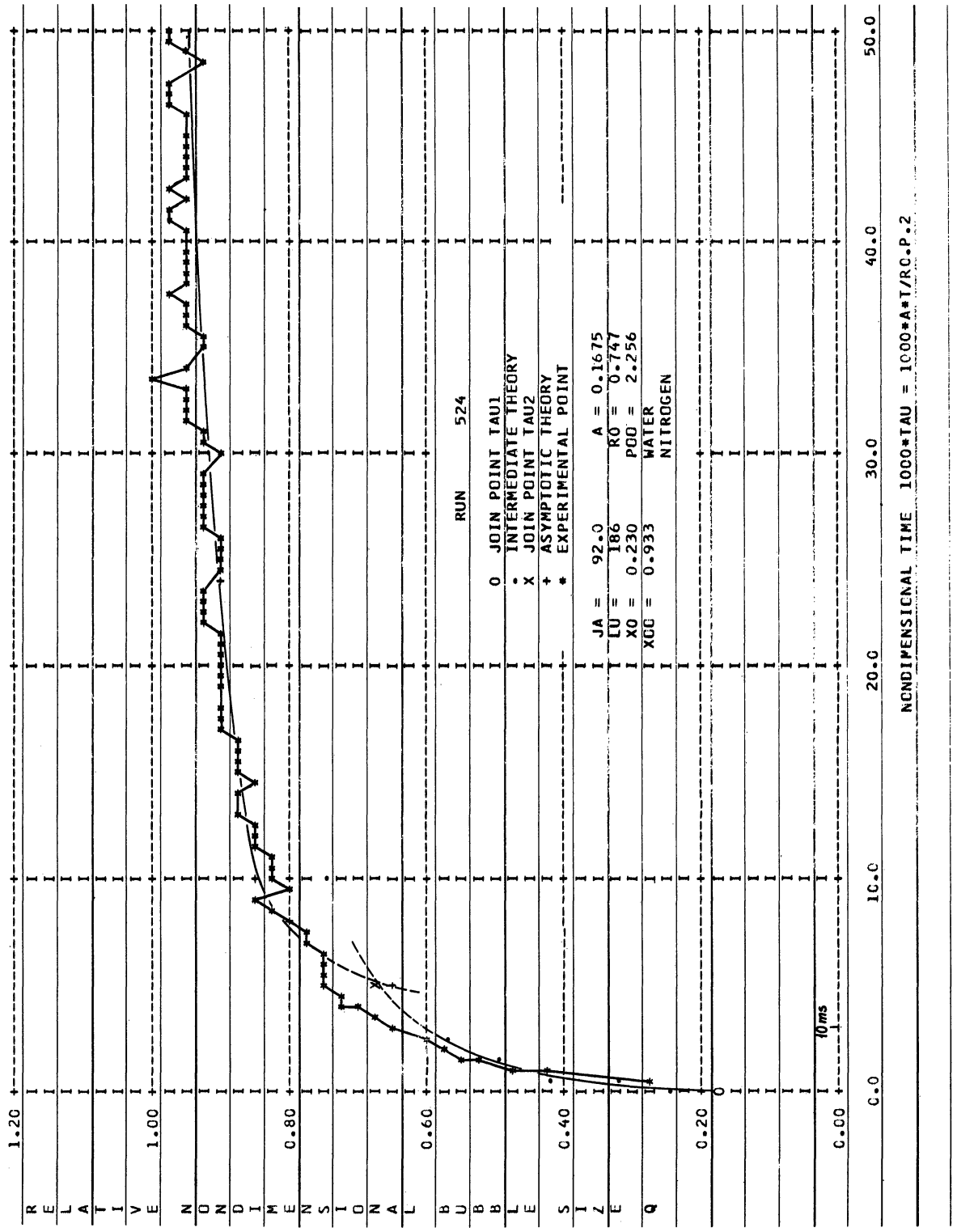

Figure 35. Bubble Growth, Run 524, Q vs τ .

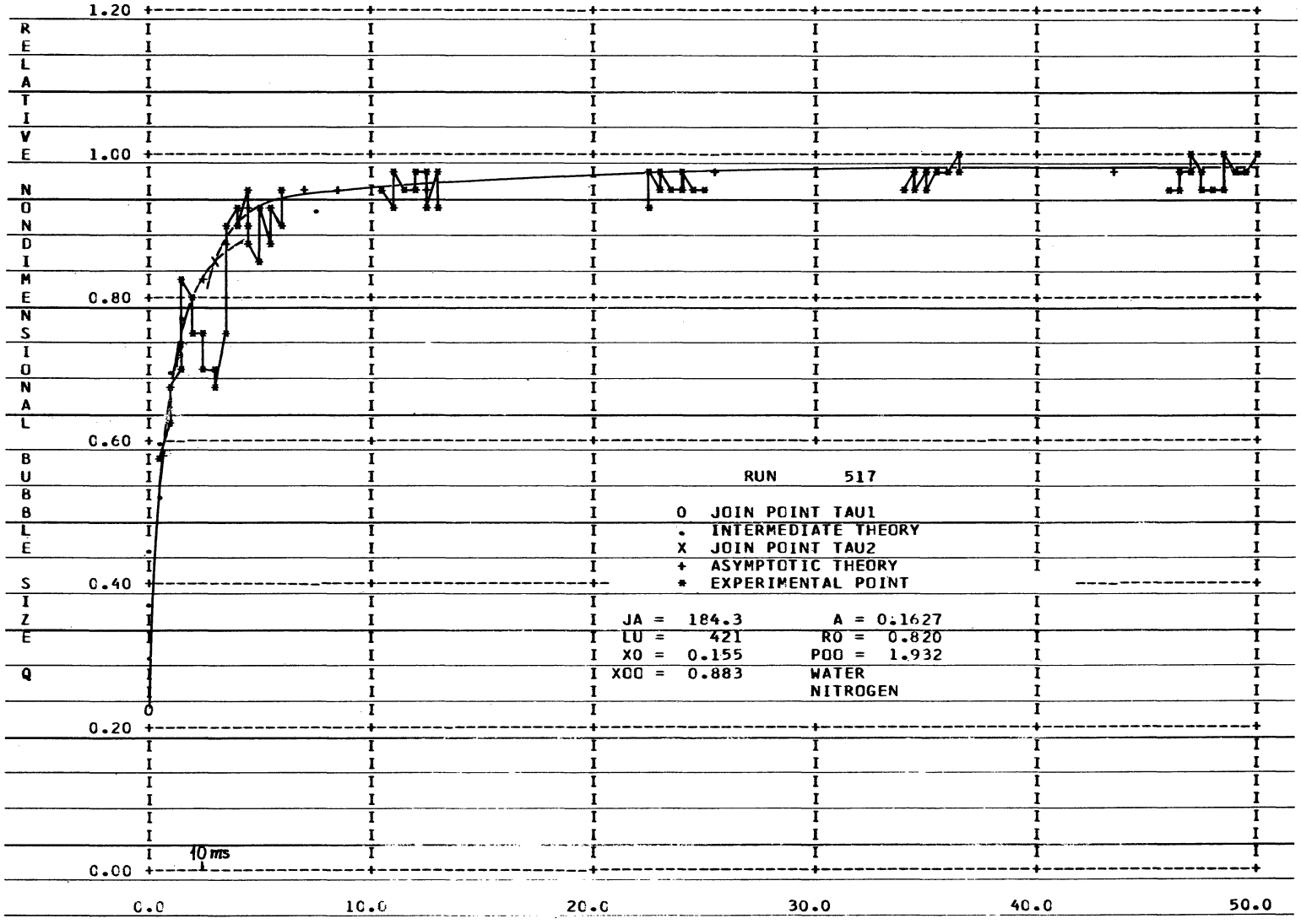

Figure 36. Bubble Growth, Run 517, Q vs τ .

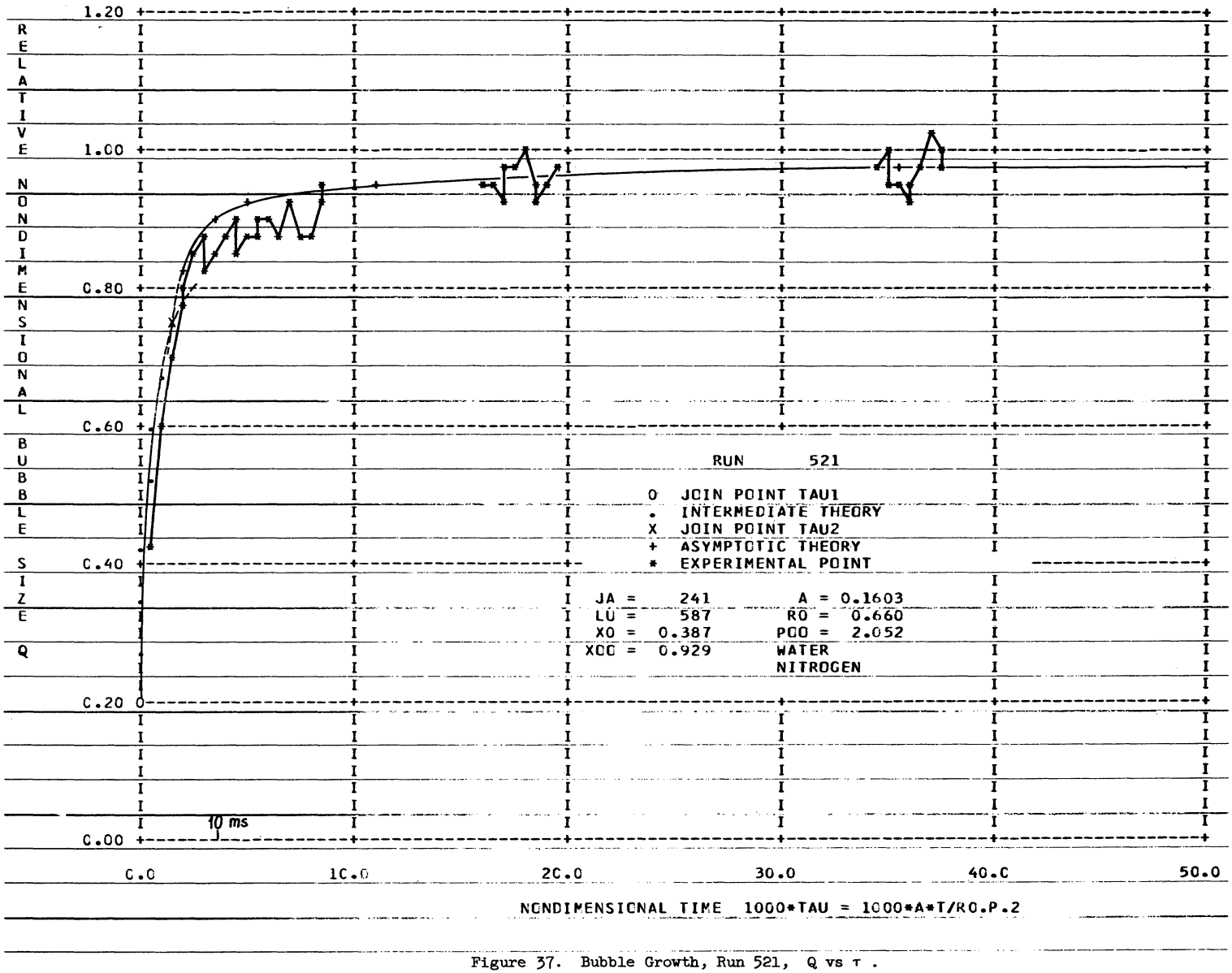

Figure 37. Bubble Growth, Run 521, Q vs τ .

amplitude of oscillation was obtained in Run 702 which, as the only run included here, was carried out with the experimental set-up inverted such that the bubble was blown vertically upwards. Despite the considerable difference in amplitude of oscillation the transient growth is virtually identical for the three runs, indicating that the second approximation to the dynamic bubble shape, Equation (19) has only at most a secondary effect on the process studied here. Although not conclusively demonstrated, this secondary effect tends to accelerate the growth.

Comparing next Figure 35 of Run 524 to e.g., Run 523 in Figure 32, the effect of a change in x_∞ and x_o resulting in an increase in P_∞ of nearly 15% shows the corresponding decrease in growth rate. Finally, Runs 517 and 521 in Figures 36 and 37 show the considerable increase in growth rate with up to a 2.5 fold and a 3 fold simultaneous increase in respectively Ja-number and Lu-number.

Figures 38-40 show Runs 601, 609, and 613, all for helium in water and for increasing Ja and Lu. For unchanged system temperature and pressure the use of a different gas implies a change in the Lu-number only, hence a change in the initial and intermediate growth rates. Comparing thus Run 504 to Run 601 the effect of a 3 fold increase in Lu-number alone is seen for the case of $Ja \cong 90$, while the similar effect for $Ja \cong 220\text{-}240$ is seen by comparing Run 521 and Run 613.

b. Case of a Soluble Gas

For the case of a stationay bubble initially containing a soluble gas four experiments are reported here in which ammonia gas was injected into water. The conditions for the experiments, Runs 951, 953, 954 and 955

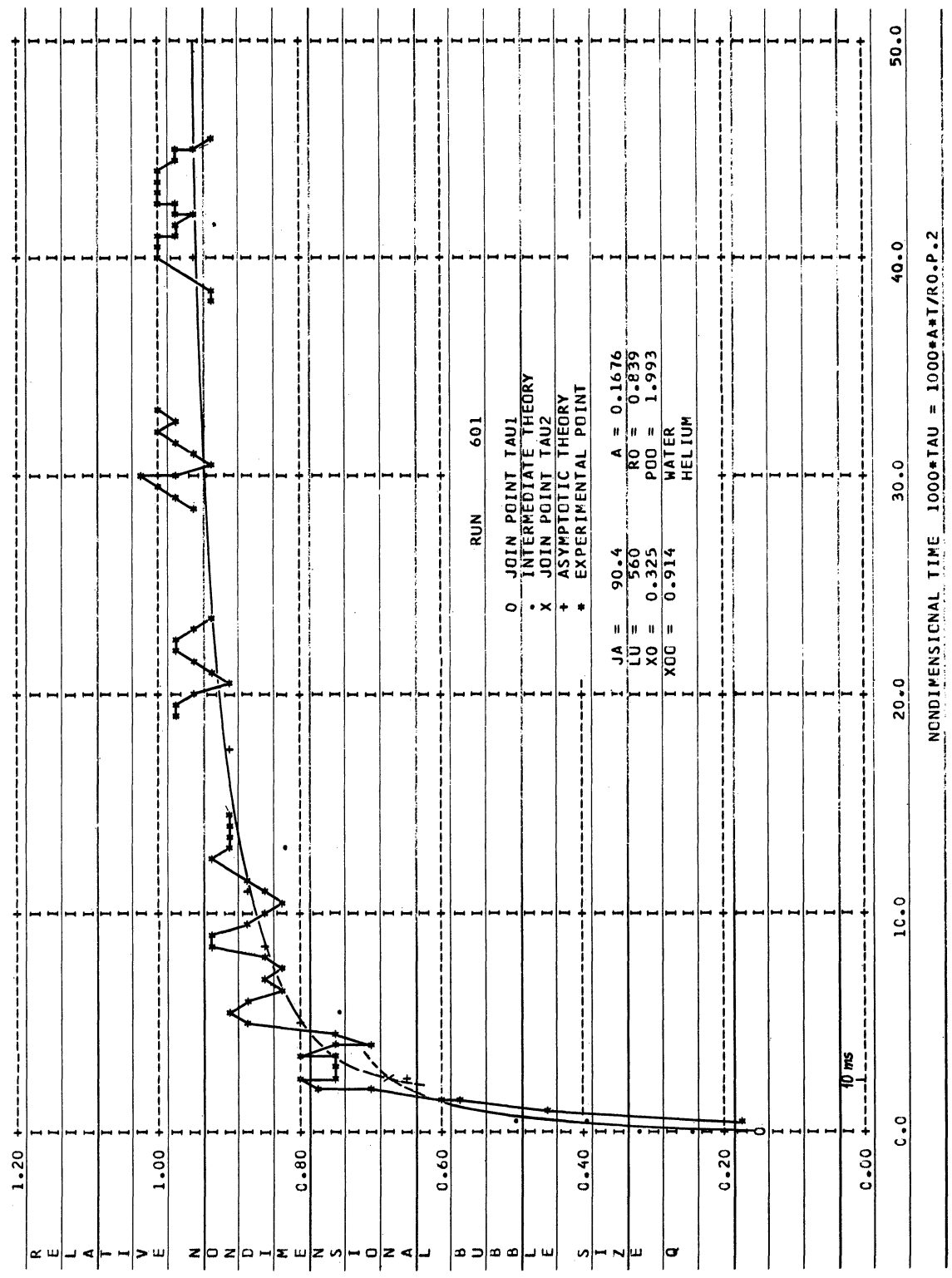

Figure 38. Bubble Growth, Run 601, Q vs τ .

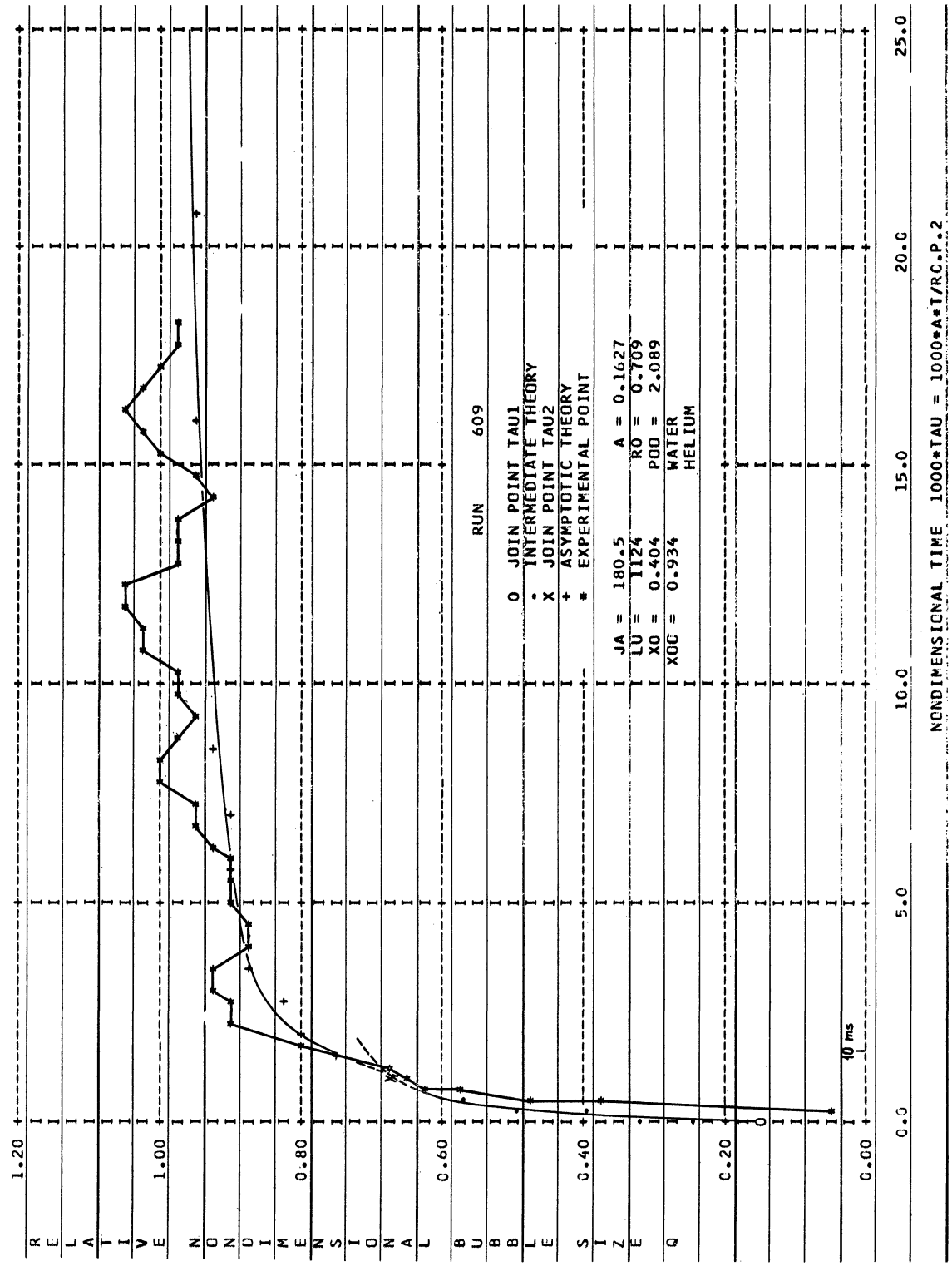

Figure 39. Bubble Growth, Run 609, Q vs τ .

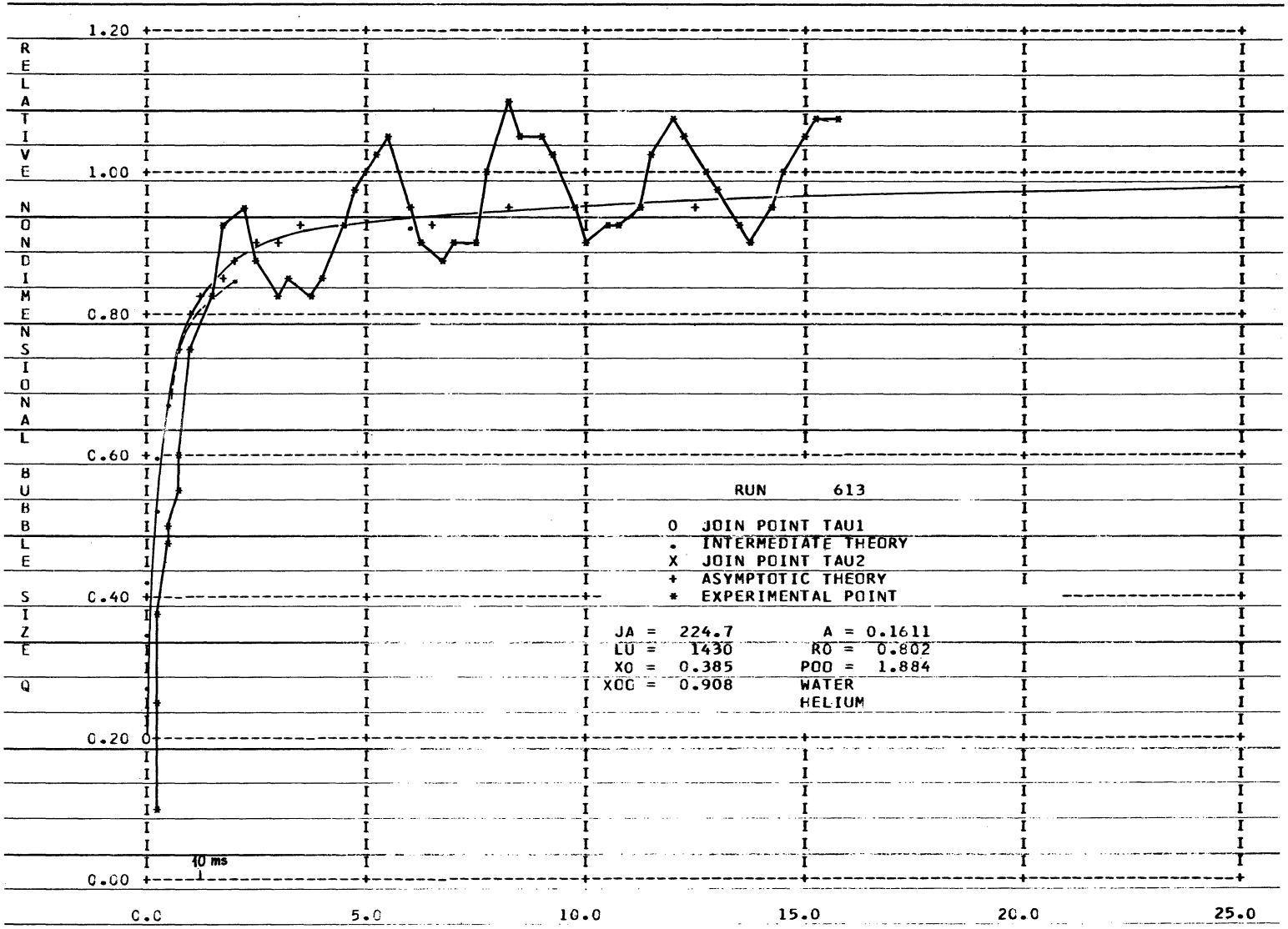

Figure 40. Bubble Growth, Run 613, Q vs τ .

are listed in Appendix VI-2 and the transient bubble collapse in the form of equivalent radius (mm) versus time (ms) is shown in Figures 41-44 directly reproduced from the print-out of the digital computer program for this case.

The study of the collapse, opposed to growth, of a stationary gas bubble initially of nearly spherical shape suspended on the injector tip, made it necessary to adopt a different procedure of data reduction. Thus, the radius plotted versus time is the equivalent radius of a spherical bubble having the actual volume of gas present on the tip, implying that the asymptotic bubble radius is zero. Consequently, the experimental results represents spherical bubble collapse only in the initial part of the transient when the bubble volume is large compared to the volume of the teflon tip, V_{tip} in Figure 30, subtracted from the visible volume

Based on the resistivity measurements of liquid samples, its composition, using the standard curve of Figure 27, ranged from 1.6 - 1.85 x 10^{-5} for the molefraction of ammonia, hence the liquid was far from saturated, providing for eventual bubble collapse in all cases. Because of this, no remanent gas phase could be present on the injector tip prior to bubble injection, and the initial gas composition could be assumed to be pure ammonia, $x''_o = 0$.

Runs 951 and 953 in Figures 41 and 42, were conducted at essentially the same, relatively high temperature, $T_\infty \cong 205°F$ but at different pressures, thus showing the effect of decreased volatility of primarily the liquid component A (water) for which the equilibrium gas composition, x''_∞ at T_∞ , is a measure. The maximum bubble radius being nearly the same, permits direct comparison of the much slower collapse in Run 951 to that in

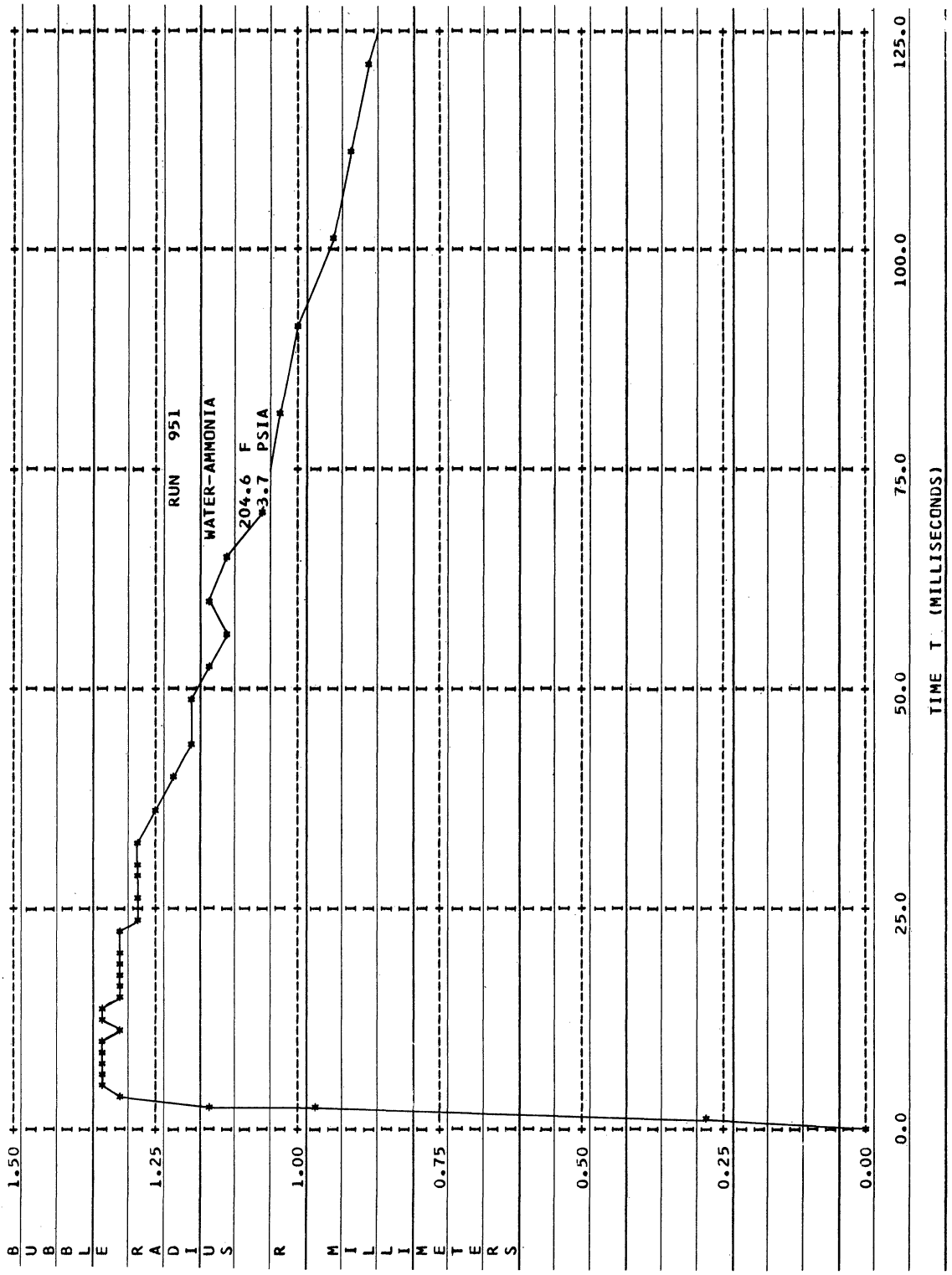

Figure 41. Bubble Collapse, Run 951, R vs t.

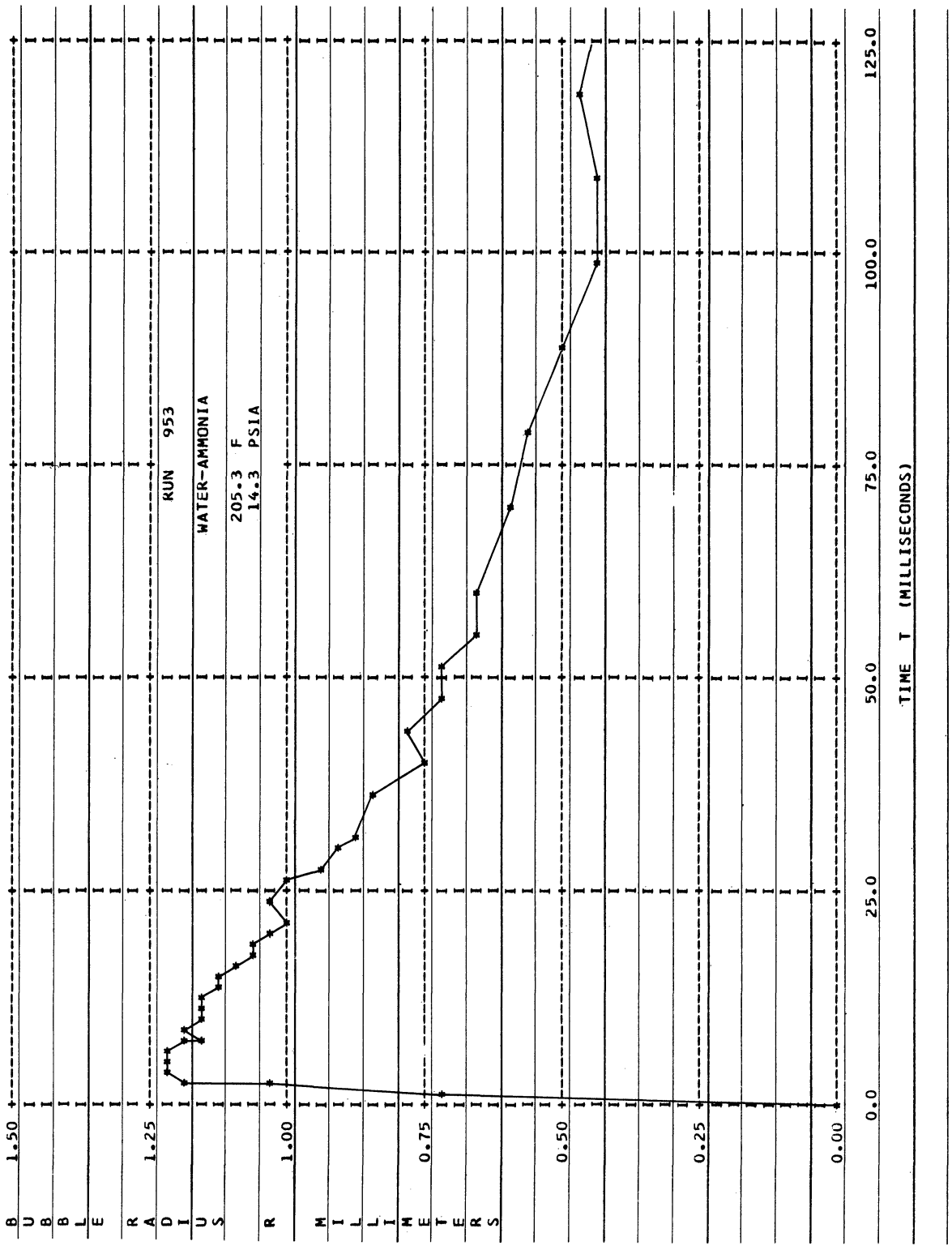

Figure 42. Bubble Collapse, Run 953, R vs t .

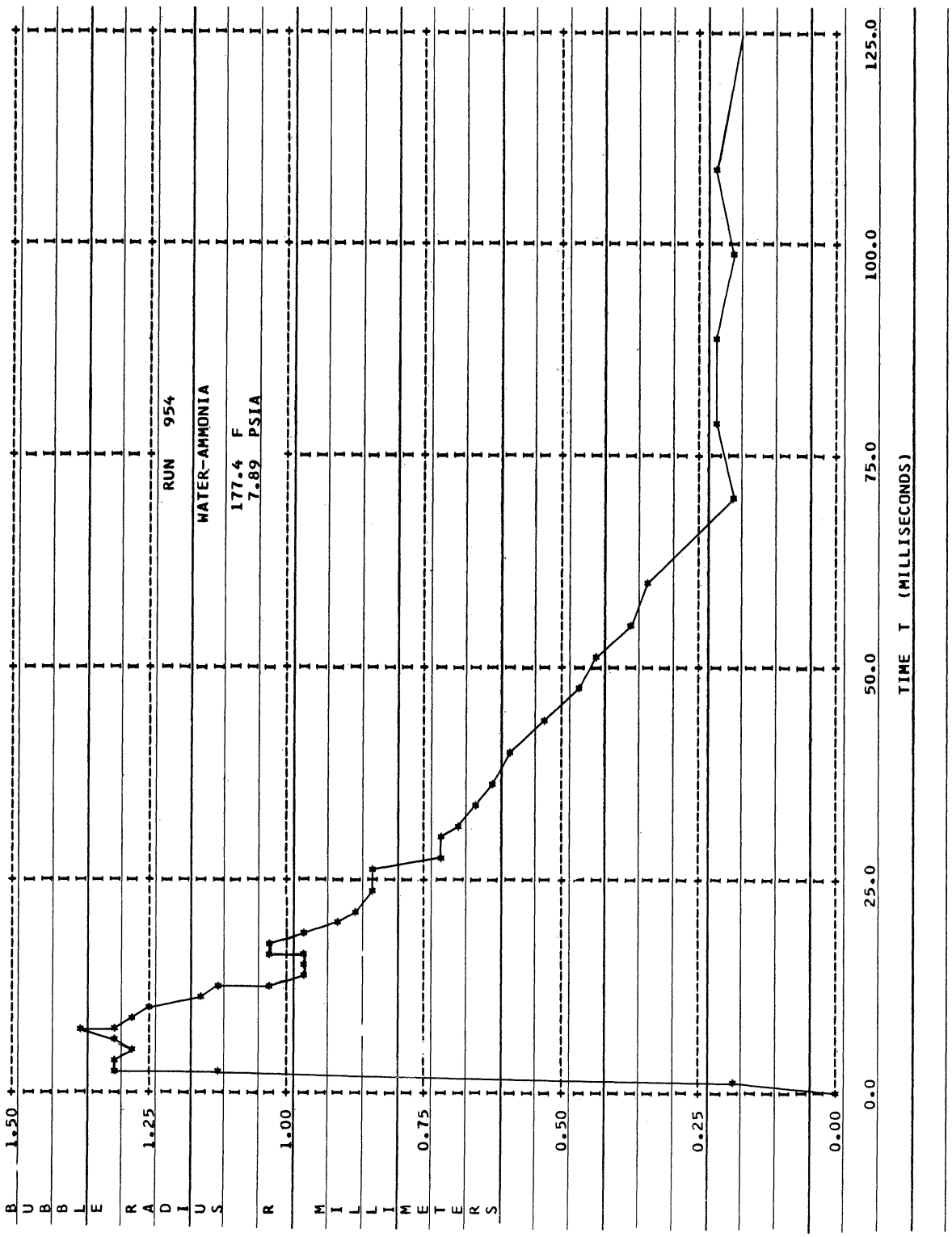

Figure 43. Bubble Collapse, Run 954, R vs t .

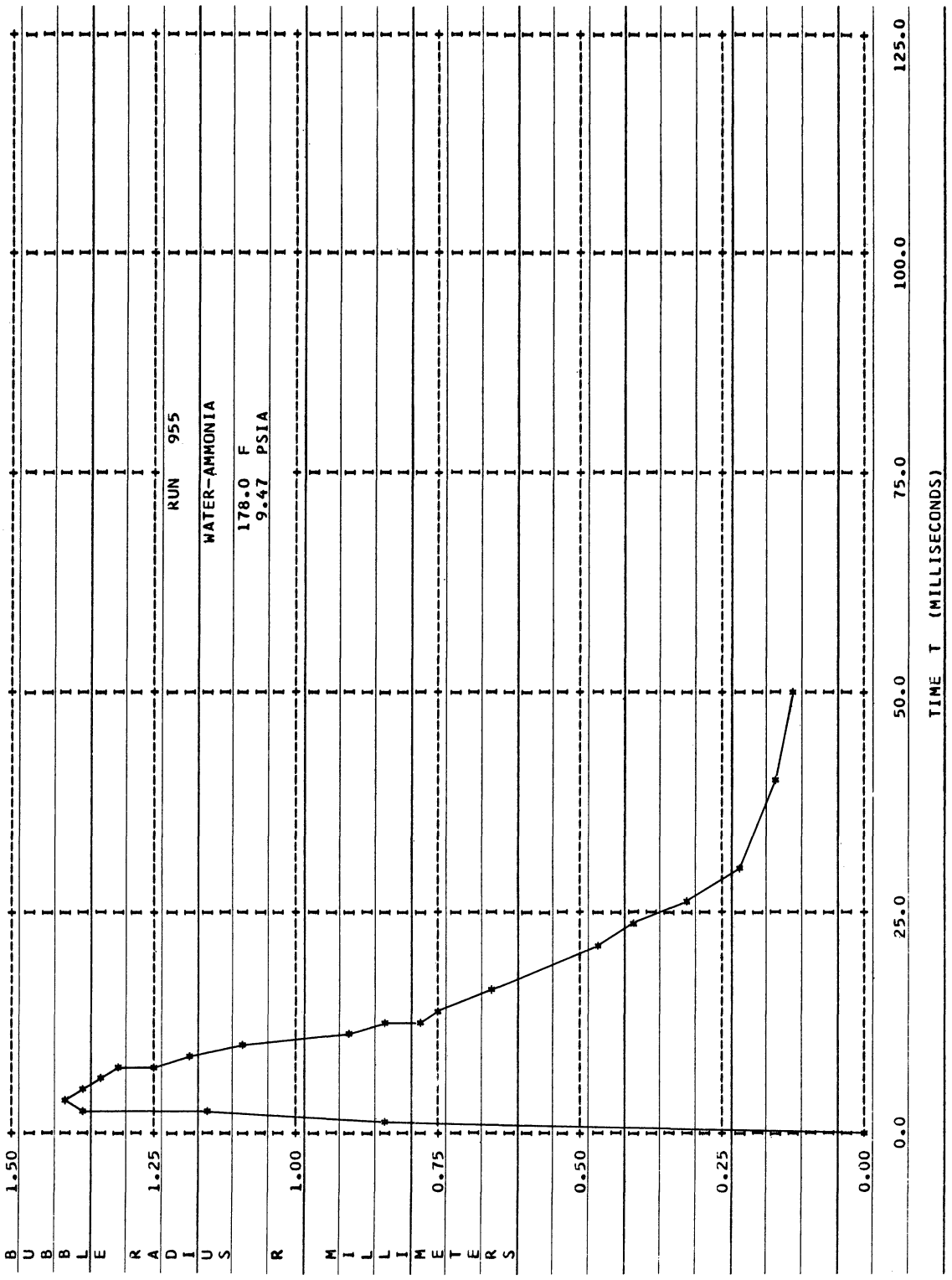

Figure 44. Bubble Collapse, Run 955, R vs t.

Run 953. According to the single 35 mm pictures taken subsequent to the high speed film, collapse was completed in the order of minutes after initiation of Run 951, while for Run 953 the gas phase had vanished when the first picture was taken 48 seconds after bubble injection.

Runs 954 and 955 were conducted to show the same trend, but at a relatively low temperature of $T_\infty \cong 178°F$, where all of the dimensionless properties for the rate of the process are greater and the solubility, x^*, of the gas higher (see Appendix VI-2). The results, shown in Figures 43 and 44, indicate the corresponding increase in the rate of collapse with decreasing volatility of the liquid, and when compared to Run 591 and 953 the much more rapid collapse is evident. The first 35 mm frame from Run 954, taken 7.8 seconds after bubble initiation, shows that collapse has been completed, while this is seen to occur at 50-75 ms directly from the high speed film in the more extreme case of subcooling ($x''_\infty = 0.758$) for Run 955.

The analytical prediction of the initial bubbles behavior, calculated according to Equation (106), is given in Appendix VI-2 in terms of the phase-growth parameter λ. The results, indicating initial growth in all cases, cannot be compared directly to the experimental results because the initial bubble size, unlike the case of a nonsoluble gas, may not be calculated from its asymptotic size. The observed bubble formation times measured from the high speed film for the case of no growth, Run 511, and measured from solenoid current, Figure 26, are in the order of 3 ms $\pm$ 1 ms. Although their smallness have been conclusively established, their exact values are not known in each experiment, and it becomes impossible to con-

clude from the plots of transient bubble size if initial bubble growth has in fact been experienced. The tendency for growth, however, compared to the tendency for collapse is clearly demonstrated by comparing, for example, Run 951 to Run 953, and noting the calculated values of the growth parameter listed in Appendix VI-2 of respectively -8.18 and -6.04.

c. The Case of Bubbles Having Translatory Motion

A number of experiments were conducted for the injection of respectively nitrogen and ammonia into water with the view tank in an inverted position from that shown in Figure 17. A sufficient amount of the gas was injected to enable bubble departure and subsequent rise through the liquid under the influence of buoyancy forces. By removing the simple 1 inch objective lens from the optical system shown in Figure 24, the view field of the camera was enlarged to cover the bubble rise up to 40 mm above the injector tip. This provided for an observation time of about 140-170 ms for the case of a growing bubble and more than 200 ms for the collapsing bubble rising more slowly.

Firstly, two experiments, Runs 805 and 806, are included to show the effect of translatory motion on the rate of growth for nitrogen bubbles injected into water. The nearly identical conditions for the two experiments, listed in Appendix VI-1, were chosen to provide growth-rates great enough to ensure completion of the growth during the available observation time. In this way the initial bubble size could be calculated and comparison made with the analysis for the case of a stationary bubble.

The resulting bubble growth, plotted in dimensionless representation as Q vs τ, is compared to the analytical solutions for the stationary

bubble in Figures 45 and 46, where for clarity the time scale has been expanded compared to Figures 32-40. The effect of translatory motion as an increase in the growth-rate does not appear significant until some time after departure and acceleration of the bubble when a flow transition has eventually occurred. This observation may be verified by comparing the bubble growth in Figures 45 and 46 to Figure 47, showing the position of the bubble center versus time for Runs 805 and 806. Bubble departure occurs at A , while the flow transition takes place over the region marked B - C . As seen from Figure 47, which also gives bubble velocity and Reynolds number, $Re = 2 \cdot R \cdot V/\nu$, for a number of bubble positions for Run 805, the bubble is practically accelerated at the time of departure to a velocity which remains nearly constant until transition occurs. Although the Reynolds number is very large the liquid motion is believed to be laminar over this part of the bubble rise. In the transition region B - C marked by an increase followed by a decrease and again an increase in bubble velocity to a nearly constant value beyond point C , a new stable flow regime is established believed to be turbulent.

In the laminar region the small departure of the measured growth-rate from the analytical prediction in case of no motion supports the "stagnant film" theory,[5] which assumes the bubble to be surrounded by a stagnant liquid film of a thickness large compared to the penetration of the potential distribution associated with the mass transfer. In the transition and turbulent regions, on the other hand, the significant departure from the analytical prediction supports the "penetration" theory[5] which assumes full slip between the liquid and the gas phase, the latter being

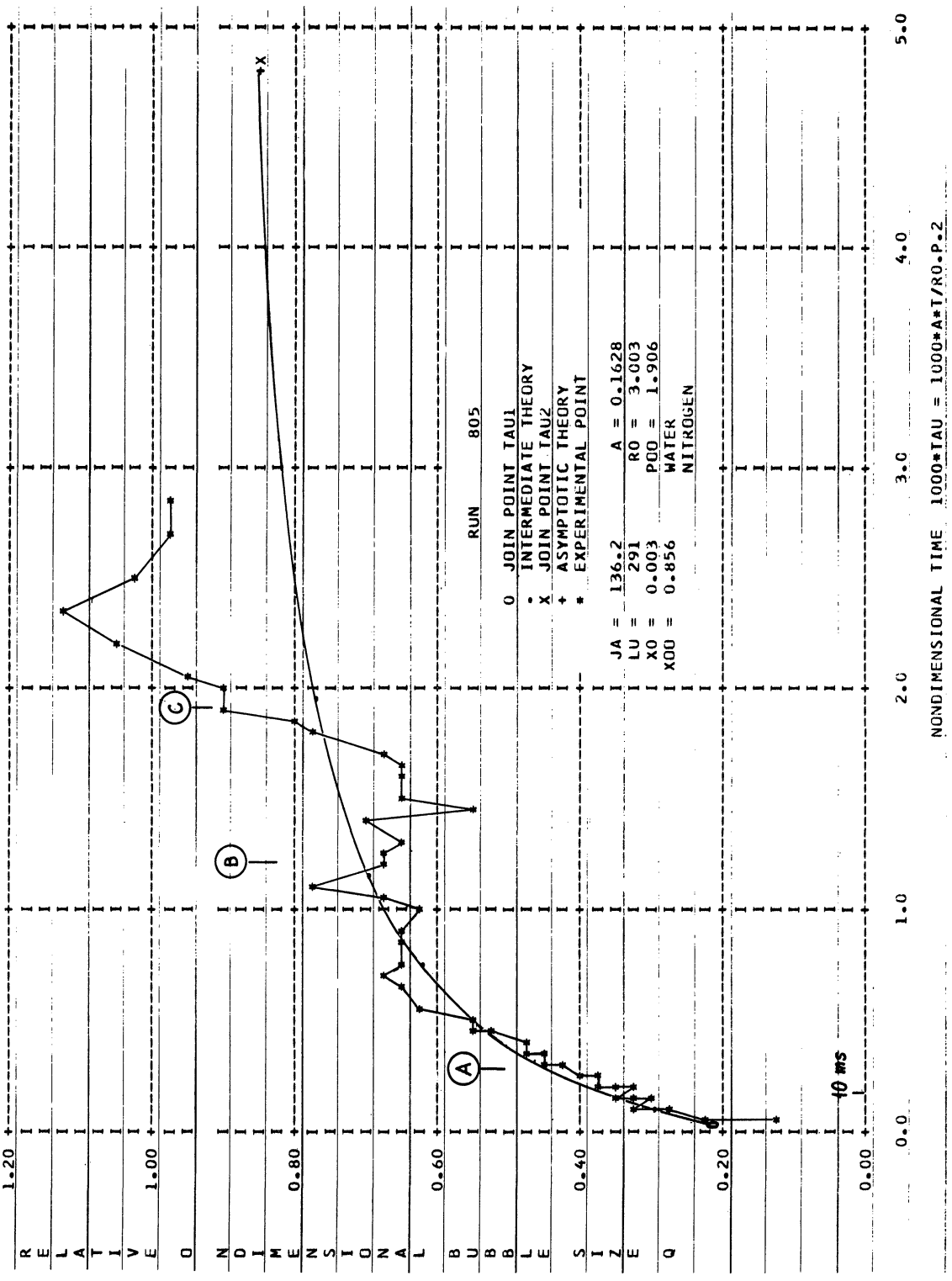

Figure 45. Growth of Moving Bubble, Run 805, Q vs τ .

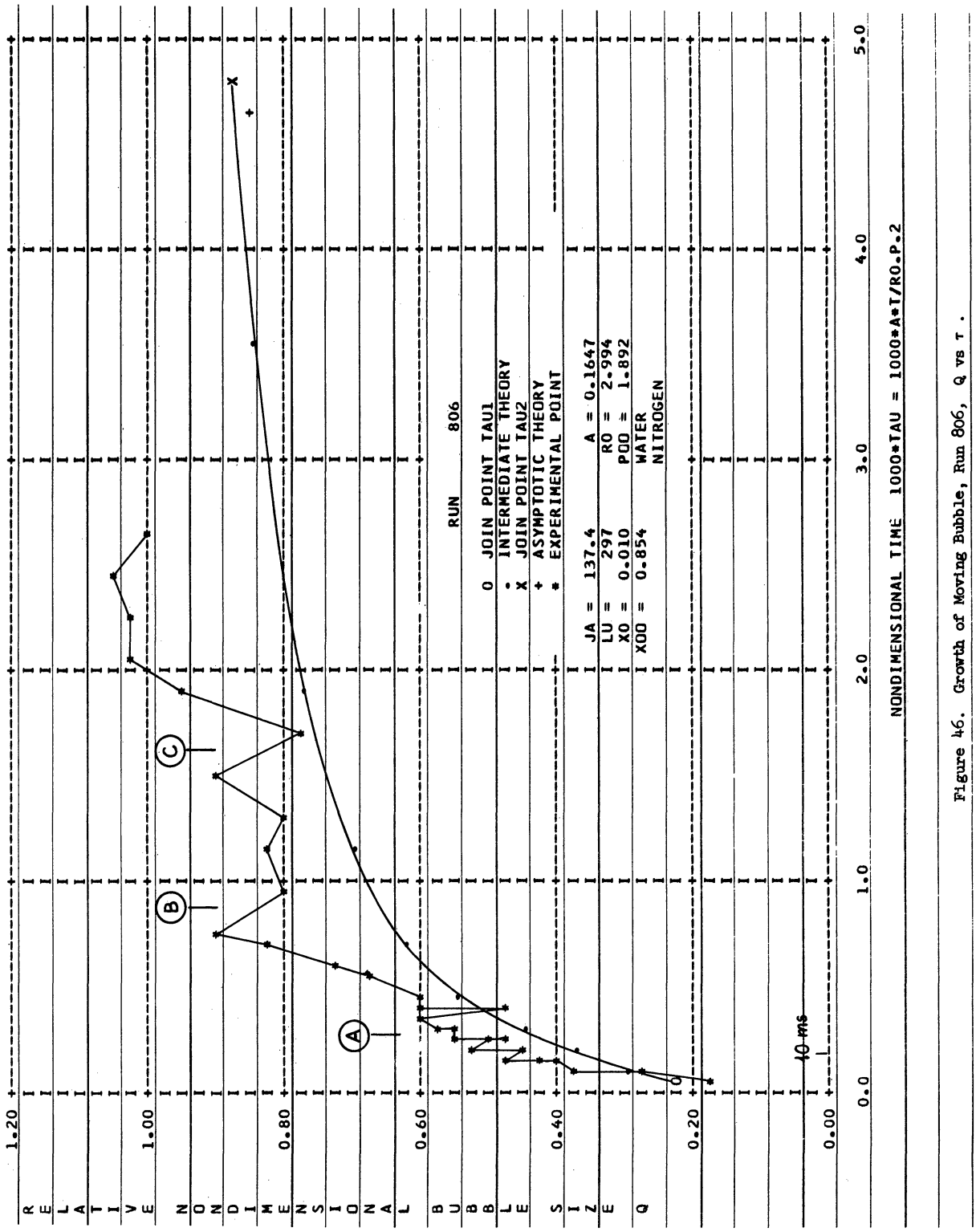

Figure 46. Growth of Moving Bubble, Run 806, Q vs τ .

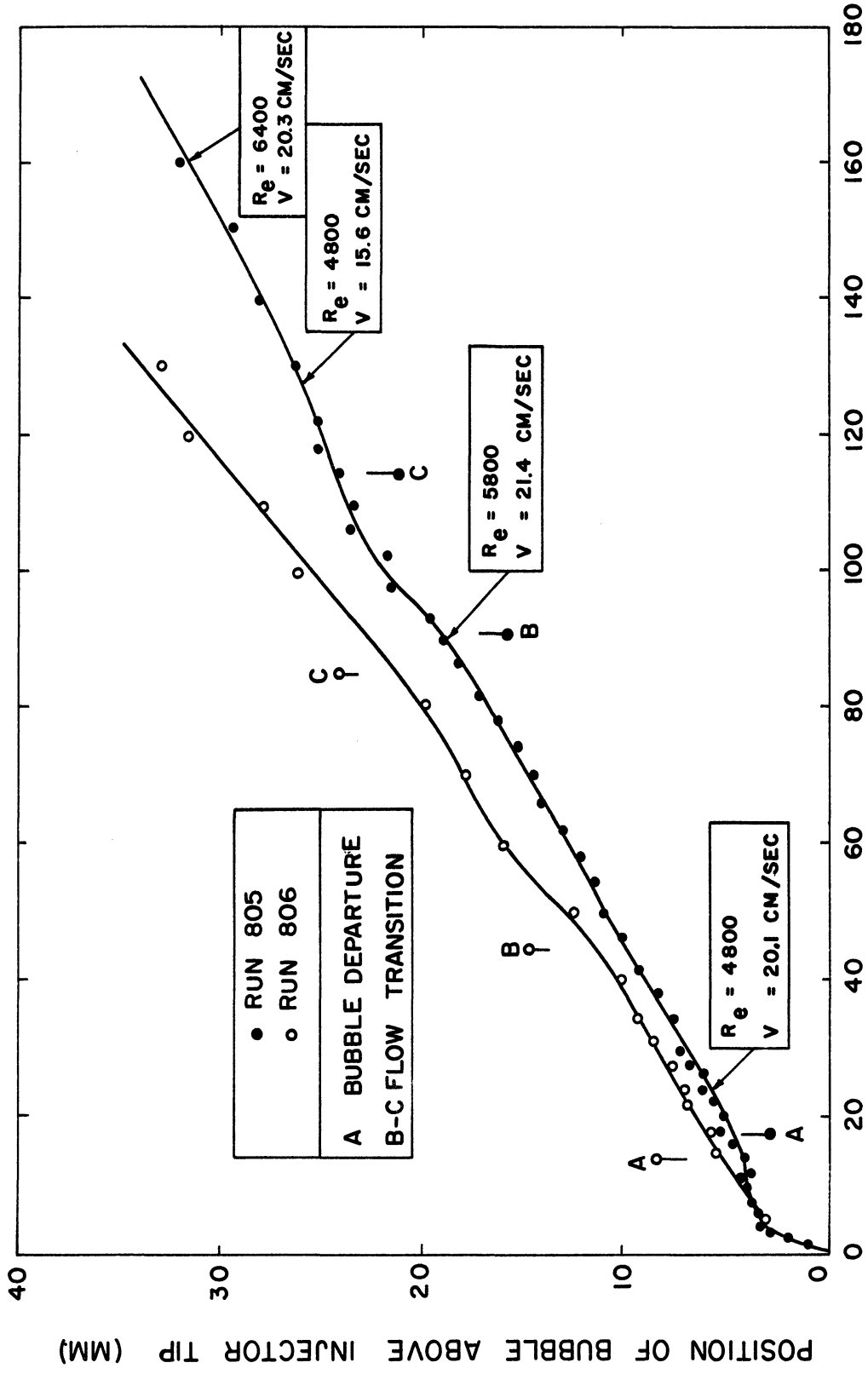

Figure 47. Bubble Position vs Time, Run 805 and 806.

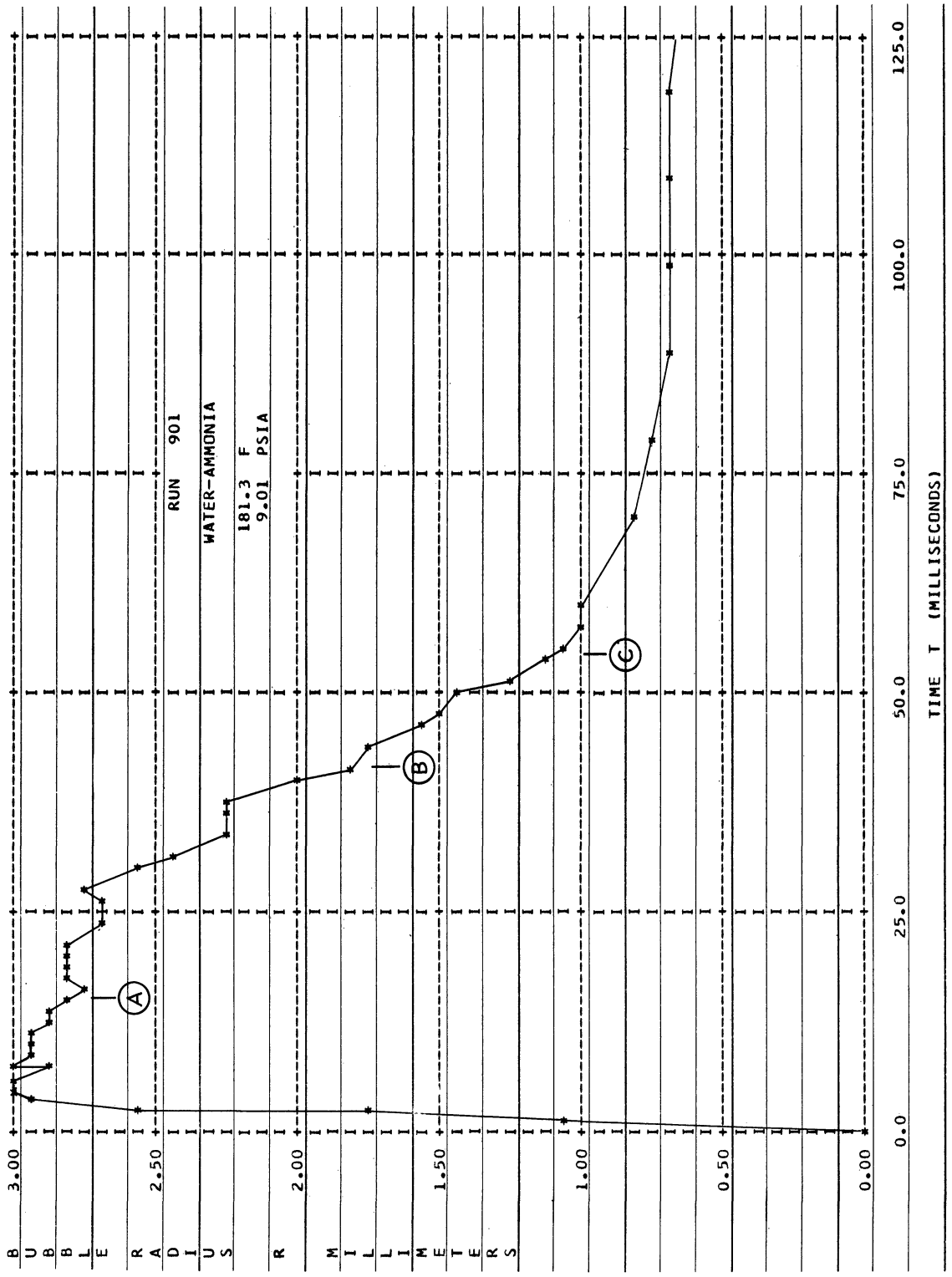

Figure 48. Collapse of Moving Bubble, Run 901, R vs t .

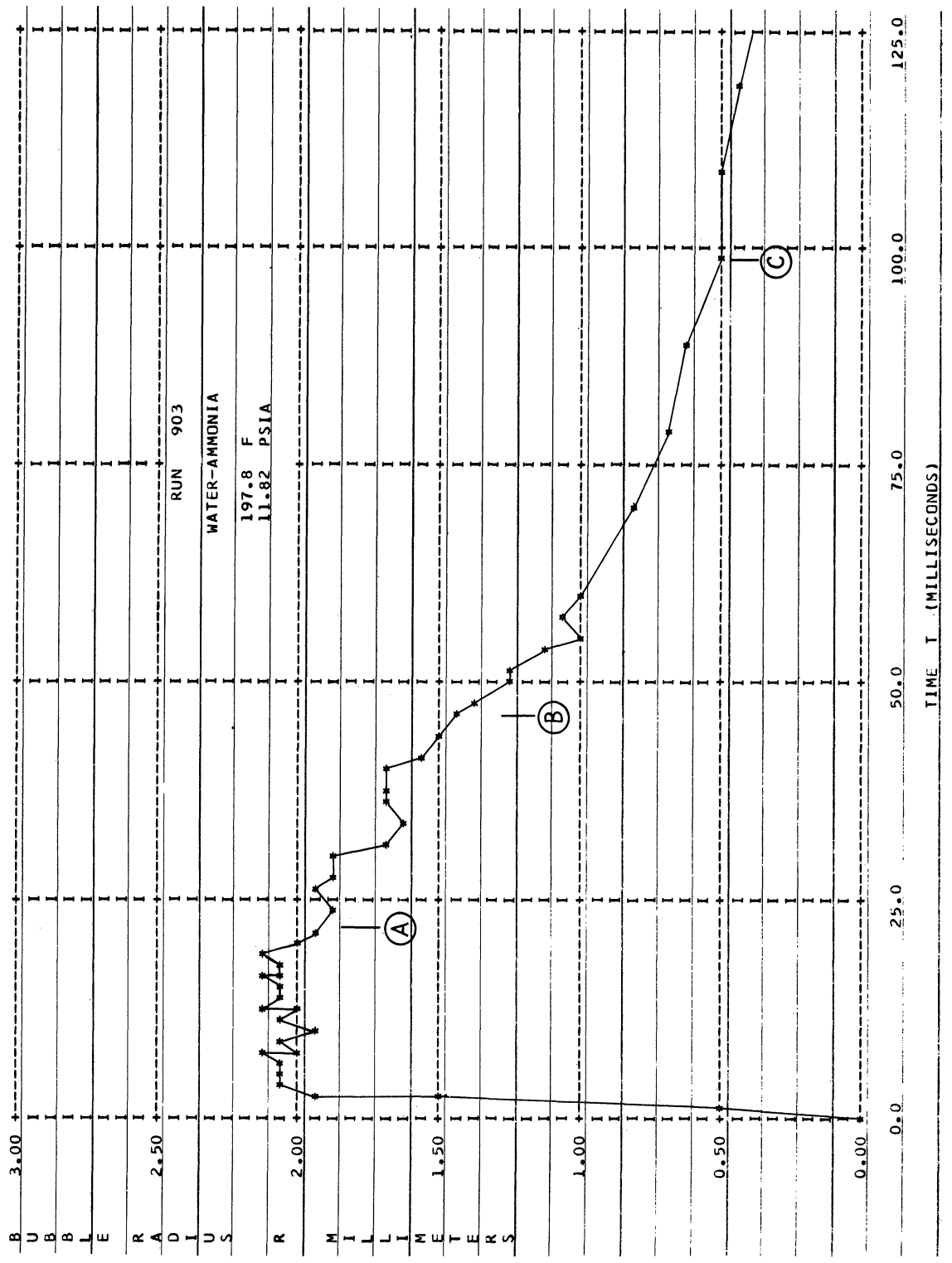

Figure 49. Collapse of Moving Bubble, Run 903, R vs t .

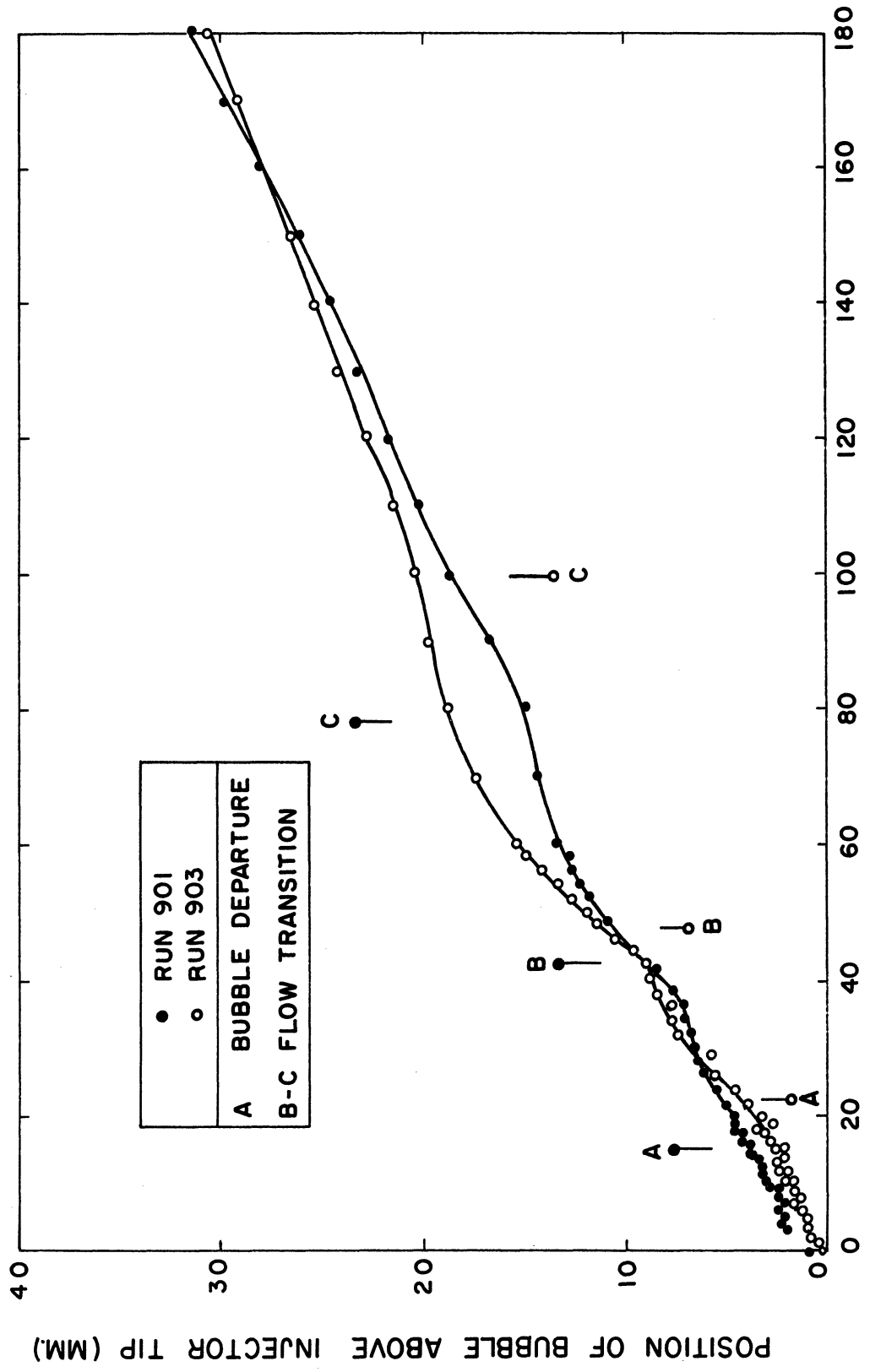

Figure 50. Bubble Position vs Time. Runs 901 and 903.

well mixed by its induced toroidal motion, hence predicting higher rates of mass transfer.

Secondly, Run 901 and 903 are included in Figures 48 and 49 to show the collapse of an injected ammonia bubble rising through water. The conditions for the experiments are given in Appendix VI-2. Despite the greater maximum bubble sizes and the higher volatility of the liquid, the resulting collapse times for Run 901 and 903 are comparable to that of Run 954 for the stationary ammonia bubble. The plot of bubble position versus time in Figure 50 for Runs 901 and 903 shows the characteristic flow transition marked B - C . The initial velocity oscillations over the region A - B are ascribed to the observed bubble oscillations.

d. Bubble Oscillations

For a number of the experiments involving the study of a stationary bubble, measurements were made of frequency and amplitude of the bubble oscillations. The results are summarized in the table in Appendix VI-3, giving Run number, the mean radius, $\bar{R}$, for which the measurements were made, experimental frequency and the theoretical frequency calculated from Equation (2) for the spherical zonal harmonics of second mode. The agreement between observed and analytical frequency indicates that the second harmonic is the dominating mode of oscillation, hence that the bubble shape could be taken to that of Equation (19) in the first approximation. Based on measured amplitudes in radius and bubble length along its assumed axis of symmetry, the relative equivalent radius, R_{eq}/R , and relative polar amplitude, a/R, of the oscillation were calculated. As seen from Figure II-1 of Appendix II only a qualitative agreement is observed with the analytical relationship given by Equation (II-5).

2. Experimental Uncertainty

A Careful evaluation of the uncertainty of the experimental results is particularly required in the present investigation because of the extensive calculations involved in the data reduction, tending to obscure the entries of uncertainty. The basic data serving as input are, liquid temperature, liquid pressure at bubble position, and bubble volumes versus time.

The uncertainty of a single temperature measurement using a Leeds & Northrup portable precision potentiometer Model 8662 is established to 0.3°F. The liquid temperature is obtained as the mean value of three readings, hence $\delta T = 0.17°F$. Despite the diverse corrections, the uncertainty on the liquid pressure remains that associated with the reading of the 30 inch mercury manometer, established to $\delta p_\infty = 0.1$ inch Hg. The reading accuracy of the bubble dimensions has been established to one or two units of the scale in the ruler system used, depending on sharpness and grain size of the film. Sample calculations of the change in bubble volume resulting from a small change in either of the dimensions indicate it reasonable to employ $\delta V(I) = V(I)\ \delta H/H$ as a measure for the uncertainty on bubble volume. H is the measured bubble length and $\delta H = 1.5$. Based on an accuracy of 0.001 inch in measuring the dimensions leading to the residual volume, VR , it is found that $\delta VR = 0.011\ mm^3$. The uncertainty of the time coordinate is related to the film speed, SPEED , read on an electronic counter connected to the camera magnetic pick-up. With a one second counting period, as used here, the accuracy for the film speed is one count in a second, or $\pm$ 16 fps , hence $\delta t/t = 16/SPEED$.

In executing the plots of $P(\tau)$ and $Q(\tau)$ as part of the digital computer program for data reduction, the plot resolution -defined as one printer space horizontally and one printer line vertically- was chosen to correspond to the uncertainty in the results. The true nature of the data is thus not obscured by the method of reproduction. Referring again to Run 523 for $P = 1.8$, for example, $\delta P/P = 1.4$ implies that $\delta Q = 0.04$, which should be compared to the resolution of 0.025 per line in the ordinate direction. In the absissa direction one printer space corresponds to 0.5 on $10^3 \cdot \tau$ while $\delta(10^3 \cdot \tau) = 0.12$ for $10^3 \cdot \tau = 4.0$.

The general expression for the accumulation of error or uncertainty, δq , on a quantity, q , given as a function of a number of observables, a_i ,

$$q = q(a_1, a_2, \ldots, a_n)$$

each encumbered with an error or uncertainty δa_i , is[31]

$$\delta q = \left[\sum_{i=1}^{n} \left(\frac{\partial q}{\partial a_i}\,\delta a_i\right)^2\right]^{1/2} \cong \frac{1}{\sqrt{n}} \sum_{i=1}^{n} \left|\frac{\partial q}{\partial a_i}\,\delta a_i\right| \qquad (129)$$

where the latter form of Equation (129) applies when the order of the individual contribution is nearly the same. Based on the approach followed in the data reduction and employing Equation (129) the uncertainties on the ultimate results are calculated. Table III shows representative values for the uncertainties for an experiment (Run 523).

TABLE III

CALCULATED EXPERIMENTAL UNCERTAINTIES FOR RUN 523

Quantity	% Uncertainty
P	2.1
τ	3.2
Ja	0.3
Lu	0.5
x_o	4.9
x_∞	0.5
R_o	1.4
P_∞	1.4

CHAPTER IV

SUMMARY OF RESULTS

In Chapter II the bubble dynamic problem was stated for a stationary spherical bubble, and approximate solutions derived for the transient growth of the bubble containing a nonsoluble gas, growth being governed by heat transport in the liquid and mass transport in the gas. The initial growth or collapse was predicted for the case of a soluble gas bubble, including the effect of mass transport in the liquid, and a solution for its collapse in a nonvolatile liquid was derived. The governing parameters were established for dimensionless bubble growth or collapse as the Ja-number and Lu-numbers, respectively characterizing the dimensionless rate of heat and mass transport. The ratios Ja^2/Lu and Ja^2/Lu' were shown to represent the relative significance of mass to heat transport for the rate of the processes.

In Chapter III the experimental simulation of the analytical model of a stationary bubble was described and the bubble formation time, although not known exactly in each experiment, was established to be about 3 ms, a time small compared to the duration of the transient growth or collapse studied.

For the nonsoluble gas case of nitrogen and helium bubbles in water the intermediate and asymptotic solutions derived in the analysis were shown to describe bubble growth adequately within the range of parameters given in Table II. The observed bubble oscillations, consistent in frequency with the second spherical zonal harmonics, could

not be concluded to cause a detectable departure from the analytical prediction of bubble growth in which oscillations were neglected. The influence of bubble oscillations on the transient heat and mass transport processes is therefore concluded to be a second order effect. The effect of translatory bubble motion was shown to appear as a significant increase in growth rates when the rising bubble had been accelerated and a transition in the fluid motion had occurred.

For the case of a soluble gas increasing collapse rates were experimentally demonstrated for increasing values of the governing rate-parameters, Ja, Lu, Lu', for decreasing liquid volatility, x_∞, and for increasing solubility of the gas, x*. The collapse rates of gas bubbles having translatory motion were shown to exceed those for the stationary bubbles.

APPENDICES

APPENDIX I

DEPARTURE FROM INTERFACE EQUILIBRIUM DURING MASS TRANSFER

The macroscopic concepts of temperature and concentration of a component in a mixture indicate these to be continuous functions in a continuum. A non-equilibrium state owing to the transfer of heat or mass inside the continuum is manifested in gradients in these continuous functions for the potentials for transfer. Near a gas-liquid boundary, however, the gas kinetic theory associates the non-equilibrium state owing to interface transfer with a temperature discontinuity (jump) proportional to the mean free path of the gas molecules, and with a discontinuity in partial pressure of the component transferred.

In the present analysis where the intra-phase energy and mass transport will be related to the interface transport in terms of macroscopic properties and potentials, the primary assumption is that the interfacial temperature discontinuity is negligible, as in all cases of a dense gas phase. The discontinuity in concentration distribution is retained and the corresponding departure from the phase-equilibrium state at the interface is evaluated for the case of the nonsoluble gas suddenly exposed to a volatile liquid.

Firstly, for a pure substance exposed to its vapor the net interfacial mole flux leaving the liquid may be written in terms of the Knudsen condensation coefficient σ_1 as[54]

$$N = \sigma_1 \frac{1}{\sqrt{2\pi MRT_s}} (p_s^* - p_\infty) \qquad \text{(I-1)}$$

where M is the molecular weight, R the universal gas constant, and T_s is the liquid surface temperature, p_s^* the corresponding equilibrium (saturation) vapor pressure, p_∞ is the actual pressure of the vapor, and σ_1 may be related to the conventionally defined condensation coefficient σ approximately by[40]

$$\sigma \cong \frac{2\sigma_1}{2+\sigma_1} \tag{I-2}$$

Introducing the Clapeyron equation integrated between p_s^* and p_∞ Equation (I-1) may approximately be written as

$$N = \sigma_1 \frac{1}{\sqrt{2\pi MRT_s}} (T_s - T^*) \frac{h_{fg}}{(1/\rho'' - 1/\rho')T} \tag{I-3}$$

where T^* is the saturation temperature corresponding to the actual vapor pressure p_∞ and the average temperature T may be taken to T_s with little error.

The effect of interfacial non-equilibrium on interface mass transfer in a one-component system may then be described in terms of macroscopic properties simply by the mass flux dependent deviation from the saturation condition at the interface given by Equation (I-3). This effect causes the so called "interface resistance to transfer," which does not manifest itself physically and mathematically as a resistance at the interface, but rather is a result of the changed conditions for the intra-phase energy transport. Consider thus evaporation at a rate $N > 0$

governed by heat conduction in the liquid. The increase in T_s above the saturation value T^*, reduces the driving potential for heat diffusion to the interface, hence facilitating an evaporation rate less than that anticipated, were the interface temperature taken to T_s.

Secondly, for the case of a binary ideal gas-liquid system the above analysis applies when Equation (I-1) is replaced by equations of the form

$$N_i = \sigma_{1i} \frac{1}{\sqrt{2\pi M_i RT}} \left(p_{is}^* - p_\infty x_{is}\right); \quad i = A,B \tag{I-4}$$

where x_{is} is the molefraction of component i in the gas at the interface and p_{is}^* is the vapor pressure of component i that would be in equilibrium with the liquid at temperature T_s and liquid composition x_{is}'. For the nonsoluble gas case, $N_B = 0$ and the mole flux for the volatile liquid component A becomes

$$N_A = \sigma_{1A} \frac{1}{\sqrt{2\pi M_A RT}} \left(x_s^* - x_s\right) p_\infty \tag{I-5}$$

where x_s is the actual gas composition at the interface, and x_s^* is the equilibrium composition corresponding to the actual temperature of the liquid

$$x_s^* = f(T_s, p_\infty) \tag{I-6}$$

Accounting for the departure from equilibrium at the interface the simultaneous intra-phase heat and mass transport in respectively the liquid and gas is subject to Equations (I-5) and (I-6), rather than the phase-equilibrium relation, $x_s = f(T_s, p_\infty)$. The resulting actual values of the interface potentials, T_s and x_s, are such that the driving potentials for both intraphase heat and mass transport are reduced.

The departure from a state of phase-equilibrium discussed above is small, except for extremely high rates of interface mass transfer. The mathematical idealization - physically approached in the gas injection process - of a sudden step change in thermodynamic state in a gas-liquid system predicts unbounded mass transfer rates during the first moments of the transient when a state of phase-equilibrium is assumed to prevail at the interface. The latter assymption is indirectly demonstrated to be satisfactory for the present study by evaluating the encountered departure from phase-equilibrium according to Equation (I-5) from the mass transfer rates predicted from the analytical model. Thus, from Equation (30) the evaporating mole flux for the expanding bubble is

$$N_A = \rho'' \dot{R} \tag{I-7}$$

Employing Equation (55) for small values of time when $\frac{4}{3} A_0 \tau \ll 1$, Equation (I-7) becomes

$$N_A \cong \rho'' \frac{\alpha'}{R_0} \frac{2}{3} A_0 \left[1 + \frac{1}{\sqrt{\frac{4}{3} A_0 \frac{\alpha' t}{R_0^2}}} \right] \tag{I-8}$$

Equating this result to the expression in Equation (I-5), the departure from equilibrium is given by

$$x_s^* - x_s = \frac{1}{\sigma_{1A}} \sqrt{\frac{2\pi}{R_A T}} \frac{\alpha'}{R_o} \frac{2}{3} A_o \left[1 + \frac{1}{\sqrt{\frac{4}{3} A_o \frac{\alpha' t}{R_o^2}}} \right] \qquad \text{(I-9)}$$

A representative numerical evaluation of Equation (I-9) is based on the following data for Run 523 taken from Appendices V-4, Part 2(a) and VI

$$R_o = 0.0877 \text{ cm}$$

$$\alpha' = 0.1675 \times 10^{-2} \text{ cm}^2/\text{sec}$$

$$T = T_\infty = 205.4 \text{ °F} = 369.7 \text{ °K}$$

$$A_o = 247.8$$

$$R_{H_2O} = 4.615 \times 10^6 \text{ erg/grams/°K}$$

using a lower value of $\sigma_{1,H_2O} = 0.5$ as measured for condensation by Nabavian.[40] The result

$$x_s^* - x_s = 0.384 \times 10^{-3} \left[1 + \frac{0.118}{\sqrt{t}} \right]$$

where the time unit is seconds, is valid for $t \ll 14$ ms. At one millisecond after the start of the process this expression indicates a deviation in interface composition of $x_s^* - x_s = 0.0018$, which is negligible compared to the driving potential for mass transfer, $x_s - x_o = 0.5544$ (see Appendix V-4, Part 2(a)).

APPENDIX II

BUBBLE OSCILLATIONS

For the case of axisymmetrical potential flow in the incompressible liquid surrounding a gas bubble, Laplace's equation becomes (see e.g., Lamb(33))

$$\frac{d}{d\mu}\left[(1-\mu^2)\frac{dY_n}{d\mu}\right] + n(n+1)\,Y_n = 0 \qquad \text{(II-1)}$$

in terms of spherical zonal harmonics Y_n of order n, where $\mu = \cos\psi$ and ψ is the polar angle. Equation (II-1) is Legrendre's equation satisfied by the Legrendre polynomials of first and second kind

$$Y_n(\mu) = A \cdot P_n(\mu) + B \cdot Q_n(\mu) \qquad \text{(II-2)}$$

Since for $n = 2$ the second term of Equation (II-2) diverges for $\mu = \pm 1$, the second zonal harmonic becomes $P_2(\mu)$, and the bubble shape for a harmonic undamped oscillation is given by

$$r = r(\psi,t) = R\left[1 + \left(\frac{a}{R}\right)\frac{3\cos^2\psi - 1}{2}\cdot \sin(\omega t)\right] \qquad \text{(II-3)}$$

where a/R is the relative polar amplitude. The variable bubble volume, $V(t)$ is obtained by integration of Equation (II-3)

$$V(t) = 2\pi\int_0^{\pi/2} r^2 \sin^2\psi \; r\sin\psi \, d\psi \qquad \text{(II-4)}$$

Introducing the equivalent radius, R_{eq}, as the radius of a sphere having the same volume as that of the oscillating bubble, V(t), the relative amplitude in equivalent radius becomes

$$\frac{R_{eq}}{R} = \left[1 - \frac{3}{5}\left(\frac{a}{R}\right)\sin\omega t + \frac{3}{7}\left(\frac{a}{R}\right)^2 \sin^2\omega t - \frac{1}{35}\left(\frac{a}{R}\right)^3 \sin^3\omega t\right]^{\frac{1}{3}} \qquad \text{(II-5)}$$

Figure II-1 shows a plot of R_{eq}/R versus a/R, indicating that the bubble of oblong shape has a smaller volume than that of the oblate shape. Hence, the effective mean radius is always less than the arithmetic mean of the maximum and mininum values. For relative polar amplitudes less than 0.2, however, this deviation is negligible.

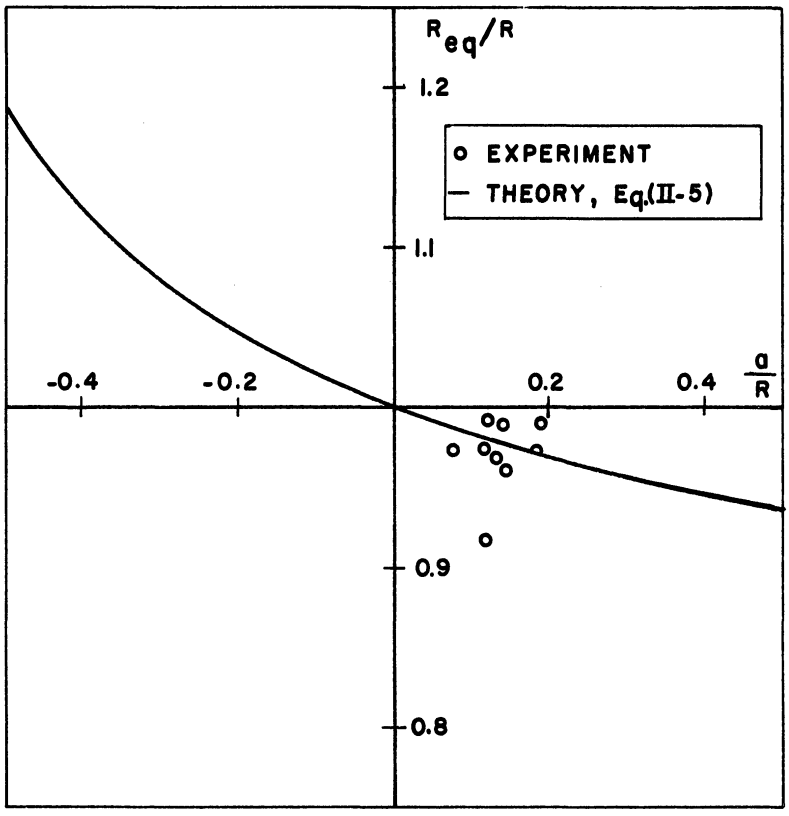

Figure II-1. Relative Equivalent Radius vs Relative Polar Amplitude for Second Zonal Harmonic Bubble Oscillation.

APPENDIX III

APPLICATION OF THE INTEGRAL TECHNIQUE TO A PROBLEM OF SPHERICAL PHASE-GROWTH

The usefulness of applying the integral technique to the problem of spherical phase-growth may be illustrated by the problem of bubble growth in a boiling one-component liquid for which an exact solution exists.

The model used considers the growth of a single stationary spherical vapor bubble, initially of zero size, growing in an inviscous infinite liquid of initial uniform superheat. Under the assumption of a single component system and in the absence of surface effects and pressure gradients, the interface temperature remains constant at the saturation value throughout the process of growth, which is now governed solely by the heat transport in the liquid surrounding the bubble.

Based on the use of the parabolic one-parameter profile of Equation (34) the formulation is analogous to Equations (45) and (47) leading to the form

$$\frac{d}{dt}\left\{Ja\,R^3\left(\frac{R}{f_T}\right)^{-3}\left[\left(\frac{R}{f_T}\right)^2+\frac{1}{2}\left(\frac{R}{f_T}\right)+\frac{1}{10}\right]\right\} = \left[1-(1-\varepsilon)\,Ja\right]\left(\dot{R^3}\right) \qquad \text{(III-1)}$$

$$R\ddot{R} = 2\alpha'\,Ja\left(\frac{R}{f_T}\right) \qquad \text{(III-2)}$$

The characteristic temperature in the Ja-number is in this case the liquid superheat, hence $Ja = (T_\infty - T^*)\cdot(\rho' c'/\rho'' h_{fg})$. Since the Ja-number is

constant, Equation (III-1) may be integrated in its entire form, subject to the initial condition $R(0) = 0$. The result,

$$\left[\frac{1}{Ja} - (1-\varepsilon)\right]\left(\frac{R}{f_T}\right)^3 - \left(\frac{R}{f_T}\right)^2 - \frac{1}{2}\left(\frac{R}{f_T}\right) - \frac{1}{10} = 0 \qquad \text{(III-3)}$$

indicates the constancy of (R/f_T), hence the similarity nature of the solution, namely, the thermal boundary layer thickness, f_T, growing proportional to the bubble radius, R. The form of the solution as obtained from Equation (III-2) is

$$R = 2\,\lambda\sqrt{\alpha' t} \qquad \text{(III-4)}$$

where the growth constant

$$\lambda(Ja,\varepsilon) = \sqrt{Ja\cdot\left(\frac{R}{f_T}\right)} \qquad \text{(III-5)}$$

is an implicit function of the Ja-number and the density deficiency $\epsilon = 1 - \rho''/\rho'$, through (R/f_T) given by Equation (III-3).

The growth-constant λ as function of the Ja-number with ϵ as parameter is compared in Figure III-1 to the exact solution by Scriven.[55] Evaluating the Ja-number at the interface condition this solution is written

$$Ja = 2\lambda^2 \exp\left[\lambda^2(1+2\varepsilon)\right]\int_{\lambda}^{\infty}\frac{1}{x^2}\exp\left[\frac{-x^3-2\varepsilon\lambda^3}{x}\right]dx \qquad \text{(III-6)}$$

Despite its simplicity, the integral technique produces a rather close approximation to the comparatively much more complicated exact solution of Equation (III-6). While the vertical asymptotes for $\epsilon < 1$ are identical in the two solutions, the case, $\epsilon = 1$, $\lambda \to \infty$, deviates slightly For completeness the asymptotic solution, $\epsilon = 1$, $\lambda \to \infty$ as obtained by a number of methods is listed in the table in Figure III-1. It may be noted that neither of the investigators, References 18 and 46, included the effect of a density deficiency different from unity, rendering their findings less general.

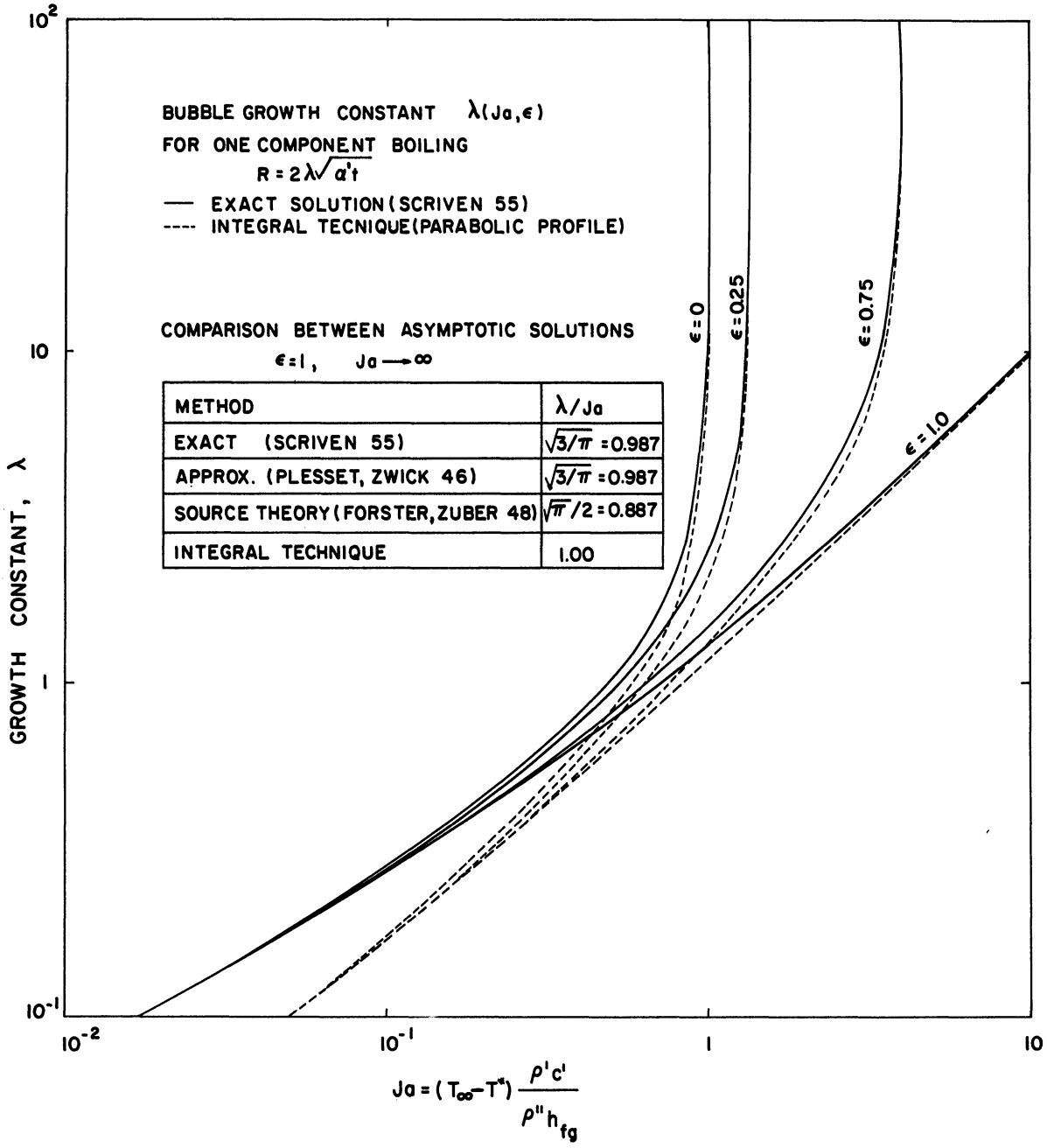

Figure III-1. Comparison Between Exact Solution and Solution by Integral Technique. Bubble Growth in One-component Superheated Liquid.

APPENDIX IV

CRITERION FOR LINEARIZATION OF EQUATION (65)

The criterion, Equation (67), for the validity of the linearization of Equation (65) by retaining its last two terms is obtained as follows. Writing for simplicity the polynomial form, Equation (65), as

$$U^3 + a_1 U^2 + a_2 U - a_3 = 0 \qquad \text{(IV-1)}$$

the coefficients can be expressed in terms of the three roots, U_1, U_2 and U_3, of Equation (IV-1) as follows

$$\begin{aligned} a_1 &= 10 - 2KL^2/N &&= -U_1 - U_2 - U_3 \\ a_2 &= 25 + 10\ KLM/N &&= U_1U_2 + U_2U_3 + U_3U_1 \\ a_3 &= 50\ KM^2/N &&= U_1U_2U_3 \end{aligned} \qquad \text{(IV-2)}$$

The linearized solution, $U^* = a_3/a_2$, in terms of the three actual roots becomes

$$U^* = U_1 \frac{1}{1 + \dfrac{U_2 + U_3}{U_2 U_3}} \qquad \text{(IV-3)}$$

Substituting from Equation (IV-2) to eliminate U_2 and U_3, Equation (IV-3) is written

$$U^* = U_1 \frac{1}{1 - \dfrac{U_1(U_1 + a_1)}{U_1(U_1 + a_1) + a_2}} \qquad \text{(IV-4)}$$

From Equation (IV-4) it is seen that $U^* = U_1$ whenever

$$\left| \frac{U_1 (U_1 + a_1)}{U_1 (U_1 + a_1) + a_2} \right| \ll 1 \qquad \text{(IV-5)}$$

Introducing in this case $U_1 \simeq a_3/a_2$, the criterion becomes

$$\left| \frac{a_3 (a_3 + a_1 a_2)}{a_2^3} \right| \ll 1 \qquad \text{(IV-6)}$$

which is the form of Equation (67) when the coefficients from Equation (IV-2) are substituted.

APPENDIX V

DATA REDUCTION BY DIGITAL COMPUTER

APPENDIX V-1

PROGRAM FOR NONSOLUBLE GAS CASE

```
          ****  DYNAMICS OF NONSOLUBLE GAS BUBBLE - INJECTION COOLING
          ****  PART (1)    REDUCTION OF EXPERIMENTAL DATA
          INTEGER I,N, RUN, I1, NUM,J,J0,J1,I2                                  *001
          DIMENSION V(300), R(300), T(300)                                      *002
          DIMENSION P(300),TAU(300),Q(300),TAU1(10),P1(10),Q1(10),              *003
        1 TAU2(25),P2(25),Q2(25)                                                *003
          VECTOR VALUES INPUT = $ I4,8F4.0*$                                    *004
          VECTOR VALUES OUTPUT = $I4, 6F15.4*$                                  *005
BEGYND    READ DATA                                                             *006
          PRINT COMMENT $1BUBBLE GROWTH   NONSOLUBLE GAS$                       *007
          PRINT RESULTS RUN                                                     *008
          PRINT COMMENT $0INPUT$                                                *009
          PRINT COMMENT $0  I   S  H1  L2  Y4  Y3  Y2  Y1  Y0$                  *010
          PRINT COMMENT $ ------------------------------------$                 *011
          EXECUTE ZERO.(T(0)...T(300))                                          *013

BEGIN     READ FORMAT INPUT, I,S,H1,L2,Y4,Y3,Y2,Y1,Y0                           *014
          PRINT FORMAT INPUT,I,S,H1,L2,Y4,Y3,Y2,Y1,Y0                           *015
          B0 = Y0                                                               *016
          B1 = -3.*Y4 + 16.*Y3 - 36.*Y2 + 48.*Y1 - 25.*Y0                       *017
          B2 = 11.*Y4 - 56.*Y3 + 114.*Y2 - 104.*Y1 + 35.*Y0                     *018
          B3 = -3.*Y4 +14.*Y3 - 24.*Y2 + 18.*Y1 - 5.*Y0                         *019
          B4 = Y4 - 4.*Y3 + 6.*Y2 - 4.*Y1 + Y0                                  *020
          INT = (B4*32./9).P.2 + B4*B3*128./9. + B4*B2*128./63.                 *021
        1 + (B3*16./3.).P.2/7. + B4*B1*32./27. + B3*B2*32./27.                  *021
        2 + B4*B0*64./15. + B3*B1*32./45. + B2.P.2*4./45.                       *021
        3 + B3*B0*8./3. + B2*B1/9. + B2*B0*4./9. + B1.P.2/27.                   *021
        4 + B1*B0/3. + B0.P.2                                                   *021
          H = H1/S                                                              *022
          V(I) = (3.141593*INT*H/4.)* (L1/L2).P.3                               *023
          R(I) = (0.75*V(I)/3.141593).P.0.3333                                  *024
          T(I) = S1*I/SPEED                                                     *025
          WHENEVER I .L. N, TRANSFER TO BEGIN                                   *026
          THROUGH SW6, FOR I = I1   , 1, I .G. (N-1)                            *027
          WHENEVER T(I) .NE. (S1*I/SPEED), TRANSFER TO SW6                      *028
          WHENEVER VIM1.G.VIM2 .AND. VIM1 .G. V(I) .AND. VIM2 .NE. 0.           *029
          WHENEVER NUM .E. 0                                                    *030
          TRANSFER TO SW6A                                                      *031
          OTHERWISE                                                             *032
          TRANSFER TO SW7                                                       *033
          END OF CONDITIONAL                                                    *034
          OTHERWISE                                                             *035
          WHENEVER NUM .E. 0, TRANSFER TO SW6B                                  *036
          END OF CONDITIONAL                                                    *037
SW6A      NUM = NUM + 1                                                         *038
          SUM = SUM + V(I)                                                      *039
SW6B      VIM2 = VIM1                                                           *040
          VIM1 = V(I)                                                           *041
SW6       CONTINUE                                                              *042
SW7       VMAX = SUM/NUM                                                        *043
```

```
            DV = V(N)/VMAX - 1.                                                    *044
            WHENEVER DV.L.E5 .AND. DV.G.0. .OR. VMAX .E. 0., VMAX=V(N)             *045
            VO = (VMAX+VR)*(1.-XOO) + XOO*(V(0)+VR)                                *046
            XO = XOO*(VR+V(0))/VO                                                  *047
            PTH = (VMAX/(VO-VR)).P.0.3333                                          *048
            POO =((1.-XO)/(1.-XOO)).P.0.3333                                       *049
            RO = (.75*VMAX/3.141593).P.0.3333/POO                                  *050
            TAUDEL = TDELAY*A/(RO.P.2)                                             *051
            TAUMS = A/(RO.P.2)                                                     *052
            ALPHA = A                                                              *053
            PRINT COMMENT $1REDUCED EXPERIMENTAL DATA$                             *054
            PRINT RESULTS SPEED,N,RUN                                              *055
            PRINT RESULTS A,L1,VR                                                  *056
            PRINT RESULTS VO, RO, XO                                               *057
            PRINT RESULTS XOO, POO, PTH                                            *058
            PRINT RESULTS VMAX, NUM,I1                                             *059
            PRINT RESULTS E5,TDELAY,TAUDEL                                         *060
            PRINT COMMENT $0I        T(I)  MSEC        R(I)  MM       V(I)        *061
          1  CU.MM      TAU * S1            P                Q$                  *061
            PRINT COMMENT $ ------------------------------------------             *062
          1 ----------------------------------------------$                        *062
            J = 0                                                                  *063
            THROUGH BETA, FOR I = 0, 1, I .G. N                                    *064
            WHENEVER T(I) .NE. (S1*I/SPEED), TRANSFER TO BETA                      *065
            TAU = A*T(I)/(RO.P.2)                                                  *066
            P = R(I)/RO                                                            *067
            Q = (P - 1.)/(POO - 1.)                                                *068
            PRINT FORMAT OUTPUT, I,T(I), R(I),V(I),TAU,P,Q                         *069
            J = J + 1                                                              *070
            TAU(J) = TAU + TAUDEL                                                  *071
            P(J) = P                                                               *072
            Q(J) = Q                                                               *073
BETA        CONTINUE                                                               *074
            JO = J                                                                 *075

           ****  PART (2)    ANALYTICAL SOLUTION

           ****  PART (2A)   SMALL VALUES OF TAU

            INTEGER I, E2, RUN, J                                                  *076
            DIMENSION XS(10), D(100)                                               *077
            VECTOR VALUES FIRST = $ 4F20.4*$                                       *078
            VECTOR VALUES SECOND = $ 8F14.4 *$                                     *079
            PRINT COMMENT $1THEORETICAL BUBBLE GROWTH - NONSOLUBLE GAS$            *080
            PRINT RESULTS JA,S1,E4                                                 *081
            PRINT RESULTS LU,E1,E7                                                 *082
            PRINT RESULTS XOO,E2                                                   *083
            PRINT RESULTS XO,E3                                                    *084
            PRINT COMMENT $0SMALL VALUES OF TAU$                                   *085
            D(0)= (XOO - XO)/2.                                                    *086
            C = LU/((1.-XO)*JA.P.2)                                                *087
            THROUGH SW1, FOR I = 0, 1, I .G. E2                                    *088
            F = D(I).P.3 + (1.-XOO-C)*D(I).P.2 + 2.*C*(XOO-XO)*D(I) -              *089
          1 C*(XOO-XO).P.2                                                         *089
            FF = 3.*D(I).P.2 + 2.*(1.-XOO-C)*D(I) + 2.*C*(XOO-XO)                  *090
            D(I+1)= D(I) - F/FF                                                    *091
SW1         WHENEVER (.ABS.(D(I+1)/D(I)-1.)) .L. E1, TRANSFER TO ALFA              *092
ALFA        D(0) = D(I)                                                            *093
            XS(0) = XOO - D(0)                                                     *094
            AO = (JA*(XOO - XS(0))).P.2                                            *095
```

```
            UX = 10.                                                                    *096
            P1 = (1.-3.*(XS(0)-X0)/(5.*(1.-X0))).P.-0.3333                              *097
            DTAU = S1*((P1.P.3+2.)/P1-3.)/(4.*A0)/E3                                    *098
            PRINT RESULTS XS(0),A0,I                                                    *099
            PRINT COMMENT $0          1000*TAU                    P                     *100
           1          UX                      Q$                                       *100
            PRINT COMMENT $          ------------------------------------             *101
           1 ----------------------------------$                                       *101
            THROUGH SW2, FOR TAU = DTAU,DTAU, UX .LE. 1.                                *102
            A = 4.*A0*TAU/3./S1                                                         *103
            P = 2.*SQRT.(1.+A)*COS.(1.0472-ATAN.(((1.+A).P.3-1.).P.0.5)                 *104
           1 /3.)                                                                       *104
            UX = (XS(0)-X0)/((1.-X0)*(1.-1./P.P.3))                                     *105
            Q = (P-1.)/(P00-1.)                                                         *106
SW2         PRINT FORMAT FIRST, TAU, P , UX, Q                                          *107

          **** PART (2B)  JOIN POINT TAU1

            PRINT COMMENT $0JOIN POINT TAU1$                                            *108
            C = C*0.6                                                                   *109
            THROUGH SW3, FOR I = 0, 1, I .G. E2                                         *110
            F = D(I).P.3 + (1.-X00-C)*D(I).P.2 + 2.*C*(X00-X0)*D(I) -                   *111
           1 C*(X00-X0).P.2                                                             *111
            FF = 3.*D(I).P.2 + 2.*(1.-X00-C)*D(I) + 2.*C*(X00-X0)                       *112
            D(I+1) = D(I) - F/FF                                                        *113
SW3         WHENEVER (.ABS.(D(I+1)/D(I) - 1.)) .L. E1, TRANSFER TO BETA1                *114
BETA1       XS(1) = X00 - D(I)                                                          *115
            P1 = (1.-3.*(XS(1)-X0)/(5.*(1.-X0))).P.-0.3333                              *116
            P1DOT = 2.*LU*(XS(1)-X0)/(P1*(1.-XS(1)))                                    *117
            UT1 = P1*P1DOT/(2.*JA*(X00-XS(1)))                                          *118
            TAU1 = S1*((P1.P.3+2.)/P1-3.)/(4.*A0)                                       *119
            P00 = ((1.-X0)/(1.-X00)).P.0.3333                                           *120
            Q1 = (P1-1.)/(P00-1.)                                                       *121
            PRINT RESULTS TAU1,P1,P1DOT                                                 *122
            PRINT RESULTS Q1,XS(1),UT1                                                  *123
            TAU1 = TAU1 + TAUDEL                                                        *124

          **** PART (2C)   INTERMEDIATE VALUES OF TAU

            PRINT COMMENT $0INTERMEDIATE VALUES OF TAU$                                 *125
            PRINT COMMENT $0TAUH/TAUM = RELATIVE SIGNIFICANCE OF HEAT TRA               *126
           1 NSPORT TO MASS TRANSPORT FOR TAU$                                          *126
            PRINT COMMENT $0        S1*TAU          P          PDOT                     *127
           1      UT          DXS          Q          TAUH/TAUM       CR              *127
           2 IT1$                                                                       *127
            PRINT COMMENT $          ------------------------------------            *128
           1 ------------------------------------------------------------             *128
           2 ------------$                                                              *128
            W0 = 1./P00                                                                 *129
            CH = S1/(2.*(JA*(1.-X0)).P.2*W0.P.8)                                        *130
            CM = 2.*S1/(5.*LU*W0.P.2)                                                   *131
            W1 = P1/P00                                                                 *132
            DW = (1.-W1)/E4                                                             *133
            J = 0                                                                       *134
            TAU2 = 0.                                                                   *135
            THROUGH SW4, FOR W = W1+DW, DW, W .G. (1.-   DW)                            *136
            J = J + 1                                                                   *137
            TAUH = (W.P.2 - W1.P.2)/2. +                                                *138
           1    (1.-W0.P.3)*(W.P.2/(1.-W.P.3) - W1.P.2/(1.-W1.P.3))/3. -                *138
           2 ((5.-2.*W0.P.3)   /9.)*                                                    *138
```

```
      3 (ELOG.(SQRT.(( 1.+W+W.P.2)/(1.+W1+W1.P.2))*(1.-W1)/(1.-W)) -                *138
      4 SQRT.(3.)*(ATAN.((2.*W+1.)/SQRT.(3.)) - ATAN.((2.*W1+1.)/                  *138
      5 SQRT.(3.))))                                                               *138
        TAUM = -(W.P.2 - W1.P.2)/2. + (1./3.)*                                     *139
      1 (ELOG.(SQRT.(( 1.+W+W.P.2)/(1.+W1+W1.P.2))*(1.-W1)/(1.-W)) -                *139
      2 SQRT.(3.)*(ATAN.((2.*W+1.)/SQRT.(3.)) - ATAN.((2.*W1+1.)/                  *139
      3 SQRT.(3.))))                                                               *139
        TAU = TAU1 + CH*TAUH + CM*TAUM                                             *140
        RATIO = TAUH*CH/CM/TAUM                                                    *141
        P = W/W0                                                                   *142
        PPDOT = S1*(1.-W.P.3).P.2/(CH*W.P.3*(W.P.3-W0.P.3)+                        *143
      1 CM*W.P.3*(1.-W.P.3))/W0.P.2                                                *143
        PDOT = PPDOT/P                                                             *144
        UT = SQRT.(PPDOT/(2.*(1.-1./P.P.3)))                                       *145
        XS = X00 - SQRT.((1.-1./P.P.3)*PPDOT/(2.*JA.P.2))                          *146
        Q = (P-1.)/(P00-1.)                                                        *147
        DXS = XS - 1. + (1.-X0)/P.P.3                                              *148
        WHENEVER TAU2 .E. 0.                                                       *149
        WHENEVER  .ABS.(DXS/XS) .L. E7                                             *150
        TAU2 = TAU - (E7-DXS/XS)*(TAU-TAU21)/(DXS1/XS1-DXS/XS)                     *151
        P2 = P - (E7-DXS/XS)*(P-P21)/(DXS1/XS1-DXS/XS)                             *152
        Q2 = (P2 - 1.)/(P00 - 1.)                                                  *153
        OTHERWISE                                                                  *154
        DXS1 = DXS                                                                 *155
        XS1 = XS                                                                   *156
        TAU21 = TAU                                                                *157
        P21 = P                                                                    *158
        END OF CONDITIONAL                                                         *159
        END OF CONDITIONAL                                                         *160
        K = JA.P.2/LU                                                              *161
        L = 1. - X00                                                               *162
        NN = 1. - 1./P.P.3                                                         *163
        M = (X00-X0) - NN*(1.-X0)                                                  *164
        A1= 10. - 2.*K*L.P.2/NN                                                    *165
        A2 = 25. + 20.*K*M*L/NN                                                    *166
        A3 = 50.*K*M.P.2/NN                                                        *167
        CRIT1 = A3*(A3+A1*A2)/A2.P.3                                               *168
        TAU1(J) = TAU + TAUDEL                                                     *169
        P1(J) = P                                                                  *170
        Q1(J) = Q                                                                  *171
SW4     PRINT FORMAT SECOND,TAU,P,PDOT,UT,DXS,Q,RATIO,CRIT1                        *172
        J1 = J                                                                     *173
        PRINT RESULTS CH, CM                                                       *174

      **** PART (2D)  JOIN POINT TAU2

        PRINT COMMENT $0JOIN POINT TAU2$                                           *175
        TAU2 = TAU2 + TAUDEL                                                       *176
        PRINT RESULTS TAU2,P2,Q2                                                   *177

      **** PART (2E)  ASYMPTOTIC SOLUTION

        VECTOR VALUES ARG = 0.,.1,.2,.3,.4,.5,.75,1.,1.5,2.,2.5,                   *178
      1 3.,3.5,4.,4.5,5.,7.,8.,10.,15.,20.,30.                                     *178
        VECTOR VALUES ER = 1.,.8965,.8090,.7346,.6708,.6157,.5069,                 *179
      1 .4276,.3216,.2554,.2108,.1790,.15529,.13699,.122485,                       *179
      2 .110705,.08059,.070524,.05642,.037613,.02821,.018806                       *179
        VECTOR VALUES THIRD = $ 3F20.4 *$                                          *180
        PRINT COMMENT $1ASYMPTOTIC SOLUTION $                                      *181
        PRINT COMMENT $0          S1*TAU                    P                      *182
```

```
      1          Q$                                                    *182
        PRINT COMMENT $          ------------------------------------ *183
      1 --------------$                                                *183
        G = 2.*JA*(XOO-XO)/(POO.P.2-1.)                                *184
        THROUGH SW5A, FOR J=1, 1, J.G.21                               *185
        P2(J) = SQRT.(POO.P.2 - (POO.P.2-1.)*ER(J))                    *186
        TAU2(J) = S1*(ARG(J)/G).P.2                                    *187
        WHENEVER P2(J) .G. P2 .AND. J .G. 1                            *188
        TAUNUL = TAU2(J-1) + (P2-P2(J-1))*(TAU2(J)-TAU2(J-1))/         *189
      1 (P2(J)-P2(J-1))                                                *189
        TRANSFER TO SW5B                                               *190
        END OF CONDITIONAL                                             *191
SW5A    CONTINUE                                                       *192
SW5B    I = 1                                                          *193
        THROUGH SW5,FOR J = 0, 1, J.G. 21                              *194
        TAU = S1*(ARG(J)/G).P.2 + TAU2 -TAUNUL                         *195
        P = SQRT.(POO.P.2 - (POO.P.2 -1.)*ER(J))                       *196
        Q = (P-1.)/(POO-1.)                                            *197
        WHENEVER P .G. P2, I = I + 1                                   *198
        TAU2(I) = TAU + TAUDEL                                         *199
        P2(I) = P                                                      *200
        Q2(I) = Q                                                      *201
SW5     PRINT FORMAT THIRD, TAU, P, Q                                  *202
        I2 = I                                                         *203

        **** PART (3)    PLOT OF ANALYSIS AND EXPERIMENT

        INTEGER ORA.                                                   *204
        INTEGER IMAGE                                                  *205
        INTEGER LINEL,IVC,IHC,IRUN,INOM                                *206
        INTEGER IJA,ILU,IXO,IXOO,IA,IRO,IPOO,CRUN,CA,CRO,GAS1,GAS2     *207
        DIMENSION IMAGE(1000)                                          *208
        VECTOR VALUES NSCALE = 1,0,2,0,1                               *209
        VECTOR VALUES ORDP = $ NONDIMENSIONAL BUBBLE SIZE P$           *210
        VECTOR VALUES ORDQ = $ RELATIVE NONDIMENSIONAL BUBBLE SIZE Q$  *211
        PRINT COMMENT $8PLOT OF P(TAU) AND Q(TAU)$                     *212
        PRINT COMMENT $00  JOIN POINT TAU1$                            *213
        PRINT COMMENT $ .  INTERMEDIATE THEORY$                        *214
        PRINT COMMENT $ X  JOIN POINT TAU2$                            *215
        PRINT COMMENT $ +  ASYMPTOTIC THEORY$                          *216
        PRINT COMMENT $ *  EXPERIMENTAL POINTS$                        *217
        PRINT RESULTS TAUMS                                            *218
        PRINT COMMENT $+                                               *219
      1 1 MILLISECOND = TAUMS$                                         *219
        PRINT COMMENT $1$                                              *220
        PRINT COMMENT $-$                                              *221
        EXECUTE PLOT1.(NSCALE,NHL,HSBH,NVL,NSBV)                       *222
        EXECUTE PLOT2.(IMAGE,XMAX,XMIN,YMAX,YMIN)                      *223
        EXECUTE PLOT3.($O$,TAU1,P1,1)                                  *224
        EXECUTE PLOT3.($.$,TAU1(1),P1(1),J1)                           *225
        EXECUTE PLOT3.($+$,TAU2(1),P2(1),I2)                           *226
        EXECUTE PLOT3.($X$,TAU2,P2,1)                                  *227
        EXECUTE PLOT3.($*$,TAU(1),P(1),JO)                             *228
        EXECUTE TITLE.                                                 *229
        EXECUTE PLOT4.(29,ORDP)                                        *230
        PRINT COMMENT $O                                               *231
      1   NONDIMENSIONAL TIME  1000*TAU = 1000*A*T/RO.P.2$             *231
        PRINT COMMENT $1$                                              *232
        PRINT COMMENT $-$                                              *233
        EXECUTE PLOT1.(NSCALE,NHL1,NSBH1,NVL1,NSBV1)                   *234
```

```
        EXECUTE PLOT2.(IMAGE,XMAX1,XMIN1,YMAX1,YMIN1)                    *235
        EXECUTE PLOT3.($0$,TAU1,Q1,1)                                    *236
        EXECUTE PLOT3.($.$,TAU1(1),Q1(1),J1)                             *237
        EXECUTE PLOT3.($+$,TAU2(1),Q2(1),I2)                             *238
        EXECUTE PLOT3.($X$,TAU2,Q2,1)                                    *239
        EXECUTE PLOT3.($*$,TAU(1),Q(1),J0)                               *240
        EXECUTE TITLE.                                                   *241
        EXECUTE PLOT4.(38,ORDQ)                                          *242
        PRINT COMMENT $0                                                 *243
      1   NONDIMENSIONAL TIME  1000*TAU = 1000*A*T/R0.P.2$               *243

        ****              TITLE FOR PLOT

        INTERNAL FUNCTION                                                *244
        ENTRY TO TITLE.                                                  *245
        IA = 10000*ALPHA                                                 *246
        IR0 = R0                                                         *247
        IR0 = (9*IR0 + R0)*1000                                          *248
        IX0 = 1000*X0                                                    *249
        IP00 = P00                                                       *250
        IP00 = (9*IP00 + P00)*1000                                       *251
        IX00 = 1000*X00                                                  *252
        CRUN = $   000$                                                  *253
        CA = $0.0000$                                                    *254
        CR0 = $ 0.000$                                                   *255
        LINEL = (NSBV*NVL+1)/6 + 1                                       *256
        THROUGH SW8 ,FOR I = IVC, LINEL, I.G.(IVC+2*(HSBH-1)*LINEL)      *257
SW8     IMAGE(I) = $       $                                             *258
        THROUGH SW9, FOR I = IHC, 1, I .G. (IHC+NSBV/3)                  *259
SW9     IMAGE(I) = $       $                                             *260
        IMAGE(IRUN) = $RUN   $                                           *261
        IMAGE(IRUN+1) = ORA.(BNBCD.(RUN),CRUN)                           *262
        IMAGE(INOM) = $0  JOI$                                           *263
        IMAGE(INOM+1) = $N POIN$                                         *264
        IMAGE(INOM+2) = $T TAU1$                                         *265
        I = INOM + LINEL                                                 *266
        IMAGE(I) = $.  INT$                                              *267
        IMAGE(I+1) = $ERMEDI$                                            *268
        IMAGE(I+2) = $ATE TH$                                            *269
        IMAGE(I+3) = $EORY  $                                            *270
        I = INOM + 2*LINEL                                               *271
        IMAGE(I) = $X  JOI$                                              *272
        IMAGE(I+1) = $N POIN$                                            *273
        IMAGE(I+2) = $T TAU2$                                            *274
        I = INOM + 3*LINEL                                               *275
        IMAGE(I) = $+  ASY$                                              *276
        IMAGE(I+1) = $MPTOTI$                                            *277
        IMAGE(I+2) = $C THEO$                                            *278
        IMAGE(I+3) = $RY    $                                            *279
        I = INOM + 4*LINEL                                               *280
        IMAGE(I) = $*  EXP$                                              *281
        IMAGE(I+1) = $ERIMEN$                                            *282
        IMAGE(I+2) = $TAL PO$                                            *283
        IMAGE(I+3) = $INT   $                                            *284
        I = INOM - 1 + 6*LINEL                                           *285
        J = I                                                            *286
        IMAGE(I) = $ JA = $                                              *287
        IMAGE(I+1)= IJA                                                  *288
        IMAGE(I+3) = $  A = $                                            *289
        IMAGE(I+4) = ORA.(BNBCD.(IA),CA)                                 *290
```

```
      I = J + LINEL                                                    *291
      IMAGE(I) = $ LU = $                                              *292
      IMAGE(I+1) = ILU                                                 *293
      IMAGE(I+3) = $ RO = $                                            *294
      IMAGE(I+4) = ORA.(BNBCD.(IRO),CRO)                               *295
      I = J + 2*LINEL                                                  *296
      IMAGE(I) = $ XO = $                                              *297
      IMAGE(I+1) = ORA.(BNBCD.(IXO),CRO)                               *298
      IMAGE(I+3) = $POO = $                                            *299
      IMAGE(I+4) = ORA.(BNBCD.(IPOO),CRO)                              *300
      I = J +3*LINEL                                                   *301
      IMAGE(I) = $XOO = $                                              *302
      IMAGE(I+1) = ORA.(BNBCD.(IXOO),CRO)                              *303
      IMAGE(I+3) = $WATER $                                            *304
      I = J + 4*LINEL                                                  *305
      IMAGE(I+3) = GAS1                                                *306
      IMAGE(I+4) = GAS2                                                *307
      FUNCTION RETURN                                                  *308
      END OF FUNCTION                                                  *309
      TRANSFER TO BEGYND                                               *310
      END OF PROGRAM                                                   *311
```

APPENDIX V-2

NOMENCLATURE FOR COMPUTER PROGRAM FOR THE CASE OF A NONSOLUBLE GAS

AO	A_o in Equation (56)
A1	Coefficient in Equation (IV-2)
A2	Coefficient in Equation (IV-2)
A3	Coefficient in Equation (IV-2)
ALPHA	α' (mm^2/sec)
ARG	$b\sqrt{\tau}$ in Equation (84) (table)
A	α' and $\frac{4}{3} A_o \tau$ in Equation (55)
BO...B4	intermediate coefficients in INT
CH	C_H in Equation (69)
CM	C_M in Equation (69)
CRIT1	Equation (67)
C	$Lu/(Ja^2(1-x_o))$
D	$x_\infty - x_s$
DXS	$x_s - x$ in Equation (85)
DTAU	$\Delta\tau$, time increment
DV	V(N)/VMAX - 1
DW	increment for w in Equation (69)
ER	$e^{b^2\tau}\text{erfc}\ b\sqrt{\tau}$ in Equation (84) (table)
F	function from Equation (56), F = 0
FF	$\partial F/\partial D$
G	b in Equation (84)

H,H1	bubble length in Equation (126), H = H1/S
I	frame number
I1	frame number from which VMAX is averaged
INT	integral of Equation (127)
JA	Ja-number
K	Equation (66)
L1	actual reference length of injector tip
L2	measured reference length of injector tip
L	Equation (66)
LU	Lu-number
M	Equation (66)
N	maximum number of pictures for a run
NUM	number of frames used in obtaining the average value of VMAX
P1DOT	$\dot{P}_1$
P1	P_1
P2	P_2
PDOT	$\dot{P}$
POO	P_∞
PPDOT	$\dot{PP}$
P	P, dimensionless bubble size $P = R/R_o$
PTH	theoretical value of P_∞ including the effect of residual volume
Q1	Q_1
Q2	Q_2
Q	Q, relative dimensionless bubble size $Q = (P-1)/(P_\infty-1)$
RO	R_o, initial radius in mm

RATIO	$C_M I_M / C_H I_H$ in Equation (70)
R	R, bubble radius in mm
RUN	run number
S1	scaling factor for time (S1=1000)
SPEED	film speed (fps.)
S	scaling factor for ruler system used in measuring bubble dimensions
SUM	sum of volumes used for determining VMAX
TAU1	τ_1 in Equation (60), join point
TAU2	τ_2 join point
TAUDEL	time delay, (here zero)
TAUH	τ_H in Equation (69) $\tau_H = C_H I_H$
TAUM	τ_M in Equation (69) $\tau_M = C_M I_M$
TAUMS	nondimensional time corresponding to 1 ms
TAUNUL	τ_o in Equation (84)
TAU	τ dimensionless time $\tau = \alpha' t / R_o^2$
TDELAY	time delay (here zero)
T	time in milliseconds
UT1	$(R/f_T)_1$ in Equation (64)
UT	(R/f_T) in Equation (52)
UX	(R/f_x) in Equation (52)
VO	V_o initial bubble volume in mm^3
VMAX	asymptotic bubble volume in mm^3
VR	residual volume Figure 30(a)
V	bubble volume in mm^3

WO	$w_o = 1/P_\infty$
W1	$w_1 = P_1/P_\infty$
W	$w = P/P_\infty$
XO	x_o
XOO	x_∞
XS1	x_{s1}
XS	x_s, interface composition
Y1...Y4	bubble diameters, $y_o \ldots y_4$ in Figure 30(e)

APPENDIX V-3

DATA INPUT FOR RUN 523

```
RUN=523,
E1=.005,E2=20.,E3=1.,E4=10.,E5=.1,VR=-.306,L1=2.082,IDELAY=0.,S1=1000.,
NHL=6,HSBH=8,NVL=5,NSBV=20,XMIN=0.,XMAX=50.,YMIN=1.,YMAX=2.2,
NHL1=6,NSBH1=8,NVL1=5,NSBV1=20,XMIN1=0.,XMAX1=50.,YMIN1=0.,YMAX1=1.2,
IVC=435,IHC=551,IRUN=451,INOM=484,
GAS1=$NITROG$,GAS2=$EN     $, E7=.005,
RUN=523,SPEED=1008.,JA=91.7,LU=185.,XOO=.8931,A=.16751,I1=170,N=195,
IJA=$  91.7$, ILU=$   185$*

000 001 058 127 094 084 055 040 000
001 001 068 127 160 167 163 130 000
002 001 084 127 160 203 205 176 000
003 001 096 127 128 207 109 160 000
004 001 115 127 128 179 198 160 000
005 001 128 127 127 165 186 180 000
006 001 139 127 125 146 179 186 000
007 001 159 127 126 149 169 175 000
008 001 177 127 126 156 160 160 000
009 001 195 127 125 160 156 138 000
010 001 207 127 126 161 154 127 000
011 001 222 127 125 163 150 119 000
012 001 230 127 125 165 155 114 000
013 001 204 127 125 165 166 136 000
014 001 179 127 126 166 173 164 000
015 001 163 127 126 164 188 176 000
016 001 154 127 126 176 193 194 000
018 001 141 127 126 194 221 191 000
020 001 134 127 150 220 220 179 000
 -
 -
 -
 -
 -
 -
 -
182 001 205 127 127 198 203 164 000
184 001 189 127 129 200 206 173 000
186 001 173 127 129 200 215 191 000
188 001 161 127 129 208 226 197 000
190 001 155 127 190 223 231 191 000
192 001 150 127 170 233 231 186 000
193 001 094 067 067 114 120 103 000
195 001 093 067 067 113 118 099 000
```

APPENDIX V-4

PRINT-OUT FOR RUN 523

PART 1 BUBBLE GROWTH NONSOLUBLE GAS

RUN = 523

(a) INPUT

I	S	H1	L2	Y4	Y3	Y2	Y1	Y0
0	1	58	127	94	84	55	40	0
1	1	68	127	160	167	163	130	0
2	1	84	127	160	203	205	176	0
3	1	96	127	128	207	109	160	0
4	1	115	127	128	179	198	160	0
5	1	128	127	127	165	186	180	0
6	1	139	127	125	146	179	186	0
7	1	159	127	126	149	169	175	0
8	1	177	127	126	156	160	160	0
9	1	195	127	125	160	156	138	0
10	1	207	127	126	161	154	127	0
11	1	222	127	125	163	150	119	0
12	1	230	127	125	165	155	114	0
13	1	204	127	125	165	166	136	0
14	1	179	127	126	166	173	164	0
15	1	163	127	126	164	188	176	0
16	1	154	127	126	176	193	194	0
18	1	141	127	126	194	221	191	0
20	1	134	127	150	220	220	179	0
22	1	135	127	180	225	212	163	0
24	1	129	127	170	224	218	166	0
26	1	130	127	140	209	221	188	0
28	1	144	127	126	194	211	194	0
30	1	163	127	130	190	196	185	0
32	1	190	127	126	184	196	161	0
34	1	216	127	126	181	189	150	0
36	1	201	127	127	180	187	167	0
38	1	185	127	128	184	197	169	0
40	1	158	127	128	191	209	186	0
42	1	146	127	128	203	217	194	0
46	1	133	127	190	228	222	179	0
44	1	138	127	135	222	228	181	0
48	1	135	127	185	230	223	179	0
50	1	144	127	155	231	227	178	0
52	1	152	127	127	208	229	200	0
54	1	164	127	126	195	218	201	0
56	1	187	127	127	190	200	180	0
58	1	208	127	128	186	189	152	0
60	1	213	127	127	184	185	148	0
62	1	184	127	127	183	197	180	0
64	1	168	127	126	191	210	195	0
66	1	157	127	127	209	228	193	0
68	1	145	127	150	231	236	191	0
70	1	134	127	200	239	231	192	0
72	1	138	127	200	243	234	180	0
74	1	139	127	170	234	232	195	0
76	1	149	127	127	214	229	200	0
78	1	165	127	126	196	215	193	0
80	1	186	127	127	190	201	177	0
82	1	202	127	127	189	196	163	0
84	1	211	127	128	187	194	158	0
86	1	194	127	126	191	201	174	0
88	1	171	127	127	200	214	194	0
90	1	159	127	125	204	227	199	0
92	1	149	127	145	215	230	199	0
94	1	144	127	170	231	228	183	0
96	1	144	127	183	230	224	176	0
98	1	143	127	160	226	224	186	0
100	1	152	127	130	216	230	186	0
102	1	161	127	128	204	220	197	0
104	1	176	127	128	201	213	187	0
106	1	200	127	128	196	204	165	0
108	1	208	127	129	194	198	165	0
112	1	179	127	129	193	211	186	0
114	1	162	127	129	202	217	195	0
116	1	153	127	127	217	228	190	0
118	1	146	127	160	231	232	196	0
120	1	140	127	185	235	232	191	0
122	1	144	127	177	235	234	188	0
124	1	152	127	150	228	234	190	0
126	1	161	127	130	212	228	201	0
128	1	176	127	129	199	217	193	0
130	1	194	127	128	193	204	175	0
132	1	206	127	127	192	196	162	0
134	1	204	127	127	193	199	161	0
136	1	180	127	127	195	209	186	0
138	1	164	127	130	206	221	200	0
140	1	155	127	130	220	234	197	0
142	1	150	127	165	233	236	190	0
144	1	146	127	190	238	232	190	0
146	1	148	127	175	237	230	185	0
148	1	151	127	145	227	233	191	0
150	1	156	127	134	209	225	200	0
152	1	170	127	127	199	216	190	0
154	1	190	127	126	198	204	175	0
156	1	203	127	128	197	202	164	0
158	1	201	127	128	195	206	171	0
160	1	185	127	127	197	211	187	0
162	1	171	127	127	204	220	195	0
164	1	160	127	128	216	228	190	0
166	1	150	127	160	225	229	193	0
168	1	146	127	172	230	232	190	0
170	1	147	127	170	231	230	185	0
172	1	149	127	160	227	228	192	0
174	1	159	127	130	218	229	188	0
176	1	169	127	127	206	222	193	0
178	1	184	127	126	199	213	189	0
180	1	199	127	128	198	207	173	0
182	1	205	127	127	198	203	164	0
184	1	189	127	129	200	206	173	0
186	1	173	127	129	200	215	191	0
188	1	161	127	129	208	226	197	0
190	1	155	127	190	223	231	191	0
192	1	150	127	170	233	231	186	0
193	1	94	67	67	114	120	103	0
195	1	93	67	67	113	118	99	0

(6) REDUCED EXPERIMENTAL DATA

SPEED =	1008.000000,	N =	195,	RUN =	523
A =	.167510,	L1 =	2.082000,	VR =	-.306000
V0 =	2.785530,	R0 =	.876954,	X0 =	.168971
X00 =	.893100,	P00 =	1.980842,	PTH =	1.922179
VMAX =	21.960408,	NUM =	5,	I1 =	170
E5 =	.100000,	TDELAY =	.000000,	TAUDEL =	.000000

I	T(I) MSEC	R(I) MM	V(I) CU.MM	TAU * S1	P	Q
0	.0000	.5837	.8330	.0000	.6656	-.3409
1	.9921	1.0608	5.0000	.2161	1.2096	.2137
2	1.9841	1.3133	9.4887	.4322	1.4976	.5073
3	2.9762	1.2774	8.7323	.6483	1.4567	.4656
4	3.9683	1.3644	10.6411	.8643	1.5559	.5667
5	4.9603	1.4058	11.6388	1.0804	1.6031	.6148
6	5.9524	1.4106	11.7594	1.2965	1.6086	.6205
7	6.9444	1.4449	12.6378	1.5126	1.6477	.6603
8	7.9365	1.4687	13.2729	1.7287	1.6748	.6880
9	8.9286	1.4739	13.4132	1.9448	1.6807	.6940
10	9.9206	1.4816	13.6236	2.1609	1.6894	.7029
11	10.9127	1.4998	14.1336	2.3769	1.7103	.7241
12	11.9048	1.5214	14.7519	2.5930	1.7348	.7492
13	12.8968	1.5196	14.7019	2.8091	1.7329	.7472
14	13.8889	1.5229	14.7963	3.0252	1.7366	.7510
15	14.8810	1.5158	14.5901	3.2413	1.7285	.7427
16	15.8730	1.5543	15.7294	3.4574	1.7723	.7874
18	17.8571	1.5744	16.3485	3.8895	1.7953	.8108
20	19.8413	1.5880	16.7755	4.3217	1.8108	.8266
22	21.8254	1.5825	16.6027	4.7539	1.8045	.8203
24	23.8095	1.5632	16.0014	5.1861	1.7825	.7978
26	25.7937	1.5614	15.9473	5.6182	1.7805	.7957
28	27.7778	1.5777	16.4531	6.0504	1.7991	.8147
30	29.7619	1.6011	17.1966	6.4826	1.8258	.8419
32	31.7460	1.6225	17.8930	6.9148	1.8501	.8667
34	33.7302	1.6537	18.9455	7.3469	1.8857	.9030
36	35.7143	1.6428	18.5732	7.7791	1.8733	.8903
38	37.6984	1.6256	17.9957	8.2113	1.8537	.8703
40	39.6825	1.6044	17.3018	8.6434	1.8295	.8457
42	41.6667	1.6114	17.5286	9.0756	1.8375	.8538
44	43.6508	1.6147	17.6386	9.5078	1.8413	.8577
46	45.6349	1.6205	17.8290	9.9400	1.8479	.8645
48	47.6190	1.6316	18.1977	10.3721	1.8606	.8774
50	49.6032	1.6590	19.1293	10.8043	1.8918	.9092
52	51.5873	1.6691	19.4800	11.2365	1.9033	.9209
54	53.5714	1.6722	19.5903	11.6686	1.9069	.9246
56	55.5556	1.6702	19.5183	12.1008	1.9045	.9222
58	57.5397	1.6502	18.8280	12.5330	1.8818	.8990
60	59.5238	1.6441	18.6195	12.9652	1.8748	.8919
62	61.5079	1.6414	18.5274	13.3973	1.8717	.8888
64	63.4921	1.6553	18.9998	13.8295	1.8875	.9048
66	65.4762	1.6756	19.7087	14.2617	1.9107	.9285
68	67.4603	1.6920	20.2944	14.6938	1.9294	.9476
70	69.4444	1.6815	19.9169	15.1260	1.9174	.9353

(PART 1(b)) CONT'D)

72	71.4286	1.6920	20.2932	15.5582	1.9294	.9475
74	73.4127	1.6842	20.0135	15.9904	1.9205	.9385
76	75.3968	1.6699	19.5090	16.4225	1.9042	.9219
78	77.3810	1.6586	19.1138	16.8547	1.8913	.9087
80	79.3651	1.6627	19.2586	17.2869	1.8960	.9135
82	81.3492	1.6722	19.5892	17.7191	1.9068	.9245
84	83.3333	1.6796	19.8511	18.1512	1.9153	.9332
86	85.3175	1.6822	19.9446	18.5834	1.9183	.9362
88	87.3016	1.6878	20.1428	19.0156	1.9246	.9427
90	89.2857	1.6811	19.9023	19.4477	1.9169	.9348
92	91.2698	1.6784	19.8078	19.8799	1.9139	.9317
94	93.2540	1.6744	19.6665	20.3121	1.9093	.9271
96	95.2381	1.6628	19.2597	20.7443	1.8961	.9136
98	97.2222	1.6556	19.0114	21.1764	1.8879	.9052
100	99.2063	1.6639	19.3000	21.6086	1.8974	.9149
102	101.1905	1.6762	19.7316	22.0408	1.9114	.9292
104	103.1746	1.6921	20.2982	22.4729	1.9296	.9477
106	105.1587	1.6994	20.5605	22.9051	1.9378	.9561
108	107.1429	1.7085	20.8930	23.3373	1.9482	.9667
110	109.1270	1.6941	20.3683	23.7695	1.9318	.9500
112	111.1111	1.6801	19.8675	24.2016	1.9158	.9337
114	113.0952	1.6684	19.4550	24.6338	1.9025	.9201
116	115.0794	1.6724	19.5976	25.0660	1.9071	.9248
118	117.0635	1.7031	20.6961	25.4981	1.9421	.9605
120	119.0476	1.6906	20.2432	25.9303	1.9278	.9459
122	121.0317	1.7007	20.6075	26.3625	1.9393	.9577
124	123.0159	1.7084	20.8909	26.7947	1.9482	.9667
126	125.0000	1.7111	20.9890	27.2268	1.9512	.9698
128	126.9841	1.7049	20.7631	27.6590	1.9442	.9626
130	128.9683	1.6940	20.3646	28.0912	1.9317	.9499
132	130.9524	1.6885	20.1692	28.5234	1.9255	.9435
134	132.9365	1.6880	20.1510	28.9555	1.9249	.9429
136	134.9206	1.6839	20.0044	29.3877	1.9202	.9382
138	136.9048	1.6983	20.5223	29.8199	1.9366	.9549
140	138.8889	1.7067	20.8280	30.2520	1.9462	.9647
142	140.8730	1.7201	21.3212	30.6842	1.9614	.9802
144	142.8571	1.7215	21.3725	31.1164	1.9630	.9818
146	144.8413	1.7103	20.9582	31.5486	1.9502	.9688
148	146.8254	1.7009	20.6160	31.9807	1.9396	.9579
150	148.8095	1.6830	19.9727	32.4129	1.9192	.9371
152	150.7936	1.6776	19.7801	32.8451	1.9130	.9308
154	152.7778	1.6928	20.3236	33.2772	1.9304	.9485
156	154.7619	1.7054	20.7801	33.7094	1.9447	.9632
158	156.7460	1.7140	21.0972	34.1416	1.9545	.9732
160	158.7302	1.7085	20.8922	34.5738	1.9482	.9667
162	160.7143	1.7061	20.8064	35.0059	1.9455	.9640
164	162.6984	1.6959	20.4328	35.4381	1.9338	.9520
166	164.6825	1.6975	20.4924	35.8703	1.9357	.9540
168	166.6667	1.6966	20.4596	36.3024	1.9347	.9529
170	168.6508	1.6914	20.2736	36.7346	1.9288	.9469
172	170.6349	1.6951	20.4039	37.1668	1.9329	.9511
174	172.6190	1.6952	20.4105	37.5990	1.9331	.9513
176	174.6032	1.7027	20.6810	38.0311	1.9416	.9600
178	176.5873	1.7159	21.1675	38.4633	1.9567	.9754
180	178.5714	1.7206	21.3390	38.8955	1.9620	.9808
182	180.5556	1.7144	21.1110	39.3277	1.9550	.9736
184	182.5397	1.6949	20.3978	39.7598	1.9327	.9509
186	184.5238	1.6909	20.2529	40.1920	1.9281	.9462
188	186.5079	1.6928	20.3213	40.6242	1.9303	.9485
190	188.4921	1.7246	21.4878	41.0563	1.9665	.9854
192	190.4762	1.7099	20.9445	41.4885	1.9498	.9684
193	191.4683	1.7662	23.0821	41.7046	2.0140	1.0338
195	193.4524	1.7371	21.9604	42.1368	1.9808	1.0000

PART 2 THEORETICAL BUBBLE GROWTH - NONSOLUBLE GAS

JA =	91.700000,	S1 =	1000.000000,	E4 =	10.000000
LU =	185.000000,	E1 =	5.000000E-03,	E7 =	5.000000E-03
XOO =	.895100,	E2 =	20		
XO =	.168971,	E3 =	1.000000		

(a) SMALL VALUES OF TAU

XS(0) =	.721422,	A0 =	247.838074,	I =	3

1000*TAU	P	UX	Q
.0927	1.1849	1.6668	.1885
.1853	1.2669	1.3080	.2721
.2780	1.3319	1.1526	.3384
.3707	1.3880	1.0619	.3956
.4633	1.4383	1.0013	.4469
.5560	1.4846	.9574	.4940

(b) JOIN POINT TAU1

TAU1(0) =	.105204,	P1(0) =	1.197641,	P1DOT =	708.997482
Q1(0) =	.201502,	XS(1) =	.747786,	UT1 =	31.861320

14113

(c) INTERMEDIATE VALUES OF TAU

TAUH/TAUM = RELATIVE SIGNIFICANCE OF HEAT TRANSPORT TO MASS TRANSPORT FOR TAU

S1*TAU	P	PDOT	UT	DXS	Q	TAUH/TAUM	CRIT1
.1980	1.2760	682.9116	28.9842	.1292	.2814	.3711	.7491
.3428	1.3543	434.1106	22.1823	.0832	.3612	.4836	.5862
.5733	1.4326	269.8927	17.1163	.0526	.4411	.6325	.4321
.9502	1.5109	162.3652	13.1431	.0323	.5209	.8334	.3019
1.5926	1.5892	93.0303	9.9223	.0189	.6008	1.1132	.1983
2.7573	1.6676	49.4700	7.2517	.0103	.6806	1.5231	.1198
5.0896	1.7459	23.2723	5.0016	.0050	.7605	2.1754	.0636
10.6663	1.8242	8.7036	3.0829	.0019	.8403	3.3823	.0267
30.6338	1.9025	1.8416	1.4316	.0004	.9202	6.5338	.0063

CH =	20.407853,	CM =	8.483750

(d) JOIN POINT TAU2

TAU2(0) =	6.395873,	P2(0) =	1.764227,	Q2(0) =	.779154

(e) ASYMPTOTIC SOLUTION

S1*TAU	P	Q
4.7370	1.0000	.0000
4.7418	1.1413	.1441
4.7564	1.2484	.2532
4.7806	1.3327	.3391
4.8145	1.4009	.4087
4.8581	1.4573	.4662
5.0096	1.5626	.5736
5.2216	1.6351	.6475
5.8275	1.7273	.7415
6.6757	1.7824	.7977
7.7662	1.8186	.8346
9.0990	1.8440	.8605
10.6742	1.8627	.8796
12.4917	1.8770	.8942
14.5515	1.8883	.9056
16.8537	1.8974	.9149
28.4858	1.9204	.9384
35.7558	1.9281	.9462
53.2039	1.9388	.9571
113.7875	1.9529	.9715
198.6046	1.9599	.9787
440.9390	1.9669	.9858

PART 3 PLOT OF P(TAU) AND Q(TAU)

0 JOIN POINT TAU1
. INTERMEDIATE THEORY
X JOIN POINT TAU2
+ ASYMPTOTIC THEORY
* EXPERIMENTAL POINTS

1000*TAUMS = .217815 1 MILLISECOND = TAUMS

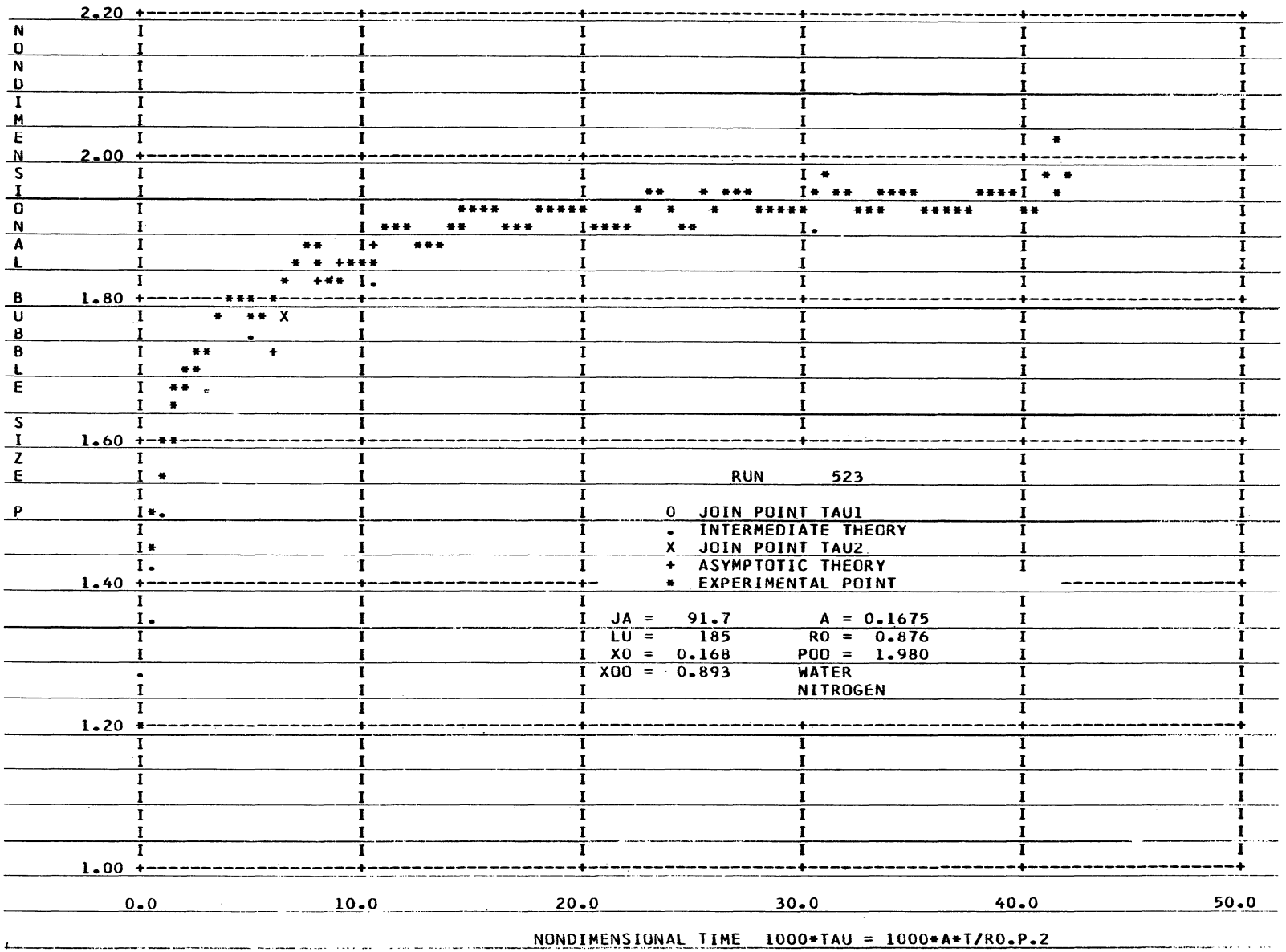
NONDIMENSIONAL BUBBLE SIZE
2.20
2.00
1.80
1.60
1.40
1.20
1.00
0.0
10.0
20.0
30.0
40.0
50.0
NONDIMENSIONAL TIME 1000*TAU = 1000*A*T/RO.P.2
RUN 523
0 JOIN POINT TAU1
. INTERMEDIATE THEORY
X JOIN POINT TAU2
+ ASYMPTOTIC THEORY
* EXPERIMENTAL POINT
JA = 91.7
LU = 185
XO = 0.168
XOO = 0.893
A = 0.1675
RO = 0.876
POO = 1.980
WATER
NITROGEN

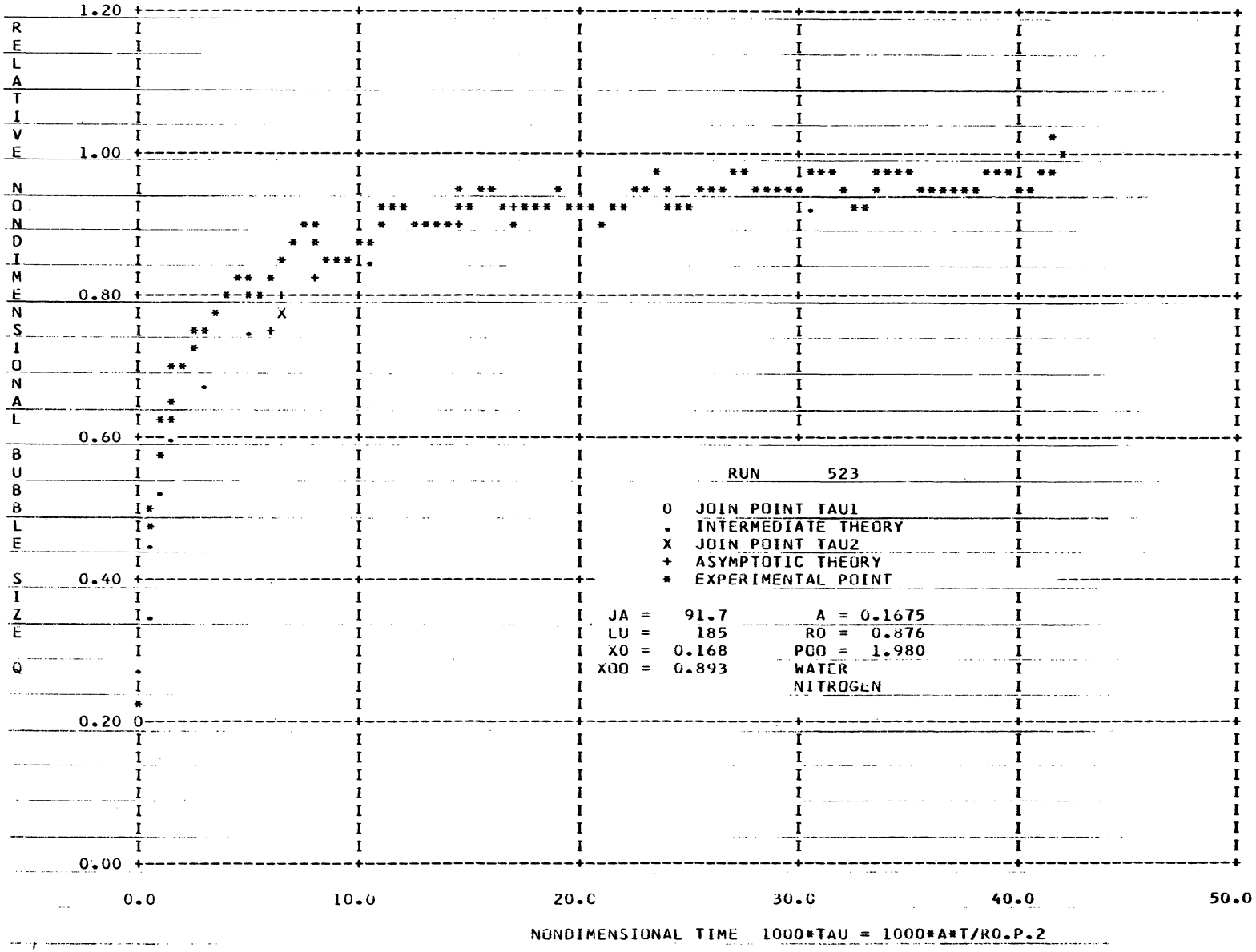
RELATIVE NONDIMENSIONAL BUBBLE SIZE
1.20
1.00
0.80
0.60
0.40
0.20
0.00
0.0
10.0
20.0
30.0
40.0
50.0
NONDIMENSIONAL TIME 1000*TAU = 1000*A*T/R0.P.2
RUN 523
0 JOIN POINT TAU1
. INTERMEDIATE THEORY
X JOIN POINT TAU2
+ ASYMPTOTIC THEORY
* EXPERIMENTAL POINT
JA = 91.7
LU = 185
X0 = 0.168
X00 = 0.893
A = 0.1675
R0 = 0.876
P00 = 1.980
WATER
NITROGEN

APPENDIX VI

SUMMARY OF EXPERIMENTAL DATA

APPENDIX VI-1

DATA FOR THE CASE OF A NONSOLUBLE GAS

Run	Liquid	Gas	SPEED (fps)	T_∞(°F)	p_∞ (inch Hg)	α' (mm^2/sec)	R_o (mm)	Ja	Lu	x_∞	x_o	P_∞	Comment
504	H_2O	N_2	1000	204.1	28.15	0.1674	0.761	93.8	191	0.903	0.227	1.999	Stationary
511	H_2O	N_2	4000	75	29.4	0.1435	1.548	450	1600	0.030	0.001	1.010	Formation
517	H_2O	N_2	1024	163.8	11.97	0.1627	0.820	184.3	421	0.883	0.156	1.933	Stationary
521	H_2O	N_2	1024	149.2	7.98	0.1603	0.661	241.0	587	0.929	0.387	2.053	Stationary
523	H_2O	N_2	1008	205.4	29.37	0.1675	0.877	91.7	185	0.893	0.169	1.981	Stationary
524	H_2O	N_2	1088	205.1	27.90	0.1675	0.747	92.0	186	0.933	0.231	2.257	Stationary
601	H_2O	He	1008	206.3	29.17	0.1676	0.839	90.4	560	0.915	0.326	1.994	Stationary
609	H_2O	He	2640	164.0	11.35	0.1627	0.709	180.5	1124	0.935	0.405	2.090	Stationary
613	H_2O	He	2672	153.2	8.92	0.1611	0.803	224.7	1430	0.908	0.386	1.884	Stationary
702	H_2O	N_2	1008	202.8	27.93	0.1672	0.764	95.4	190	0.890	0.203	1.935	Injector Facing up
805	H_2O	N_2	1072	180.7	18.14	0.1648	3.010	136.2	291	0.856	0.010	1.902	Moving
806	H_2O	N_2	977	180.3	18.00	0.1647	2.994	137.4	297	0.854	0.010	1.892	Moving

APPENDIX VI-2

DATA FOR THE CASE OF A SOLUBLE GAS

Run	901	903	951	953	954	955
Liquid	H_2O	H_2O	H_2O	H_2O	H_2O	H_2O
Gas	NH_3	NH_3	NH_3	NH_3	NH_3	NH_3
SPEED fps	1008	1008	992	1008	1008	1008
T_∞ °F	181.3	197.8	204.3	205.3	177.4	178.0
p_∞(psia)	9.01	11.8	13.7	14.27	7.87	9.48
α' (mm^2/ sec)	0.1649	0.1667	0.1674	0.1675	0.1644	0.1645
$\rho_e x10^{-3}$ (ohm-cm)	30	30	38	36	35.5	36
p^*_B(psia)	642	779	835	846	613	617
K_B ref.(47)	0.0578	0.0588	0.0600	0.0788	0.0526	0.0624
Ja	135.4	104.0	93.2	91.5	144.0	142.5
Lu	405	285	258	252	312	308
Lu'	9×10^{-3}	9×10^{-3}	9×10^{-3}	9×10^{-3}	9×10^{-3}	9×10^{-3}
x''_∞	0.858	0.932	0.920	0.901	0.901	0.758
$(1-x'_\infty)x10^5$	2.5	2.5	1.6	1.8	1.85	1.8
x''_o	~ 0	~ 0	~ 0	~ 0	~ 0	~ 0
$1-x^*$	0.0082	0.0040	0.0048	0.0078	0.0052	0.0151
$F = h_{fgB}/h_{fgA}$	0.8	0.8	0.8	0.8	0.8	0.8
$(1-\epsilon)x10^4$	3.3	4.5	5.0	5.0	2.9	2.9
λ, Eq.(106)	-8.76	-9.00	-8.18	-6.04	-8.97	-4.63
Comment	Moving	Moving	Stationary	Stationary	Stationary	Stationary

APPENDIX VI-3

DATA FOR BUBBLE OSCILLATIONS

RUN	Mean Radius $\bar{R}$ (mm)	Measured Frequency f (sec^{-1})	Theoretical Frequency Eq. (20) f_{th} (sec^{-1})	Relative Polar Amplitude a/R	Relative Equivalent Radius Req/R
504	1.49	77	76	.073	.973
510	1.46	79	83	.194	.972
511	1.51	78	79	.116	.934
513	1.61	70	66	.142	.987
522	1.30	96	93	.122	.992
523	1.69	56	63	.177	.991
601	1.57	67	69	.115	.974
609	1.48	77	78	.130	.970
613	1.50	74	76	.138	.960
702	1.47	80	77	.061	.973

BIBLIOGRAPHY

1. Bankoff, S. G. and Mikesell, R. D. Growth of Bubbles in a Liquid of Initially Non-uniform Temperature. ASME-58-A-105 Annual Meeting, New York, Dec., 1958.

2. Barlow, E. J. and Langlois, W. E. "Diffusion of Gas From a Liquid Into an Expanding Bubble." IBM Jour., 6 (1962), 393.

3. Benjamin, J. E. and Westwater, J. W. "Bubble Growth in Nucleate Boiling of a Binary Mixture." International Development in Heat Transfer, 24, 1961.

4. Besant. Hydrostatics and Hydrodynamics. Cambridge, 1859.

5. Bird, R. B., Stewart, W. E. and Lightfoot, E. N. Transport Phenomena. John Wiley and Sons, 1960

6. Birkhoff, G., Margulies, R. S. and Horning, W. A. "Spherical Bubble Growth." Phys. of Fluids, 1, No. 3 (1958), 201.

7. Carslaw, H. S. and Jaeger, J. C. Conduction of Heat in Solids. 2nd Ed., Oxford, 1959.

8. Chambré, P. L. "On the Dynamics of Phase Growth." Quart. J. Mech. and Appl. Math., 9 (1956), 224.

9. Clark, J. A., et al. Pressurization of Liquid Oxygen Containers. UMRI Project 2646, University of Michigan Research Inst., Sept., 1959.

10. Coppock, P. D. and Meiklejohn, G. T. "Behavior of Gas Bubbles in Relation to Mass Transfer." Trans. Inst. Chem. Eng., 29 (1951), 75-86.

11. Dankwerts, P. V. "Significance of Liquid Film Coefficients in Gas Absorption." Ind. Eng. Chem., 43 (1951), 1460-67.

12. Datta, R. L., Napier, D. H. and Newitt, D. M. "The Properties and Behavior of Gas Bubbles Formed at a Circular Orifice." Trans. Inst. Chem. Eng., 28 (1950), 14-26.

13. Dergarabedian, P. "Observations on Bubble Growth in Various Superheated Liquids." J. Fluid Mech., 9 (Sept., 1960), 39-48.

14. Dodge, B. F. Chemical Engineering Thermodynamics. McGraw-Hill Book Co., 1944.

15. Ellion, M. E. A Study of the Mechanism of Boiling Heat Transfer. JPL, Memo 20-88, Pasadena, Calif., March, 1954.

16. Emmert, R. E. and Pigford, R. L. "Interfacial Resistance. A Study of Gas Absorption in Falling Liquid Films." Chem. Eng. Prog., 50 (1954), 87-93.

17. Epstein, P. S. and Plesset, M. S. "On the Stability of Gas Bubbles in Liquid-Gas Solutions." J. Chem. Phys., 18, No. 11 (1950), 1505.

18. Forster, H. K. "On the Conduction of Heat Into a Growing Vapor Bubble." J. Appl. Phys., 25, No. 8 (1954), 1067-68.

19. Forster, H. K. and Zuber, N. "Dynamics of Vapor Bubbles and Boiling Heat Transfer." AIChE Journal, 1 (1955), 531-35.

20. Forster, H. K. "Diffusion in a Moving Medium With Time Dependent Boundaries." AIChE Journal, 2, No. 4 (Dec., 1957), 535-38.

21. Goodman, T. R. "The Heat-Balance Integral and Its Application to Problems Involving a Change of Phase." Trans. ASME, 80 (1958), 335-42.

22. Griffith, P. "Bubble Growth Rates in Boiling." Trans. ASME, 80 (1958), 721-27.

23. Grigor'ev, L. N. and Usmanov, A. G. "Heat Transfer During Boiling of Binary Mixtures." Soviet Physics, Tech. Phys., 3, No. 2 (Feb, 1958), 297-305.

24. Groothuis, H. and Kramers, H. "Gas Absorption by Single Drops During Formation." Chem. Eng. Science, 4 (1955), 17-25.

25. Hammerton, D. and Garner, F. H. "Gas Absorption from Single Bubbles." Trans. Inst. Chem. Eng. (London), 32 (1954), 18-24.

26. Higbie, R. "The Rate of Absorption of a Pure Gas Into a Still Liquid During Short Periods of Exposure." Trans., AIChE, 31 (1935), 365-89.

27. Hsieh, D-Y and Plesset, M. S. "Theory of Rectified Diffusion of Mass Into Gas Bubbles." J. Acoust. Soc. Amer., 33 (1961), 206.

28. Jakob, M. and Hawkins, G. A. Elements of Heat Transfer. John Wiley and Sons, 3rd Ed., 1959.

29. Kaplan, W. Advanced Calculus. Addison-Wesley Pubs. Co., Inc., Mass. (1952), 220.

30. Keenan, J. H. and Keyes, F. G. Thermodynamic Properties of Steam. John Wiley and Sons, Inc., 1st Ed., 1958.

31. Kline, S. J. and McClintock, F. A. "Describing Uncertainties in Single-Sample Experiments." Mechanical Engrg., 75 (1953), 3-8.

32. Klinkenberg, A. and Mooy, H. H. "Dimensionless Groups in Fluid Friction, Heat and Material Transport." Chem. Eng. Progr., 44 (1948), 17-36.

33. Lamb, H. Hydrodynamics. Dover Publ., 6th Ed., 1945.

34. Larsen, P. S. Transient One-Dimensional Mass and Heat Transfer in Two-Phase, Two-Component Systems. Heat Transfer and Thermodynamics Lab, University of Michigan, (unpublished), Sept., 1962.

35. Larsen, P. S., Clark, J. A., Randolph, W. O. and Vaniman, J. L. "Cooling of Cryogenic Liquids by Gas Injection." Advances in Cryogenic Engineering, 8, Plenum Press, 1963.

36. Lienhard, J. H. A Study of the Dynamics and Thermodynamics of Liquid-Gas-Vapor Bubbles. Washington State Inst. of Tech. Bulletin 266 (about 1963).

37. Lightfoot, E. N. "Steady State Absorption of a Sparingly Soluble Gas in an Agitated Tank with Simultaneous Irreversible First Order Reaction." J. AIChE, 4 (1958), 499.

38. Lykov, A. V. and Mikhaylov, Y. A. Theory of Energy and Mass Transfer. Prentice-Hall, Int. Ser. in Eng., 1961.

39. Mikhaylov, Y. "Highly Intensive Heat and Mass Transfer in Dispersed Media." Intl. J. Heat and Mass Transfer, 1 (1960), 37-45.

40. Nabavian, K. and Bromley L. A. Condensation Coefficient of Water. Sea Water Conversion Program, Univ. of Calif. Water Resources Center contribution No. 62, Oct., 1962. (See also: Ph.D. Thesis, Aug., 1962).

41. Pattle, R. E. "The Aeration of Liquids - Part I, The Solution of Gas from Rising Bubbles." Trans., Inst. Chem. Engrg., 28, 27-31.

42. _____, "Part II, Factors in the Production of Small Bubbles." Ibid, 32-37.

43. Perry, J. H. Chemical Engineers' Handbook. McGraw-Hill Book Co., Inc., 3rd Ed., 1950.

44. Plesset, M. S. "The Dynamics of Cavitation Bubbles." J. Appl. Mech., 16 (1949).

45. Plesset, M. S. and Zwick, S. A. "A Non-steady Heat Diffusion Problem with Spherical Symmetry." J. Appl. Physics, 23 (1952), 95.

46. Plesset, M. S. and Zwick, S. A. "Growth of Vapor Bubbles in Superheated Liquids." J. Appl. Phys., 25 (1954), 493-500.

47. Plesset, M. S. and Zwick, S. A. "On the Dynamics of Small Bubbles in Liquids." J. Math. and Phys., 33, No. 4 (1955), 308-330.

48. Plesset, M. S. Bubble Dynamics. Calif. Inst. of Tech., Report No. 85-23, February, 1963).

49. Pohlhausen, K. "Zur naherungsweisen Integration der Differentialgleichung der laminaren Reibungsschicht." ZAMM, 1 (1921), 252-268.

50. Poots, G. "An Approximate Treatment of the Heat Conduction Problem Involving a Two-Dimensional Solidification Front." Intl. J. Heat and Mass Transfer, 5 (1962), 339-48.

51. _____, "An Application of Integral Methods to the Solution of Problems Involving the Solidification of Liquids Initially at Fusion Temperature." Loc. cit., 525-31.

52. Rayleigh, L. Phil. Mag., 34 (1917), 94.

53. Savic, P. "The Dynamics of an Expanding Vapor Bubble in a Boiling Liquid." Can. J. Chem. Eng., 40, No. 6 (1962), 238-45.

54. Schrage, R. W. Interphase Mass Transfer. Columbia Univ. Press, 1953.

55. Scriven, L. E. "On the Dynamics of Phase Growth." Chem. Eng. Science, 10 (1959), 1-13.

56. Scriven, L. E. and Pigford, R. L. "On Phase Equilibrium at the Gas Liquid Interface During Absorption." Journal AIChE, 4, 439-44.

57. van Stralen, S. J. D. "Heat Transfer to Boiling Binary Liquid Mixtures at Atmospheric and Subatmospheric Pressures." Chem. Eng. Science, 5 (1956), 290-96.

58. Strasberg, M. "Pulsation Frequency of Non-Spherical Gas Bubbles in Liquids." J. Acoust. Soc. Amer., 25 (1953), 536.

59. Treybal, R. E. Mass Transfer Operations. McGraw-Hill Book Co., Inc., 1955.

60. Tung, L. N. and Drickamer, H. G. "Diffusion Through an Interface Binary System." J. Chem. Phys., 20 (1952), 6-9.

61. Vos, A. S. and van Stralen, S. J. D. "Heat Transfer to Boiling Water-Methyl Ethylketone Mixtures." Chem. Eng. Science, 5 (1955), 50-56.

62. van Wijk, W. R., Vos, A. S., and van Stralen, S. J. D. "Heat Transfer to Boiling Binary Liquid Mixtures." Chem. Eng. Science, 5 (1956), 68-80.

63. Yang, K-T, and Szewczyk, A. An Approximate Treatment of Transient Heat Conduction in Semi-Infinite Solids with Variable Thermal Properties. Dept. of Mech. Eng. Univ. of Notre Dame, Notre Dame, Indiana (Internal technical note.)

64. Yang, W-J, and Clark, J. A. On the Application of the Source Theory to the Solution of Problems Involving Phase Change, Part I - Growth and Collapse of Bubbles. ASME Paper 63-H-45 (to be published in ASME J. Heat Transfer).

UNIVERSITY OF MICHIGAN
3 9015 03023 1925